Image Processing Solutions for Precise Road Profile Measurement Systems

AGO MÕLDER

TALLINN UNIVERSITY OF TECHNOLOGY

Faculty of Information Technology

Thomas Johann Seebeck Department of Electronics

This dissertation was accepted for the defense of the degree of Doctor of Philosophy in Computer and Systems Engineering on May 04, 2015.

Supervisor: Dr. Olev Märtens
Thomas Johann Seebeck Department of Electronics,
Faculty of Information Technology, Tallinn University of
Technology

Opponents: Res. Prof. Andi Kivinukk
Tallinn University, Estonia

Assoc. Prof. Gholamreza Anbarjafari
University of Tartu, Estonia

Dr. Ints Mednieks
Institute of Electronics and Computer Science, Riga, Latvia

Defense of the thesis: 04.06.2015

Declaration:

Hereby I declare that this doctoral thesis, my original investigation and achievement, submitted for the doctoral degree at Tallinn University of Technology has not been submitted for any academic degree.

/Ago Mõlder/

Pilditöötluse lahendused täpsetele tee profiili mõõtesüsteemidele

AGO MÕLDER

CONTENTS

APPROBATION AND LIST OF PUBLICATIONS

Portions of this thesis material were presented and published in the following publications in fulfillment requirements for the PhD of Tallinn University of Technology. Copies of the publications I - III can be found in appendices.

Publications related to thesis topic, published

I   **A. Molder**, O. Martens, T. Saar, and R. Land, "Laser Line Detection with Sub-Pixel Accuracy," *Elektron. Ir Elektrotechnika*, vol. 20, no. 5, May 2014, pp. 132-135.

II **A. Mõlder**, O. Märtens, T. Saar, and R. Land, "Extraction of the Variable Width Laser Line," in *Proceedings of the 14th Biennial Baltic Electronics Conference (BEC)*, Tallinn, Estonia, Oct. 06, 2014, pp. 157-160.

III **A. Molder**, O. Martens, T. Saar, and R. Land, "Adaptively undersampled image processing for fast multiline laser detection," in *2013 IEEE 8th International Symposium on Intelligent Signal Processing (WISP)*, 2013, pp. 60–64.

Publications related to thesis topic, in print

IV O. Märtens, **A. Mõlder**, R. Land, T. Saar, M. Reidla, D. Reid, and A. Girfanov, "Meetod ja seade täpsete ajatemplitega pideva pildivoo hõivamiseks," Estonian Patent Application No. P201400044, Dec. 18, 2014.

V   **A. Mõlder**, O. Märtens, T. Saar, and R. Land, "Laser Scanner Calibration Dependency on the Line Detection Method," *Elektron. Ir Elektrotechnika*, accepted Feb. 18, 2015, in print.

Author other publications, published during the same period, listed below, are not directly related to the current thesis, but will give in one or another way, an inspiration for future works in the thesis field.

Author's other publications

- Gavrijaseva, **A. Molder**, O. Martens, C. Kyrkou, and T. Theocharides, "Cross-correlation-based image matching of coins," in *Proceedings of the 13th Biennial Baltic Electronics Conference (BEC), Tallinn, Estonia,* 2012, pp. 319–322.

- **A. Molder**, O. Martens, and T. Saar, "Adaptively undersampled, circular histogram based image processing for rotation invariant coin detection," in *Electronics Conference (BEC), Tallinn, Estonia,* 2012, pp. 137–140.

- **A. Molder**, M. Reidla, O. Martens, and R. Land, "Feasibility study: A DM3730-based data acquisition and processing solution," in *Education and Research Conference (EDERC), 2012 5th European DSP*, 2012, pp. 58–61.

- O. Martens, T. Saar, A. Gavrijaseva, and **A. Molder**, "Variable-resolution image processing for validation of coins," in *2011 IEEE 7th International Symposium on Intelligent Signal Processing (WISP)*, 2011, pp. 1–4.

- O. Martens, R. Land, A. Gavrijaseva, and **A. Molder**, "Adaptive-rate inductive impedance based coin validation," in *2011 IEEE 7th International Symposium on Intelligent Signal Processing (WISP)*, 2011, pp. 1–4.

- **A. Molder** and O. Martens, "Image Processing in the Woodworking Industry: Challenges, Solutions and Platforms," *Elektron. Ir Elektrotechnika*, vol. 113, no. 7, Sep. 2011, pp. 43-46.

- **A. Mõlder** and J. Mullo, "Meetod käsitööpalkseinte varamiseks," Estonian utility model, U201000047, Apr. 12, 2010.

The results of the thesis have been and will be presented and discussed at various conferences:

A. Baltic Electronics Conference (BEC), Tallinn, Estonia, 2014.
B. International Symposium on Intelligent Signal Processing (WISP), Madeira, Portugal, 2013.
C. Electronics, Palanga, Lithuania, 2014 and 2015.

Some of the thesis results have been also included into the reports of the EU FP7-SME project "Hermes" ("Innovative, Highly Efficient Road Surface Measurement and Control System") and some of the solutions proposed in the thesis have been also tested and evaluated during this project.

Author's Contribution to the Publications

Here is the list of author's contributions to the publications related to current thesis.

- **I.** Development of the laser line detection software; setting up and making of experiments to compare different laser line detection methods with sub-pixel resolution, analysis and recording of the results; writing of the paper.
- **II.** Development of the variable width laser line detection software; making the graphs of the laser line detection with optimal standard deviation of the convolution kernel; analysis and recording of the results; writing of the paper.
- **III.** Development of the adaptively undersampled image processing algorithm and software; making of experiments on different computation platforms; analysis and recording of the results; writing of the paper.
- **IV.** Setting up and making of experiments with different excitation signals and frequencies; analysis of the results; preparation of the patent application figures; review of the patent application text.
- **V.** Development of the calibration software; setting up and conducting of experiments with different laser line detection methods, analysis and recording of the results; writing of the paper.

.

INTRODUCTION

About road measurement systems

Road measurement system usually consists of instruments to measure road parameters like transverse and longitudinal profiles, macro-texture properties, rut depth and width, cross fall, curve radius, cracks, international roughness index (IRI), mean profile depth (MPD), relative position since the start of measurement, vehicle (measurement platform) speed, global positioning system (GPS) position, pavement imaging, but can also include systems to capture road markings, friction, quality of road markings in center and sides, crack level, crack area, holes, structural changes, manholes, and asphalt joints.

Figure 0.1 Example of „Furgo Roadware" road measurement system [1].

Road measurement systems are used by different customers for various purposes. The main users of the road measurement system are listed below.

- Road maintainers - to locate quickly and automatically locations requiring urgent repair. If the measurement of the road would be made regularly, the measurement results can be used for keeping track of the wear of the road and also, on this basis, the build quality and the material needed for repair can be assessed.
- Road constructors - to calculate the amount of material for new road construction in the same location. Also road constructors can verify if the newly built road meets all the required existing road building standards (all the road markings are at the right spot, the manholes are

at the right height, the slopes are right, there are no cracks, the Roughness Index is within limits, etc).

- National technical control centers responsible for roads – they are the supervisors who control that all the new roads and maintenance are made according to existing standards. This enables to maintain the quality of the roads within limits, despite the fact that the construction and maintenance of the roads are made by different companies.
- Air-fields - to ensure the safety of the airplane landing sites to detect cracks and holes from the runway.
- Road engineers - to plan and design new and better roads with better materials, resulting in roads that are more durable.
- Car drivers - the collected information can also be used in road-hazard avoidance systems. Through these systems, car drivers could get real-time warnings from forthcoming road surface condition like roughness, holes and bigger cracks. This enables the car drivers to act accordingly to actual road conditions.

About road profile scanners

One of the main instruments of the road measurement systems is typically a 3 dimensional (3D) road profile scanner to acquire road profile data and convert this to digital domain.

Two main technologies for road pavement scanning exist currently: light detection and ranging (LIDAR) and structured light methods. LIDAR based technology uses time-of-flight (TOF) of the light wave. Usually phase shift in modulated laser light is measured and used to calculate the distance between the laser light source and reflected surface [2]. Structured light methods are based on the measurements of the projections of the predefined light shape. Based on the deformations of the light, the road pavement profile can be calculated, using a simple triangulation transform.

One of the structured light methods, used in 3D laser line scanners, contains a camera and a line laser. The camera sensor and the line laser have a fixed position and orientation relative to each other. The laser projects a plane of light to the object under measurement. The laser light plane is created with special optics in front of the laser beam. The laser light plane creates a line on the object visible by the camera. The line is straight if the object height compared with the measurement base plane is zero. Depending of the object height the line shape is deformed and so the profile and the measurement results of the object cross section can be calculated. If the object moves through the laser light plane, several profiles are taken and eventually a complete distance map or a 3D model can be generated.

In case of road profile scanners typically one profile covers full lane witdh (3-4 meters) of the road.
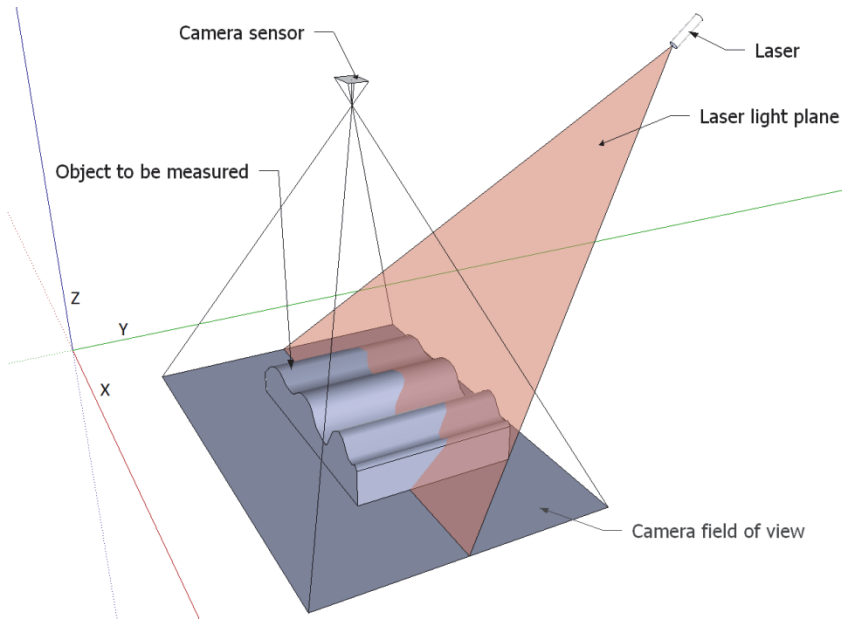
Figure 0.2 Working principle of 3D laser scanner.

Such road profile scanner, attached to the measurement vehicle, allows the measurement of the road profile, cracks, potholes, bumps and other irregularities or unknown objects. If the acquired 3D road profile data is sufficiently accurate and with sufficient density/resolution, then most of the road parameters can be calculated from this data.

Figure 0.3 Example of 3D road profile data from road profile scanner.

Overview of the state of the art

Patent information

Around 40 patent specifications have been found on the thesis topic. Some of the solutions [3-14] describe non-contact methods for scanning the road surface by using different projected structured light or laser line patterns, multiple laser combinations or fan-shaped light beams in conjunction with a camera. Other solutions [9, 15-20] use contact or contact and non-contact combined methods for scanning of the road surface parameters.

Many road scanner solutions [16, 21-27] use TOF-based distance measurement scanners, charge coupled device (CCD) sensor-based cameras [12, 20, 23] or multi-camera systems [8-9, 23, 28]. Additional or substitution measurement instruments for road surface scanners like global positioning system (GPS), acceleration sensors or radiation based scanners [9, 16, 23-24, 29-30] are also used.
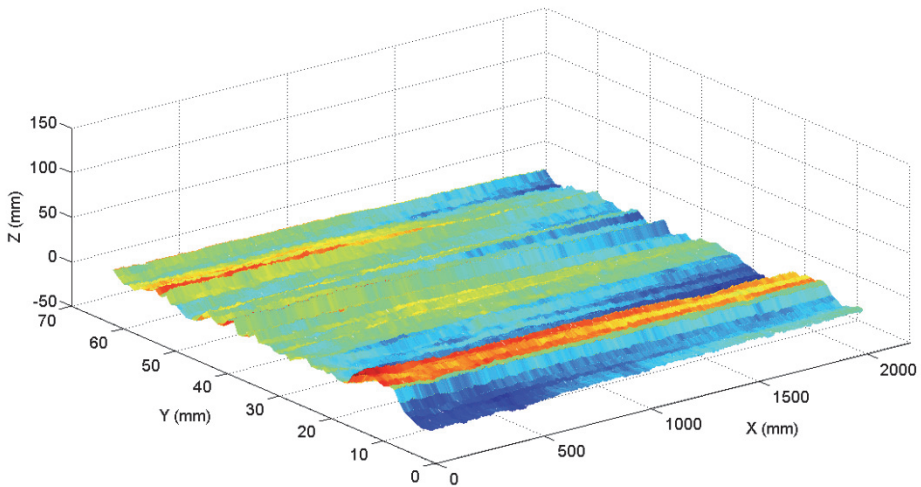
Some of the patent specifications describe improvements of existing systems [20, 29, 31], using scanned data to control vehicle suspension [4, 32], repair the road right after scanning [31], measuring features and their positions located on the road or on the side of the road [33] or describe hand operated high resolution road profile scanners[25].

A large proportion of patents [5, 7-9, 17-19, 21, 24, 30, 34-40] describe the scanners used to measure different road parameters like transverse and longitudinal profile, transverse and longitudinal cracks, alligator cracks, design cracks, potholes, rutting, cross fall and friction.

The main objectives of patented solutions are listed below.

- To increase the measurement speed.
- To improve the immunity to surrounding light condition variations.
- Improvements in data analysis.
- Creating of a mathematical model of the road.
- Simultaneous measurement of several parameters.
- Synchronous measurement of transverse and longitude road profile.
- Simultaneous measurement of the pavement profile and its deflection under load.
- Improvements in accuracy.

The analysis of the patent and other information confirms efficiency of using of the laser beam(s) in combination with camera to scan the profile of the road and retrieve other useful information from the pavement using the same camera.

Commercial solutions

There are many commercial road measurement systems available, most of which contain also a road profile scanner. The most known of them are, GIOVE, ViaTech, Pathway Services, Pavemetrics Systems, ARAN, Fugro Roadware, International Cybernetics, Roadscanners OY, Siteco [1, 41-47].

From the road profile measurement perspective the most important parameters of the road profile measurement scanners are horizontal accuracy, profile vertical accuracy, update rate (Hz), maximum measurement speed of the platform, the laser type, the laser output power, number of cameras and the maximum measurement width. Following table (Table 0.1) concludes the known parameters for the state of the art solutions [1, 41-50].

Table 0.1 Comparison of known commercial road profile scanner parameters.

Parameters	Manufacturer							
	GIOVE	ViaTech	Pathway Services	Pavemetrics	International Cybernetics	Fugro adware	Roadscanners OY	Siteco
No. of transverse profile points	-	580	1500	4096	1280	4096		
Horizontal accuracy	±1 mm	±2 mm	-	±1 mm	±1 mm			
Vertical accuracy	±1 mm	±1 mm	-	±0.5 mm				
Laser type	3B	3R	-	4	-			
Laser output power	-	-	-	6000 mW	-			
Number of cameras		0	3	2	4	4	0	
Number of lasers	-	1	4	2	4	4	1	
Transverse scan width	-	4 m	-	4 m		4 m		
Update rate	-	140 Hz	-	11200 Hz	150 Hz			100 Hz
Maximum measurement speed	50 km/h	40 km/h	112 km/h	100 km/h	108 km/h	100 km/h		

Motivation, research objectives and challenges

Motivation

The analysis of the patents, existing commercial solutions and other information shows that the existing road profile measurement systems are fairly complex, consisting of several sophisticated instruments which are necessary to collect the data required by the users of the road profile measurement systems. This however, has made the road profile measurement systems quite expensive and thus not affordable for smaller companies who would benefit of owning such systems. Several aspects of the existing solutions, as shown in this thesis, can be improved, while reducing the complexity of the road profile measurement system and reducing the number of instruments required to acquire necessary road profile data. This helps to reduce the cost of the road measurement systems, making it more affordable to be used in several business sectors and companies.

One of the challenges of the FP7-SME project "Hermes", related to the current thesis, was just to develop the efficient road measurement system suitable for cost-sensitive SMEs.

Research objectives and challenges

The purpose of the work, described in the thesis has been to develop, optimize, implement and evaluate new 3D laser scanner solution and its image processing algorithms for the road profile measurement system. Following objectives of the new 3D laser scanner for the road profile measurement system have been set.

O1. Reduce the number of cameras and lasers to cover full lane width for both transverse and longitudinal road profiles.
O2. Increase the vertical accuracy of the road profile data to sub-millemeter level.
O3. Improve the calibration process of the whole scanner system to be more automatic, more accurate and easier to use.
O4. Improve the laser line detection in case of different road surfaces conditions and variable laser line width.
O5. Improve the laser scanner profile scanning speed without using more expensive equipment.
O6. Improve the safety of the laser scanner by reducing the output power of the laser line scanners used by the current road profile scanning systems.
O7. Simplifying the installation and usage of the road profile measurement system on different vehicles.
O8. Lower the cost of the road profile measurement system.

Existing road profile measurement systems usually consist of two or more laser scanners to measure transverse and longitudinal road profile data

separately. However longitudinal scanner camera and laser can be removed by increasing the transverse profile scanning rate and calculating the longitudinal road profile from transverse road profile data.

Vertical accuracy of the transverse road profile data is an important aspect for the users of the road scanning systems. Existing road scanning systems allow up to ±1 mm of transverse profile vertical accuracy. The limiting factor of the existing solutions is the fact that most of the laser line detection algorithms detect the laser line from the laser scanner images with 1 pixel resolution and the accuracy of the vertical road profile data is thus directly dependent of the camera sensor resolution. Higher resolution cameras are more expensive and requiring more processing power to detect the laser line, thus making the scanners more expensive. The vertical road profile accuracy can be improved by using laser line detection algorithms which can detect the laser line with sub-pixel resolution.

Calibration, needed to convert the detected laser line in pixels of the camera sensor to real world 3D millimeters is often not implemented correctly. Most of the laser scanner calibration algorithms does not take into account the distortions, caused by the optics used in front of the laser to generate the line and in several cases the camera lens optics distortions are also not taken into account. This will lead to inaccurate calibration and thus wrong measurement results. Some of the existing calibration processes are quite complicated making them difficult to implement to calibrate the scanner accurately. Calibration process and the accuracy of the calibration results can be improved by using simple methods and proper calibration procedure.

Due to the fact that different surfaces reflect light in different ways the laser line on captured images has not always constant width. The line width also depends on the laser optics used. In order to achieve greater autonomy of the laser line extraction algorithm from the line width and reduce the corresponding uncertainty the variable width laser line detection algorithms can be used.

Road profile scanning speed determines directly the time needed to measure the road section at required resolution. One way to increase the speed is by developing adaptive laser line extraction algorithms for transverse profile measurement.

Requirement for the road profile scanner to be safer is related to the fact that some of the most known road profile laser line scanners use very powerful laser, up to 6000 mW. These scanners belong to the class 4 of lasers and are considered the highest and most dangerous class of the lasers. Class 4 lasers can burn the skin, or cause devastating and permanent eye damage as a result of direct, diffuse or indirect beam viewing. The main reason of using of such high power lasers in existing commercial solutions is to reduce the effects of ambient light conditions, caused mainly by fairly strong solar illumination and rapidly changing road surface reflection conditions. The output power of the laser lines

can be reduced by creating more sophisticated laser line detection algorithms which work well on various light conditions.

By removing some of the measurement instruments the road profile measurement system will be easier to use and install on various measurement vehicles making the cost of the measurement system smaller.

Outline of the thesis

This thesis is structured as follows.

In chapter 1 and paper [51 (II)] a new method based on second order Gaussian derivative convolution with different standard deviation convolution kernel parameters taking into account the variable laser line width was developed and tested. In paper [52 (I)] two laser line detection methods "Parabola method" and "Upsampling method" and the combination of those were developed and tested to improve the laser line detection resolution from pixel to sub-pixel level.

In chapter 2 and paper [66 (III)] a new "Adaptive Undersampling Method" to increase the road profile scanning speed without increasing the camera frame rate or using custom, expensive hardware was developed and tested.

In chapter 3 a new "Laser Light Plane Linear Interpolation Method" for finding the laser light plane parameters together with the complete scanner calibration procedure and flowchart were developed and experimentally evaluated (in paper [76 (V)]) in the lab with objects of known dimensions as well as on real pavement (together with road maintenance authorities in Estonia).

In chapter 4 and in the patent application [88 (IV)] a novel solution to precisely time-stamp the laser line profile (road transverse profile) with absolute time and thus location on road was described.

In chapter 5 the developed hardware and software is described.

In chapter 6 the main results of the thesis are listed. Future improvements are proposed.

LIST OF ABBREVIATIONS

3D	3 Dimensional
ABCD	A, B, C, D parameters
BEC	Baltic Electronics Conference
CCD	Charge Coupled Device
EDERC	Education and Research Conference
EU	European Union
FP7	Seventh Framework Programme
FPS	Frames Per Second
GNSS	Global Navigation Satellite System
GPS	Global Positioning System
GUI	Graphical User Interface
IEEE	Institute of Electrical and Electronics Engineers
IRI	International Roughness Index
LED	Light Emitting Diode
LIDAR	Light Detection And Ranging
LSF	Least Square Fitting
MPD	Mean Profile Depth
PC	Personal Computer
PhD	Doctor of Philosophy
PPS	Pulse Per Second
RGB	Red Green Blue
RMSE	Root Mean Square Error
DSP	Digital Signal Processor
ROI	Region Of Interest
SME	Small and Medium-sized Enterprises
TOF	Time Of Flight
USB	Universal Serial Bus
WISP	International Symposium on Intelligent Signal Processing

1. LASER LINE DETECTION

Laser line detection is one of the key elements in 3D laser scanner system. The quality of the laser line detection algorithm influences directly the detected road profile measurement results. The quality in this context means how accurately and at which resolution can the laser line be detected from the camera image and thus from the road surface, as well as how unaffected is the laser line detection from external conditions like light conditions and variation of the line width. Also the computational efficiency is an important quality aspect determining how efficiently the laser line can be detected without excessive hardware cost, energy and time.

In this chapter and in papers [51 (II) – 52 (I)] several novel methods are investigated to improve the laser line detection resolution compared to existing solutions and reduce the dependency of the laser line detection algorithm from the noise and the variation of the laser line width.

1.1. Laser line detection with pixel resolution

Over time many laser line detection methods have been developed and used to extract laser line(s) from 3D laser scanner images. The most used and the simplest of these are the methods that are based on the use of the most intensive pixel [53-54] or so called peak detection methods. Unfortunately those methods can produce inaccurate results while processing over saturated, noisy or wider than 1 pixel laser line profile peaks. Figure 1.1 shows an example of the laser line gray value profile, where those methods will probably cause an inaccurate result due to the flat top of the laser line profile.
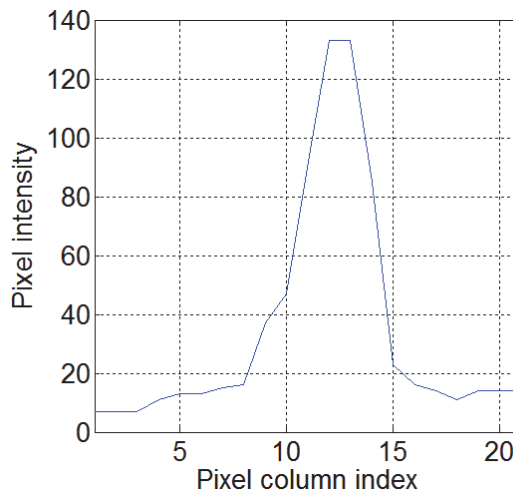

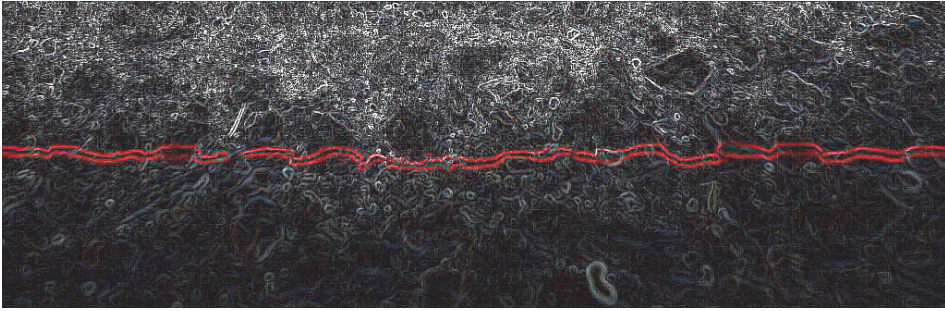*Figure 1.1 Laser line profile with flat peak.*

Figure 1.2 Laser scanner image filtered with Canny operator.

Various edge detection methods [55-56] are also very popular. Those methods are usually based on various Canny, Sobel and Prewitt operators to find the laser line edges. Based on the found edges a laser line center can be calculated. Due to the fact that the road profile surface is usually quite multicolored, containing often small and very reflective rocks that can cause sharp edges and laser light scattering, the laser line profile can become asymmetric which can cause the mathematical mean point to deviate from the actual laser line center. Figure 1.2 represents laser scanner image with the laser line on the road surface filtered by Canny operator. It can be clearly seen that the laser line is not always with constant width nor symmetric.

The disadvantage of this method is also the fact that some of the edges that are not acctually part of the laser line can influence the laser line detection.

Template matching is also a known method for line detection. Haar features [57] can be used to detect different parts of laser lines. Figure 1.3 shows an example of templates that have a good match for the laser line detection.

Since the laser line width, shape and the position of it on the image changes quite a lot, an enormous amount of correlation calculations with different templates has to be performed in order to find the optimal laser line position.
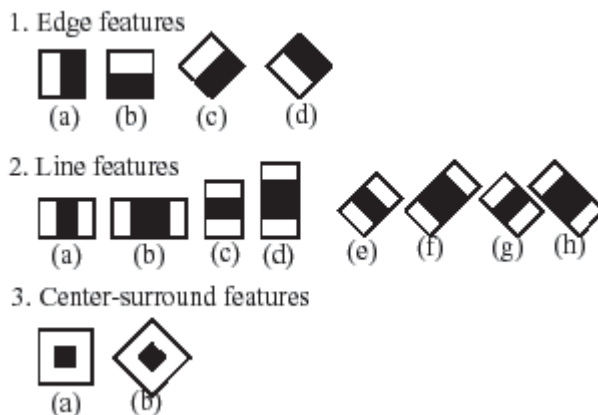

Figure 1.3 Different Haar features for template matching [57].

Also the relative position between the found templates has to be taken into account. Thus this method is not very optimal solution for high speed laser profile measurement systems from the resource usage perspective. Furthermore this method has also the same risk to detect the laser line parts that actually does not belong to the real laser line.

Some of the laser line detection algorithms use first order Gaussian derivative zero crossings [58] to extract the laser line center positions. Another method [59] uses multiple first order Gaussian derivatives to extract laser line edges instead of usual edge detection operators and then uses fixed distance of those found first order derivatives to find the laser line. With those methods the variations of the laser line width is not taken into the consideration and random noise peaks influence the result quite a lot.
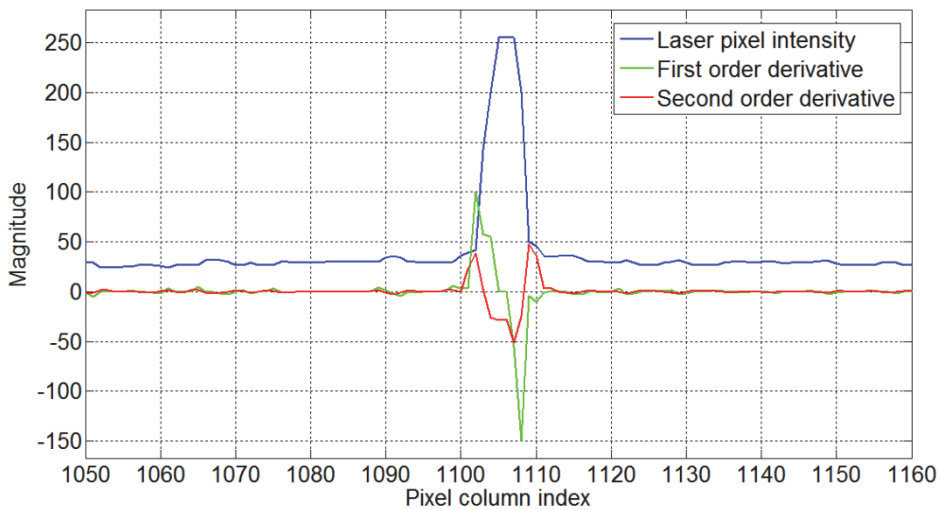

Figure 1.4 Laser line intensity profile and its Gaussian derivatives.

As known, cross-section of the laser line (Figure 1.1 for example) is similar to the Gaussian distribution from the image pixel intensity perspective. Thus many laser line extraction methods [60, 61] are based on this fact, giving quite reasonable results and hope to develop a good laser line detection algorithm based on this approach for high speed and accurate 3D road profile measurement system.

The method uses Gaussian second order derivative mask to find the laser lines from images. Gaussian distribution is described as

$$g(n, \sigma) = \frac{1}{\sqrt{2\pi}\sigma} e^{-\frac{n^2}{2\sigma^2}}, \qquad (1.1)$$

with a width of N in pixels where

$$-\left(\frac{N-1}{2}\right) \leq n \geq \left(\frac{N-1}{2}\right) \qquad (1.2)$$

and σ is the standard deviation of a Gaussian random variable.

To find a convolution mask an inverted second order derivation of the Gaussian distribution is taken:

$$g''(n,\sigma) = -\frac{n^2 - \sigma^2}{\sqrt{2\pi}\sigma^5} e^{-\frac{n^2}{2\sigma^2}}. \qquad (1.3)$$

This mask is then convolved with the gray value profile $f(n)$ of each image column:

$$s''(n,\sigma) = g''(n,\sigma) * f(n). \qquad (1.4)$$

In the center position of the laser line the convolution result has a local maximum.

1.2. Variable width laser line detection method

Most of the laser line detection algorithms assume that the laser line is of constant width over the whole image, but in reality this is not always the case. Depending on the 3D laser scanner application area this is not taken into account, but in 3D road profile measurement scanner the variable laser line width affects the laser line extraction algorithm and thus the whole road profile measurement system precision. In sub-millimeter level this is a critical factor.
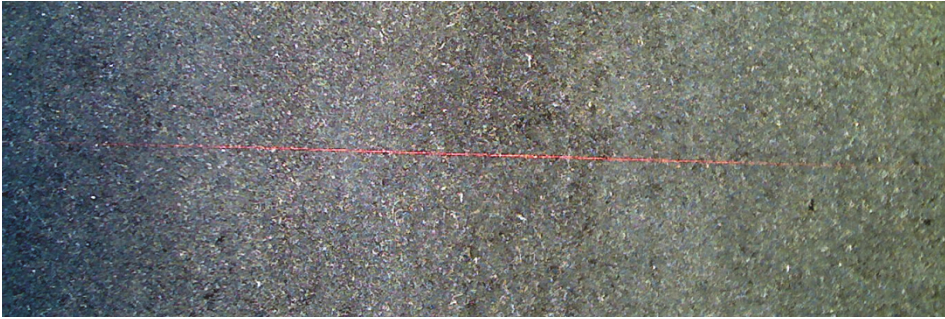
Figure 1.5 Variable width laser line on a pavement surface.

The variable laser line width is caused by the fact that various surfaces reflect light in different ways. Some materials reflect more energy back to the camera sensors than others. Road profile is usually full of small multicolored rocks and dust with different reflection properties. As a consequence, some areas of the laser line on image are wider and some laser line areas are narrower. The laser line shape (including the width) depends on the implementation of optics used in front of the laser beam. Gaussian distribution optics has more energy in the middle part of the laser line thus causing wider line area in the middle part of the line and converging line widths at the ends of the laser line. In addition, the laser line width varies at different distances from the camera. Closer to the camera the laser line is wider. Figure 1.5 shows an example of laser line on a pavement surface with Gaussian distribution optics.

In order to reduce the uncertainty, caused by the unknown laser line width and to increase the autonomy of the laser line extraction algorithm, the laser line width has to be taken into account and included into the laser line detection method. For every laser line section there is an optimal laser line width, that can estimated. This laser line width parameter, for every laser line section, can be used for one time system calibration or for real-time system optimization.

As it has been previously described, the laser line cross-section is similar to the Gaussian distribution from the image pixel intensity perspective, thus the variable width laser line extraction method is based on the Gaussian second order derivative method. To take the laser line width into account over the entire image the inverted second order derivations of the Gaussian distribution has to be taken with several different standard deviations. Having more different deviation values gives better optimal laser line width detection. The range of $1 \leq \sigma \geq 4$ with an increment of 0.5 steps can be chosen for example, as this range is quite big to cover good laser line width variations and on the other hand is small enough. So the method will not be very calculation intensive and can thus be used in real-time 3D scanner systems.
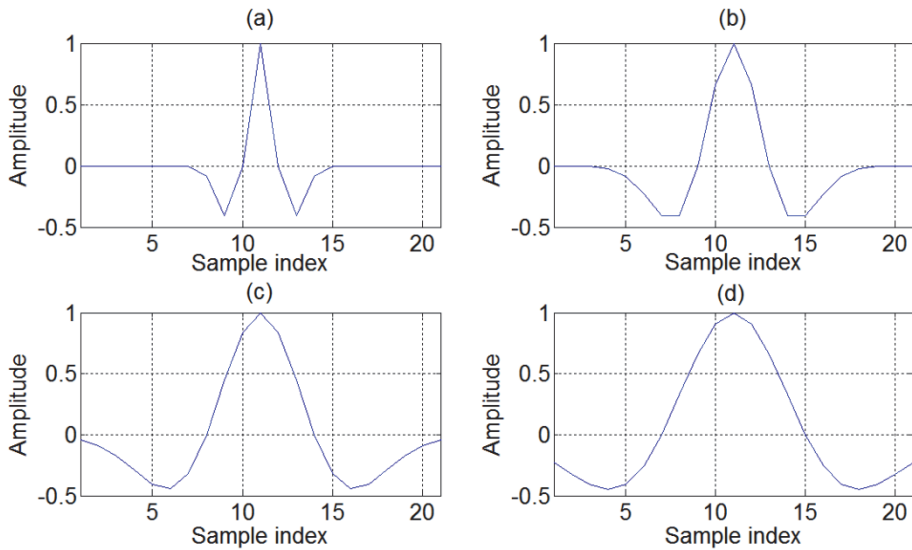
Figure 1.6 Inverted second order Gaussian derivatives with different σ-s [51 (II)].

Figure 1.6 presents inverted second order Gaussian derivatives with different standard deviations. These derivatives are used as masks or so called kernels for convolutions with the gray value profile of every image column. In the laser line center positions the convolution has a local maximum with every convolution mask. The maximum value per convolution mask is different. Out of those maximums a maximum of maximums for the final laser line is selected. Figure 1.7 presents a block diagram of the variable width laser line detection method.

The optimal standard deviation value out of which the convolution was the maximum is stored for every image column or a section of the laser line. The vector of optimal deviations can be used for one-time system calibration or for real-time system optimization during the laser line extraction process.
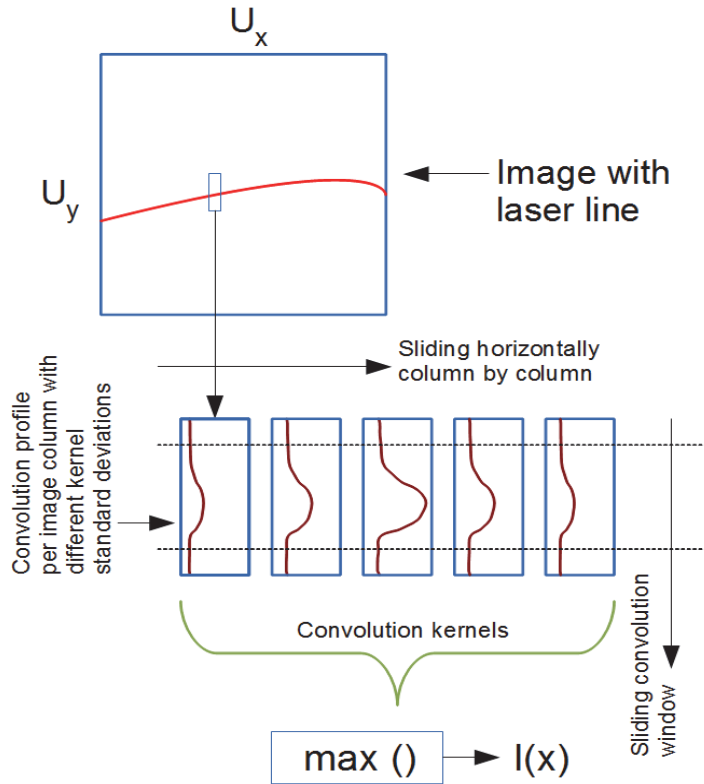
Figure 1.7 Block diagram of variable width laser line detection method [51 (II)].

1.3. Experiments - variable width laser line detection

Experiments of the method were made with several real life images. The goal was to find the optimal standard deviation for every image column for better laser line extraction. Figure 1.8 shows the relation between the standard deviation of the convolution kernel and the maximum of the convolution results with different standard deviation convolution kernels. Three different laser line width values where used, as line a = 3 px, line b = 5 px and line c = 7 px marked on Figure 1.8. It can be seen from the Figure 1.8, that using different laser line width values the maximum convolution result is different as expected. The optimal or the maximum of the maximum convolutions is clearly visible and depends on the used standard deviation value.
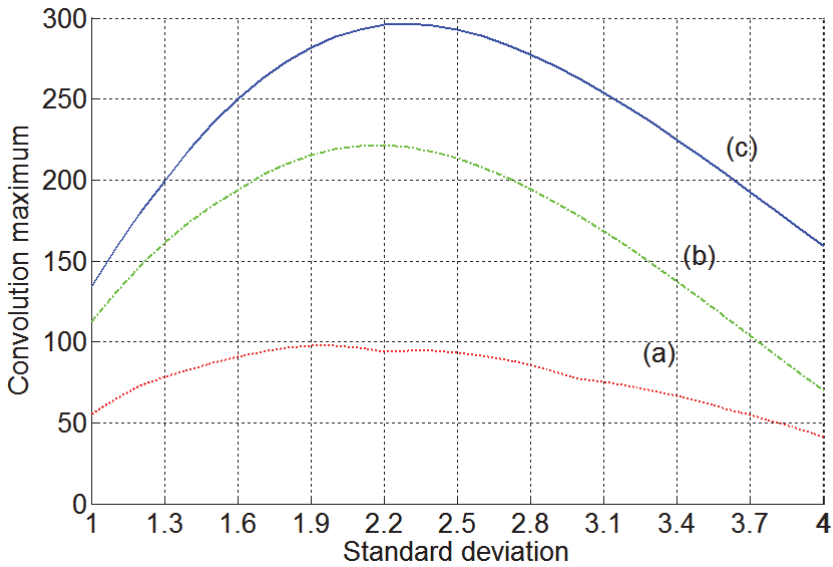
Figure 1.8 Maximum convolution compared to standard deviation with the convolution mask width of 13 pixels [51 (II)].
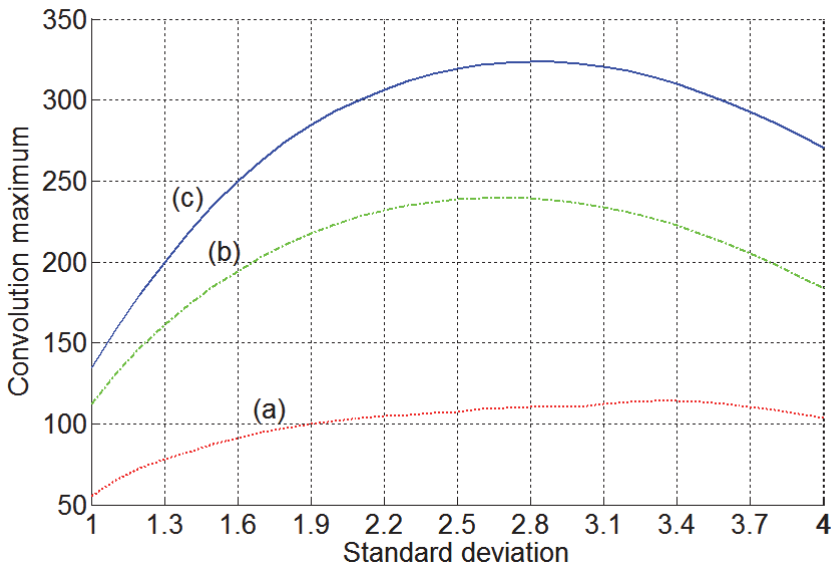

Figure 1.9 Maximum convolution compared to standard deviation with the convolution mask width of 19 pixels [51 (II)].

It was also noticed, that with different convolution mask sample count (the convolution mask width) the optimal standard deviation of the convolution kernel was changing. Figure 1.8 shows a shifted optimal convolution kernel standard deviations compared to Figure 1.9.

Figure 1.10 shows an example of the image used to test the proposed method. It can be seen that the laser that is used is with Gaussian distribution optics, meaning that in the middle of the laser line the line is wider and it is narrower at the ends of the laser line. It can be also seen that on the darker squares of the chessboard there is much less energy on the laser line, so the line is narrower there.
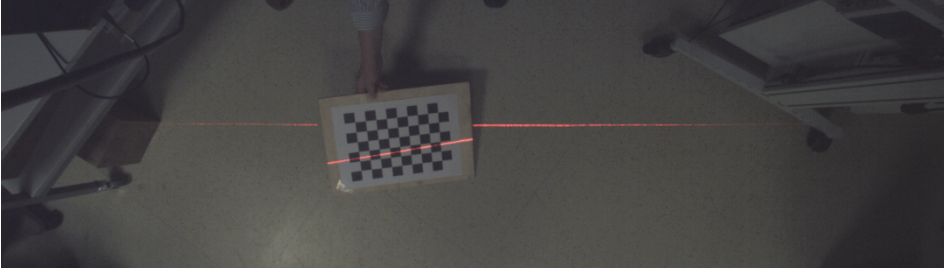

Figure 1.10 Example test image with Gaussian distribution optics [51 (II)].

Figure 1.11 (a-d) represents an extracted laser line with different fixed standard deviation convolution kernels. Figure 1.11(e) shows an extracted laser line with optimal standard deviation convolution kernels for every pixel column. It can be seen that the laser line (Figure 1.11 (e)) has been detected with less missing samples than with the fixed standard deviation convolution kernels. Although some fixed standard deviation convolution kernels (Figure 1.11 (b)) can give quite good results, it is not an optimal standard deviation for every pixel column. Closer inspection shows that the laser line, detected with fixed standard deviation convolution kernels, deviates from the laser line, detected with the optimal standard deviation convolution kernel. Figure 1.12 shows a laser line section deviation from the optimal laser line. It can be seen that in some points the deviation from the optimal laser line is in several pixels. This deviation becomes critical when it is necessary to detect the laser line with sub-pixel/sub-millimeter accuracy.
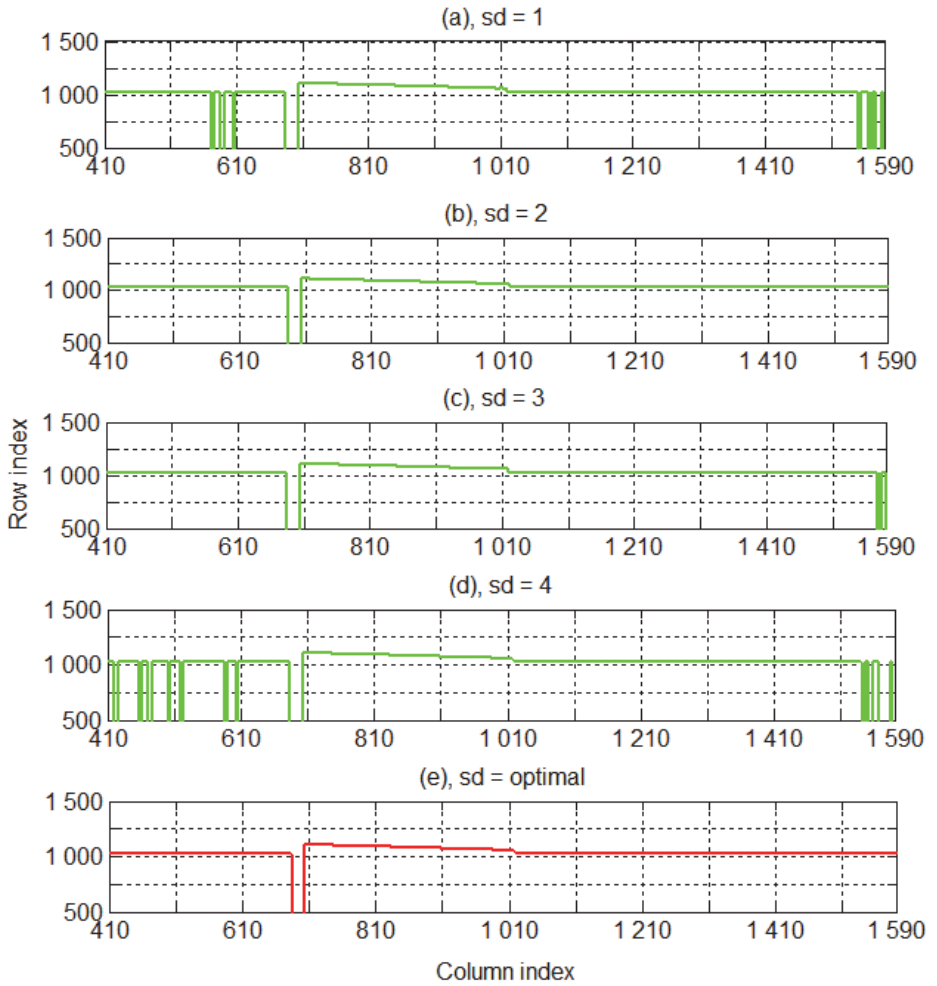
Figure 1.11 Extracted laser line with fixed and optimal standard deviation [51 (II)].
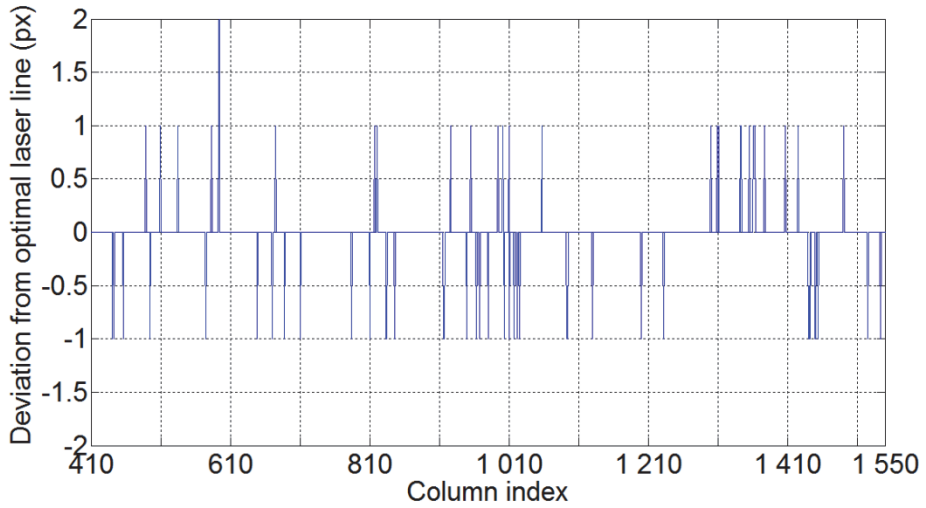
Figure 1.12 Laser line deviation from the optimal laser line [51 (II)].
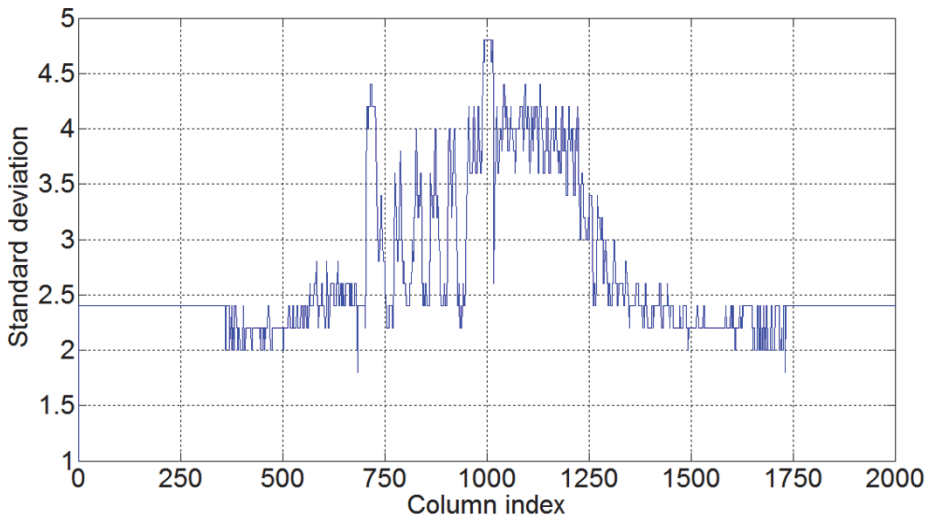
Figure 1.13 Standard deviation distribution over the whole laser line [51 (II)].

Figure 1.13 shows the distribution of standard deviations of the maximums of convolution kernels over the whole laser line image. As seen from the graph the optimal standard deviation is not a constant over the laser line, furthermore, the standard deviation is higher in the middle part of the laser line and lower in the both ends of the laser line. This is within correlation with the Figure 1.10 laser line width. It can be also seen from Figure 1.13 that in places, where the laser line was on dark squares and is thus narrower due to less energy - the optimal standard deviation is smaller than on white squares.

1.4. Laser line detection with sub-pixel resolution

Many laser line detection algorithms [54, 62] for 3D laser line scanners detect the laser line with pixel resolution. This is mainly related to the fact that the camera sensor, capturing the laser line image, has a fixed resolution and the pixel size. In one aspect-the theoretical limit for the spatial resolution is determined by the Nyquist - Shannon sampling theorem. Changes at higher frequencies, than the half of the sample rate cannot be accurately detected. The laser line is typically 1 to 10 pixels wide, in real images of interest. This one pixel accuracy however is not sufficient in many cases, if going into sub-millimeter measurements with line laser scanners. The accuracy of the laser scanner is directly related to the precision of the laser line detection algorithm and in many cases the actual laser line center position is located between two pixels. This is highlighted particularly in a linearly growing or declining surfaces, but also on very rough surfaces, as for example the pavement surface with small rocks.

Several laser line sub-pixel resolution detection methods exist. Some of them are proposing to first detect the laser line edges [59] and then to estimate the real laser line center position by interpolation. Furthermore, sub-pixel edge detection [63] by cubic interpolation has been also proposed to enhance this method. Unfortunately this method can produce inaccurate results, if laser scattering can cause asymmetric laser line profile with non precise edge positions. This can cause the mathematical mean point of the laser line to deviate from the actual laser line center.

Other method [64] proposes to detect the laser line center position with sub-pixel resolution by calculating the weighted average of the "brightest" pixel coordinates in each column. This method can still cause inaccurate results, if the laser line peak has a flat top and uneven number of brightest pixels. The result in this case is also affected by the fact, how many pixels are chosen as "brightest" pixels and how the threshold level has been set.

As known, cross-section of the laser line is similar to the Gaussian distribution from the image pixel intensity perspective. Thus Gaussian profile fitting is also a popular method [60] to detect laser line center position with sub-pixel resolution. With this method, however, a maximum position of the fitted Gaussian profile is detected instead of the actual laser profile peak position. This can lead to inaccurate results when the laser line width is changing. In case, if the laser line has multiple peaks a specially modified Gaussian function has to be used.

1.5. Sub-pixel resolution with parabola method

The inverted second order Gaussian derivative is used for the laser line extraction as a kernel for convolution to the brightness (e.g. gray value) profile. Furthermore, variable width kernels are used and the best kernel with the

maximum convolution value is selected. The convolution is calculated for every image column to detect the laser line position with pixel accuracy. Figure 1.14 shows the laser line gray value profile and its convolution results with optimal inverse Gaussian second order derivation kernel. As seen from Figure 1.14 the actual gray value profile (a) is rather flat in the laser line center position. By looking the convolution curve (b) around the maximum area more closely, it can be seen, that the top of the curve is not symmetrical.
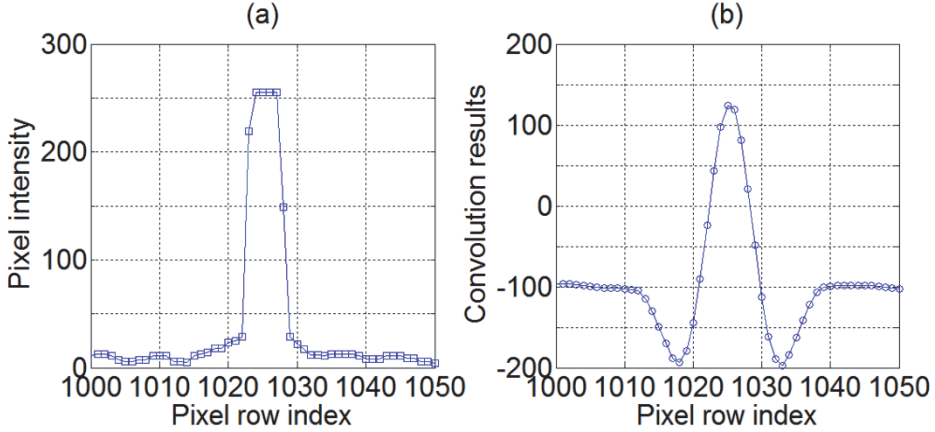
Figure 1.14 Laser line gray value profile and its convolution curve [52 (I)].

To estimate the real center position of the laser line a point before the maximum (x_1, y_1), the maximum point (x_2, y_2) and one point after the maximum (x_3, y_3) can be taken. With those points it is possible to find a parabola equation

$$y = ax^2 + bx + c, \tag{1.5}$$

that passes through all these points. By solving the equation system

$$y_1 = ax_1{}^2 + bx_1 + c, \tag{1.6}$$

$$y_2 = ax_2{}^2 + bx_2 + c, \tag{1.7}$$

$$y_3 = ax_3{}^2 + bx_3 + c, \tag{1.8}$$

the constants *a, b* and *c* can be easily found:

$$a = \frac{((y_2 - y_1)(x_1 - x_3) + (y_3 - y_1)(x_2 - x_1))}{((x_1 - x_3)(x_2{}^2 - x_1{}^2) + (x_2 - x_1)(x_3{}^2 - x_1{}^2))}, \tag{1.9}$$

$$b = \frac{((y_2 - y_1) - a(x_2{}^2 - x_1{}^2))}{(x_2 - x_1)}, \tag{1.10}$$

$$c = y_1 - ax_1{}^2 - bx_1. \tag{1.11}$$

With those constants the parabola vertex x_{max} and y_{max} coordinates can be expressed with the following equations:

$$x_{max} = -\frac{b}{2a}, \tag{1.12}$$

$$y_{max} = ax_{max}{}^2 + bx_{max} + c. \tag{1.13}$$

Figure 1.15 shows an example of the parabola constructed from the points x_1, y_1, x_2, y_2 and x_3, y_3 and its real maximum located at x_{max}, $y_{max.}$ This parabola vertex is found for every convolution maximum of every pixel column. It can be seen that the maximum is between two pixels and by this the laser line has been found by sub-pixel accuracy.
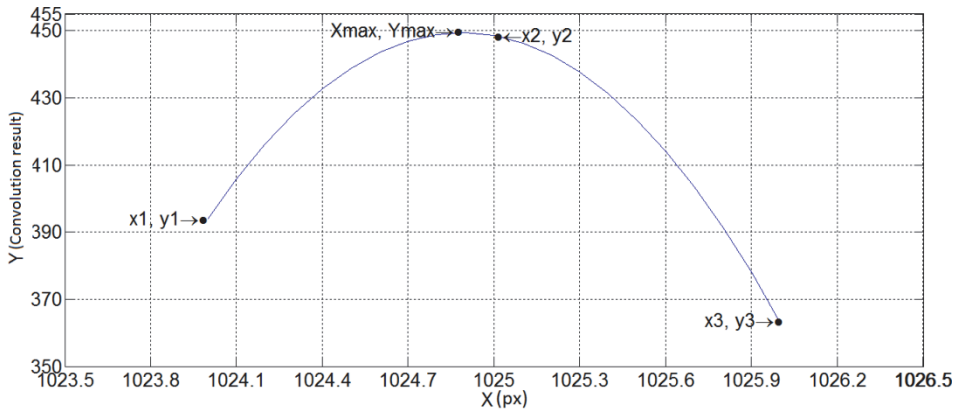
Figure 1.15 Example parabola constructed with 3 points and its vertex [52 (I)].

1.6. Sub-pixel resolution with upsampling method

One efficient approach to increase the laser line resolution and thereby the accuracy is to upsample the images. After upsampling the image, the laser line can be found in sub-pixel accuracy compared with the original image. Many algorithms exist [65] to upsample the image, using different methods. Many image editing software like Irfanview and image processing libraries like OpenCV already include those various upsampling methods, making this quite robust and easy method to implement. Figure 1.16 shows a laser line image before upsampling and Figure 1.17 after the upsampling Lanczos method.

Figure 1.16 Laser line image before upsampling [52 (I)].

Figure 1.17 Laser line image after upsampling 2 times with Lanczos method [52 (I)].

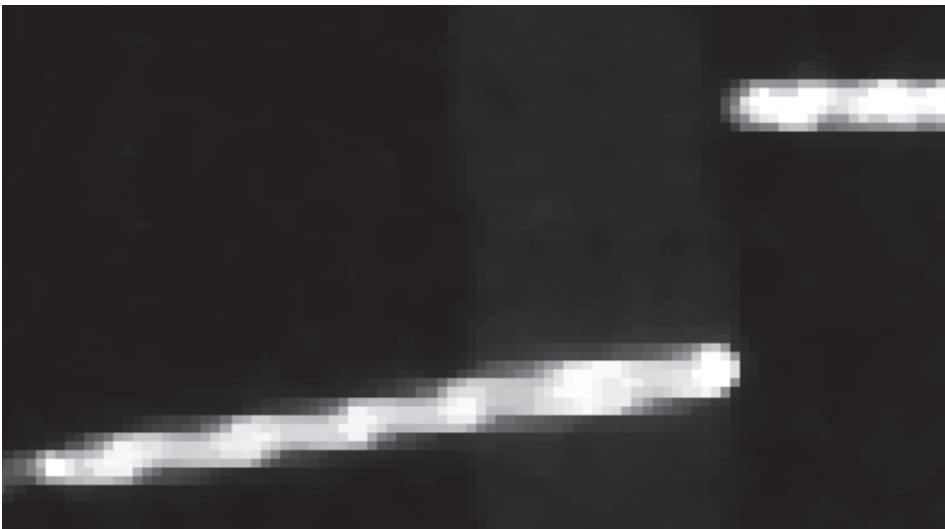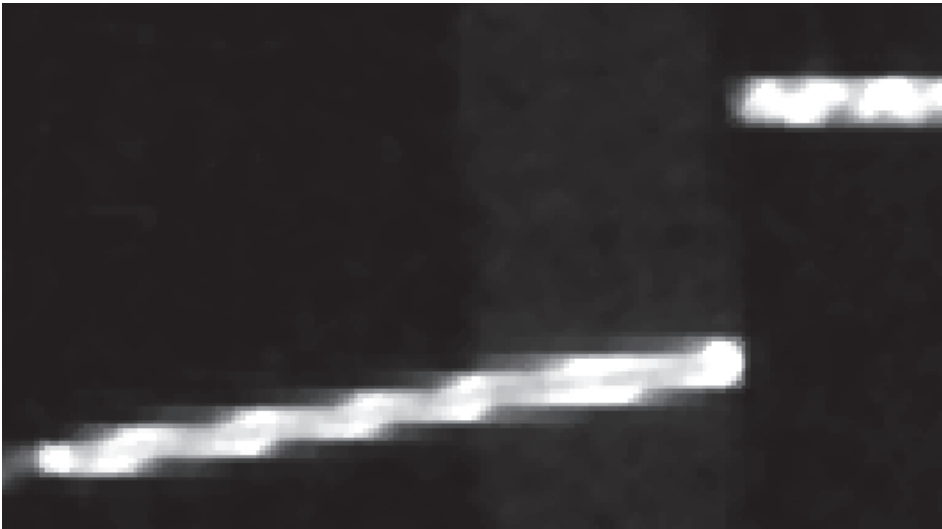## 1.7. Experiments – laser line detection with sub-pixel resolution

Experiments to asses the method were performed with several real life images. Laser lines were extracted with pixel and then with sub-pixel resolution (and accuracy). In particularly, as the problem is especially highlighted in the linearly growing or declining surfaces, but also in strait lines where the actual laser line center position is between two pixels, these parts of the test images were selected to verify the proposed methods. First the convolution maximum correction with parabola method was tested. Figure 1.18 shows a linearly growing laser line and a detected laser line with pixel accuracy and Figure 1.19 with sub-pixel accuracy. It can be seen, that the proposed method has significantly improved the laser line detection accuracy.

Secondly, the upsampling method with the same image was tested. For comparison purpose the same image region of interest was selected to verify the method. Figure 1.20 shows for demonstration the detected laser line with upsampled image. It is clearly visible, that the upsampling method also improves the laser line detection accuracy. Furthermore the results are similar or even better for the first proposed method.

For experimental purposes the convolution maximum correction with parabola method was also tested on the upsampled image. Figure 1.21 shows the result of this combined method. It can be seen, that the accuracy has been significantly improved, compared also with the upsampled image.

The disadvantage of these upsampling methods is, that the upsampling increases the number of pixels by the power of the upsampling level selected.

This in turn decreases the laser line detection speed and increases the required processing power, which is often critical in real-time systems. The

speed decrease can be compensated with adaptively undersampling the image, as proposed by [66 (III)]. Finding the optimal up- and downsampling level is probably the key element of this method.
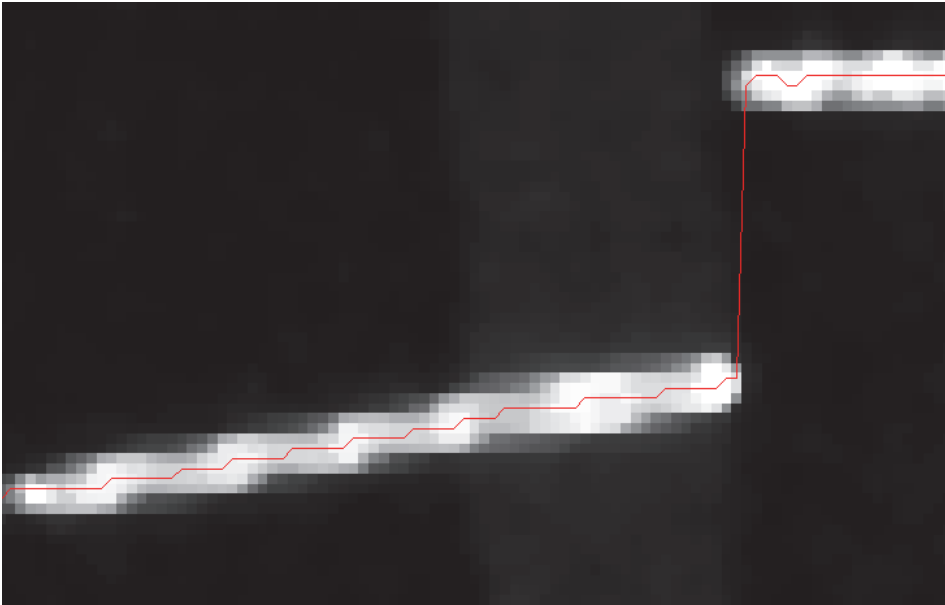

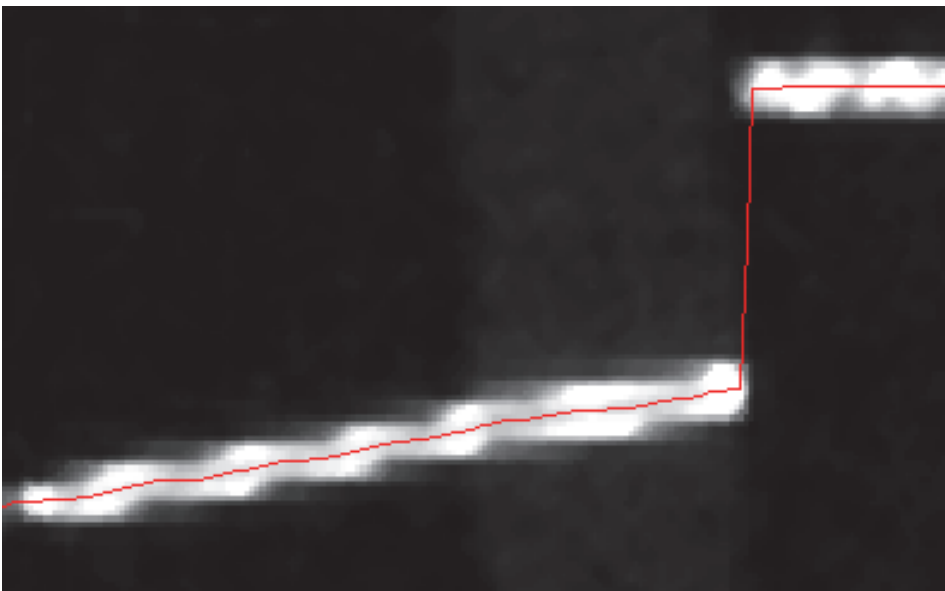*Figure 1.18 Detected laser line with 1 pixel resolution from original image [52 (I)].*

Figure 1.19 Detected laser line with sub-pixel resolution (parabola method) [52 (I)].
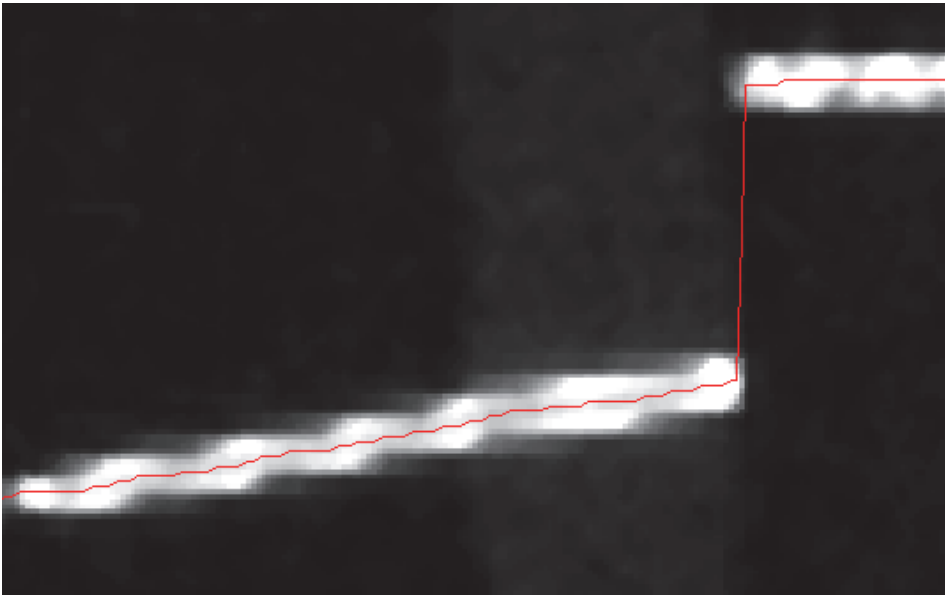
Figure 1.20 Detected laser line from upsampled image with pixel resolution [52 (I)].
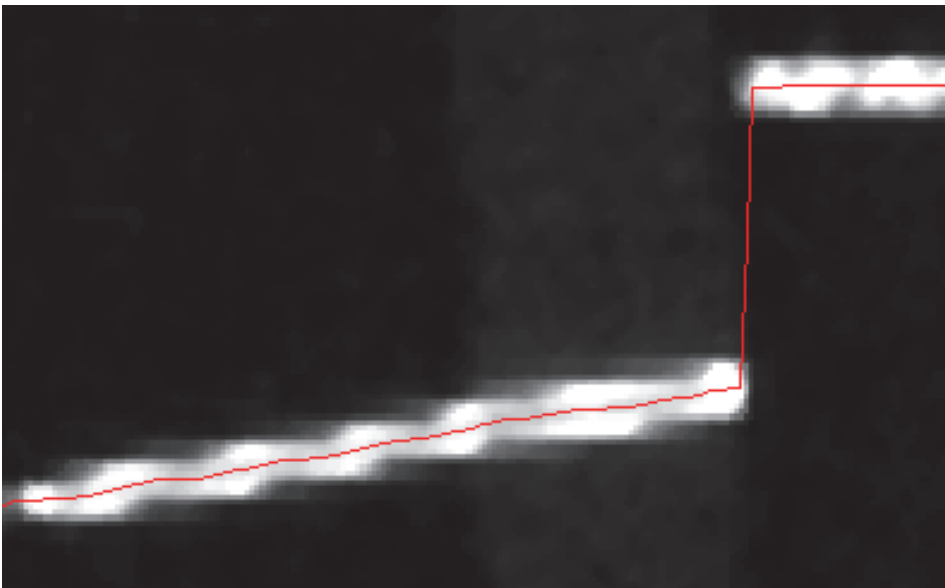
Figure 1.21 Detected laser line from upsampled image with sub-pixel [52 (I)].
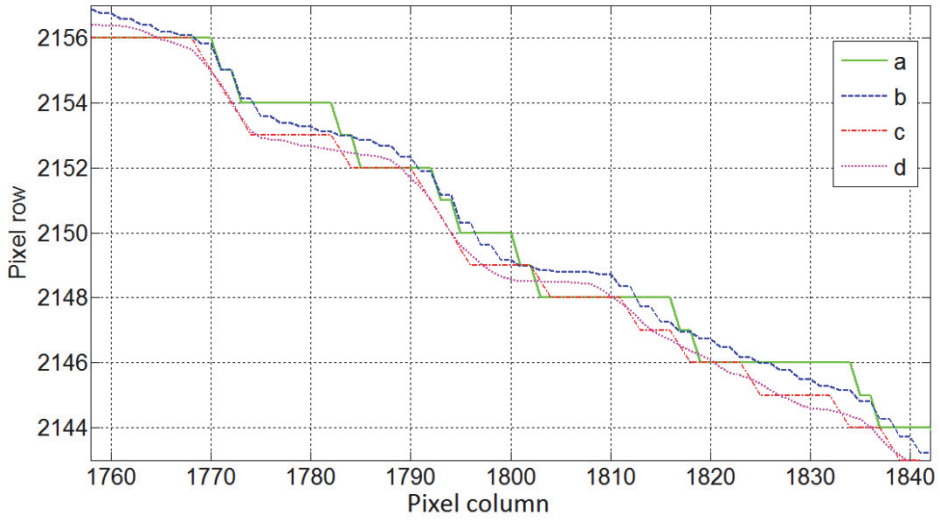
Figure 1.22 Detected laser line on linearly declining surface [52 (I)].
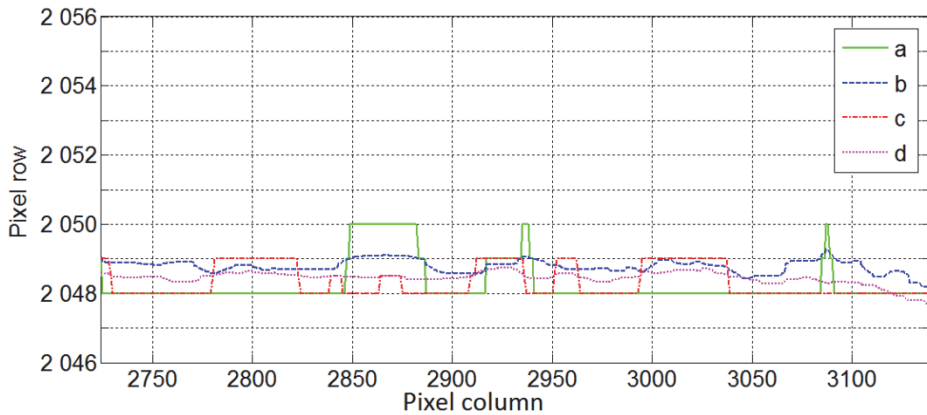
Figure 1.23 Detected laser line on fairly strait floor surface [52 (I)].

Figure 1.22 and Figure 1.23 present 2 laser line sections: laser line on fairly straight (few pixel fluctuations over 2 meters) floor surface and on linearly declining surface, detected with pixel resolution form original image (a); sub-pixel accuracy with convolution maximum correction method from original image (b); pixel resolution (sub-pixel resolution compared to original image) from upsampled image (c) and sub-pixel resolution (sub-sub-pixel compared to original image) with convolution maximum correction and upsampling method combination (d). It can be seen from Figure 1.22 and Figure 1.23, that all of the proposed methods improve the laser line detection accuracy.

In order to assess the real improvement the methods are compared to reference. It is known that in the real world both those laser line sections (linearly declining surface and strait floor surface) are straight (ideal) lines.
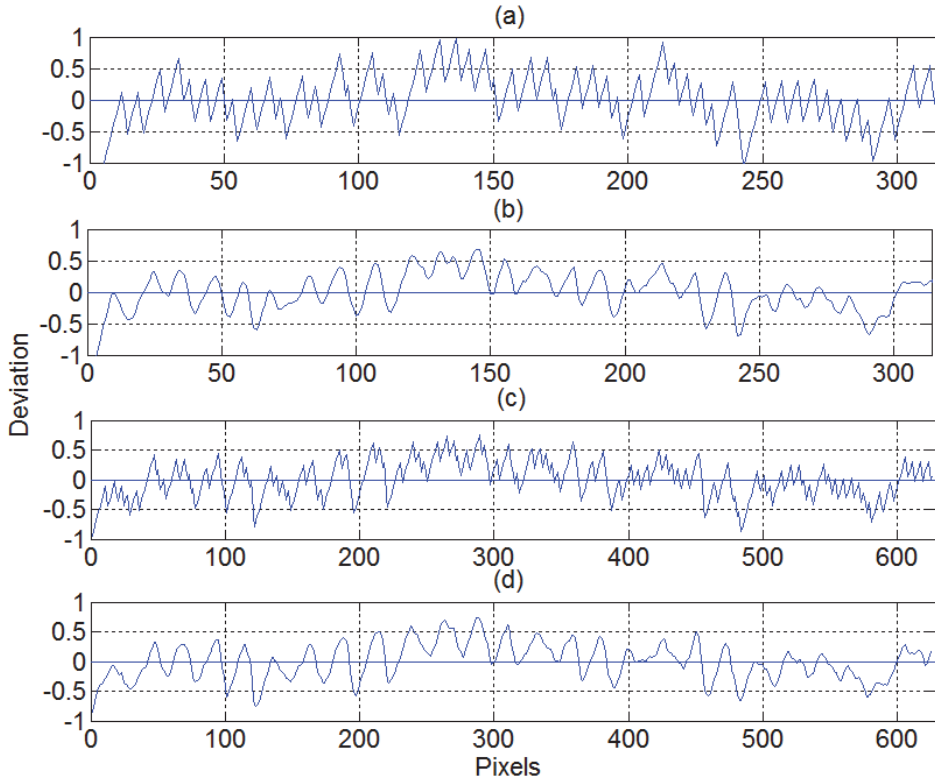
Figure 1.24 Deviation from the ideal line at position 0 [52 (I)].

By fitting the ideal line through the detected laser line points for every method the deviation from the ideal line can be found. This indicates how good the method is compared to the original pixel accuracy method from original image. The less the deviation from the ideal line is, the better is the method. Figure 1.24 shows the deviation in pixels from the reference (ideal) line at position 0 on linearly declining surface. It can be seen that in the case of the pixel accuracy method from the original image Figure 1.24 (a) the deviation varies from 1 to -1, while for all the proposed methods Figure 1.24 (b, c, d) much less - between 0.6 to -0.6.

Root mean square error (RMSE) was calculated for all the methods by ideal lines for both line sections (declining surface and straight floor surface). Average RMSE for the both line section was calculated. It can be seen from the Table 1 that all the methods have improved the laser line detection accuracy. The RMSE has decreased more than 20% for all the proposed methods. The most accurate method is the upsampled one. The RMSE has decreased more than 25% compared to original image for this method.

Table 1.1 RMSE of methods by ideal line fitting [52 (I)].

Method name	RMSE (declining surface)	RMSE (straight floor surface)	RMSE (Average)	Δ%
Pixel accuracy, upsampled image	0.304	0.365	0.335	25.294
Sub -pixel with parabola method, original image	0.319	0.379	0.349	22.019
Sub -pixel with parabola method, upsampled image	0.304	0.402	0.354	21.032
Pixel accuracy, original image	0.414	0.481	0.448	0

1.8. Conclusion of chapter 1

In the first part of this chapter, methods used to detect the laser line with pixel resolution are described. The second order Gaussian derivative convolution based method was chosen as the starting point to investigate the laser line detection from different surfaces and a new method with different standard deviation convolution kernels taking into account the variable laser line width was described. The dependencies, optimal standard deviations and the reduced uncertainties in case of variable laser line width caused by different material reflection constants were shown with experiments.

In the second part of this chapter two main ideas and the combination of those regarding how to improve the laser line detection resolution were presented. All the methods improved the laser line detection accuracy more than 20%. The parabola method is not as accurate as upsampling method, but is more computationally efficient, making it more preferable in the limited hardware embedded systems.

2. INCREASING THE SCANNING SPEED

One important aspect of road profile measurement scanners is the scanning speed. This influences the time spent on scanning of a specific section of the road or the longitudinal profile resolution at the fixed measuring platform speed. In order to scan the road with regular speed with good longitudinal resolution and not disturb the ongoing traffic the laser line detection must be done in real-time (requiring expensive and usually custom developed hardware) or after image acquiring, off-site, needing a lot of disk space to store all the acquired images to be processed. In either case the laser line detection algorithm has to be fast and computationally efficient.

In this chapter and in paper [66 (III)] a novel adaptive undersampling method is described and tested to increase the laser line detection speed from images without increasing the camera frame rate or using custom hardware.

2.1 Various road profile scanning speed aspects

Several structured light based so called "one shot" scanning technologies exist [67-68], which have the advantage of a high scan rate compared to the laser line scanners, but they are significantly more sensitive to illumination changes and are thus more sophisticated to implement for road profile measurement system. Also using of special projector to generate structured light projections makes the cost of scanning system much higher compared to laser scanners.

Most of the laser scanners consist of one camera and one laser. One camera frame will typically give one transverse road profile. In such case the number of laser profiles of the road, gained per second, depends greatly on the camera capturing speed. In order to speed up the scanning the camera frame rate could be increased. For this high speed cameras can be used [69]. However higher frame rate cameras are significantly more expensive and with the increasing of frame rate the data transfer rates and thus image processing performance must be significantly increased. This is especially important in the case, if embedded real-time image processing systems are used with very limited processor resources. Therefore the image acquisition and processing algorithms should be robust, fast and smart.

One fairly reasonable approach to decrease the number of calculations needed for laser line extraction is to use region of interest (ROI). By only detecting laser line on some specific region the area to be processed could be rather small decreasing significantly the processing capacity. ROI on images can be set by either in the horizontal, vertical or in both directions at the same time. However in case of setting of the ROI one must take into account the measurement profile maximum deviations from the normal of the measurement

profile. It may happen that some of the laser line parts may fall out of ROI making the measurement results unreliable.

Another efficient approach to increase laser scanner speed is to use multiline lasers or multiple lasers at the same time. This allows to gain more laser profiles from one image thus increasing the laser scanner speed without increasing the camera frame rate and therefor the amount of data to be processed. This method has been successfully used in welding industries [54] to check the quality of welding joints and on road profile systems for crack detection [70]. A critical part of this method is to be able to distinguish which part of the laser lines belongs to which laser line profile. Some of the methods propose to segment the laser lines and match the laser line segments from multiple images [71]. Second option is to choose sufficient distances between two laser profiles so they would not ovelap each other in any case. One drawback of using of the multiline lasers is that the special optic lenses, splitting the laser beam to multiple laser lines, are rarely with perfect lens surface smoothness and perpendicular to the laser beam. Laser lines located farther from the lens optical center are more distorted than the laser lines located closer to optical center [71]. This makes the 3D reconstruction more complex. The power of the multiline laser must also be relatively high because the laser beam energy is divided between the multiple lines. So such lasers are more dangerous to use and also quite expensive. Therefore it is more reasonable to use multiple lasers, each with smaller output power.

Using of solely multiple lasers to increase the profile scanning speed is unfortunately mostly not sufficient on embedded real-time image processing platforms, which have limited processing power.

2.2 Adaptive undersampling method

A large part of image processing algorithms process the images independently from the content of the images. This burdens the processor by processing actually image areas that are not relevant or not so highly interesting. Instead only areas of high interest should be processed. Resulted from the fact that the laser line(s) to be detected on an image, captured by the camera, have usually marginal size - in sense of the line width (typically some to ten pixels), compared, with the camera image height (2048 pixels, for example) - a lot of processor resources are wasted for processing of the non-relevant parts of an image. Consequently the idea to process images partially (only high interest areas) is reasonable.

Adaptive undersampling is an efficient method to speed up laser profile scanning and to reduce the processing of non relevant image areas. By combining adaptive undersampling with multiline or multiple laser lines on the images of the laser profile - the scanning speed can be increased significantly.

To do this an image taken by the camera of the laser scanner shown in Figure 2.1 with multiple (2 in the example) laser lines on the road surface is first preprocessed. As the lasers used are mostly red colored due to more favorable production prices a red channel image or weighted RGB image (image with weighted color channel scales added or subtracted together) is constructed. Red channel image is shown in Figure 2.2. Additionally methods like constant stretch [72] or using of other color spaces [73] can be considered to enhance the laser line signal on camera image.

Figure 2.1 Image captured by the scanner camera with multiple lasers [66 (III)].

Figure 2.2 Red channel image from the laser scanner camera [66 (III)].

After the preprossessing the images are horizontally undersampled. This means that only some of the columns are chosen for further processing. The amount of columns that are chosen for further processing can be determined by
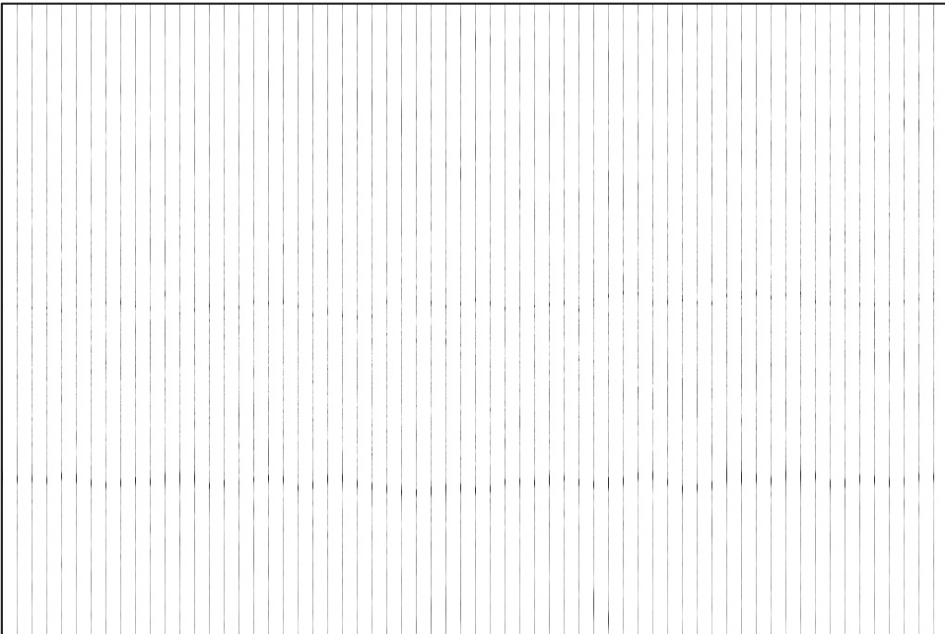

Figure 2.3 Horizontally undersampled image [66 (III)].

analyzing the laser line detection error compared to images without undersampling. Figure 2.3 represents the horizontally undersampled image. The image was horizontally undersampled by factor of 15, in this example.

From horizontally undersampled image an initial laser line locations are detected. Those locations indicate the areas around which the laser lines are more likely to be detected. Since the image contains multiple of laser lines all initial laser line locations are detected and stored. For laser line detection the proposed sub-pixel resolution parabola method can be used. Figure 2.4 represents an initially detected laser line locations from horizontally undersampled image.
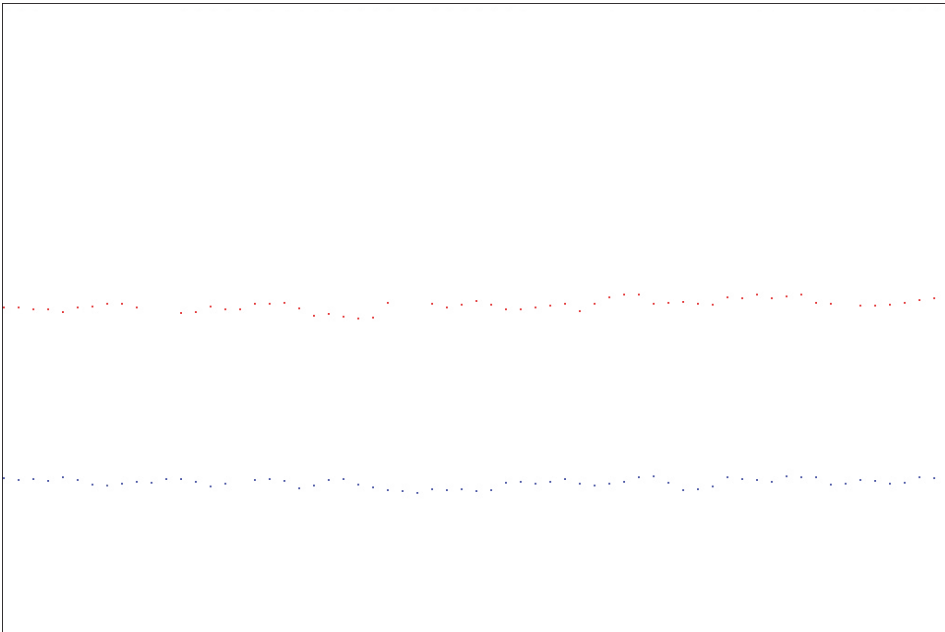
Figure 2.4 Initial laser locations from horizontally undersampled image [66 (III)].

After the initial laser line detection an adaptively undersampled image is created from the red channel image by using the points of the initial laser line as references. A predefined number of pixels are taken from the red channel image, around the initial laser line position for every column. The amount of pixels that are taken can be determined by analyzing the laser line detection error compared to images without undersampling. For columns which does not have initial laser line locations the last known initial laser line locations are used. The resulting image is an adaptively undersampled image, where only all relevant regions of the image would be highlighted and all the unnecessary and non-relevant parts of an image are excluded. In such way adaptively undersampled image is shown on Figure 2.5. From the adaptively undersampled image final laser line can be extracted. For this the sub-pixel resolution parabola method can be used for the next image processing step on the areas which are

part of the undersampled image. Figure 2.6 shows the extracted laser lines from the adaptively undersampled image.

Figure 2.5 Adaptively undersampled image [66 (III)].

Figure 2.6 Final laser lines detected from the undersampled image [66 (III)].

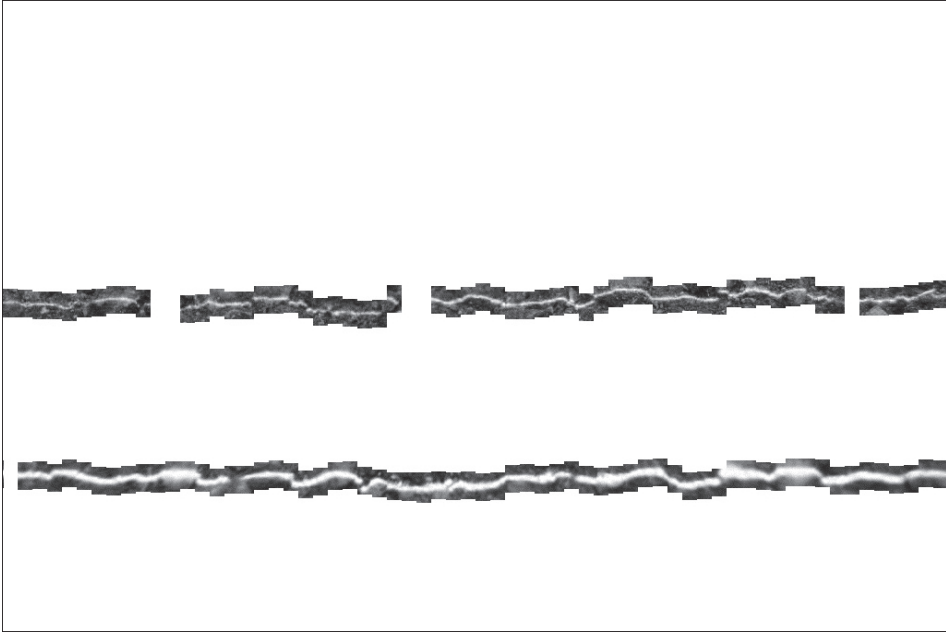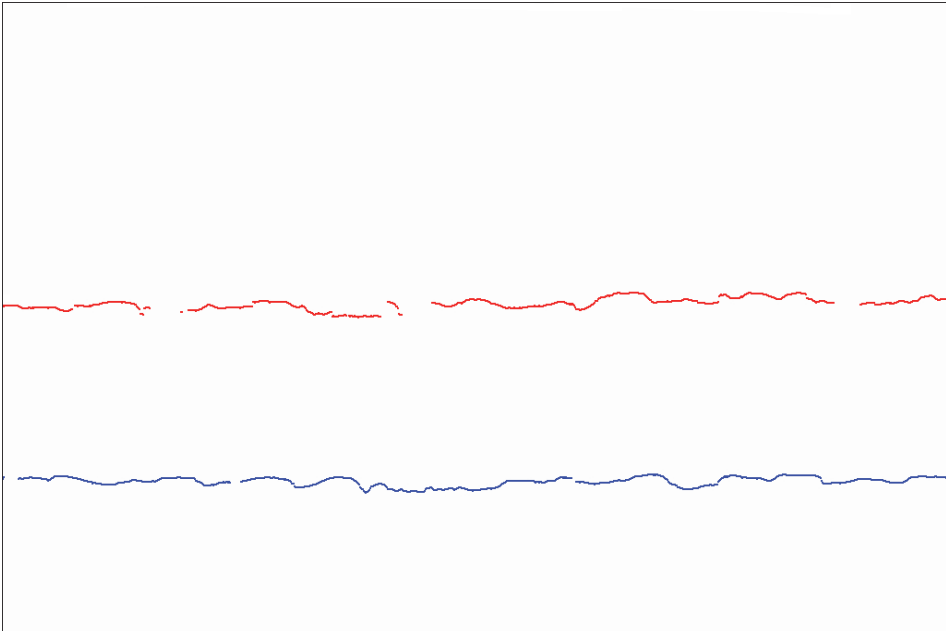A key aspect of this method is to find the optimal level of undersampling so, that the substantial part of the laser line is not lost during the undersampling

process. This can be analyzed by finding the laser line detection error compared to images without undersampling. The optimal threshold can be determined according to the required detection speed and available hardware performance.

As seen from the Figure 2.6, some of the line parts have not been fully detected thus the undersampling level might not be optimal in this case. Alternatively, a variety of sample recovery methods [74] and spline [75] (or other) fitting methods exist to interpolate those missing samples.

2.3 Experiments – increasing laser line detection speed

As discussed before, one of the key aspects of road profile measurement scanners is the scanning speed. A set of experiments were made in order to assess the adaptive undersampling method and verify that the laser line detection speed is increased compared to the conventional method (not using undersampled images).

C++ code was developed with using of the OpenCV libraries in order to be able to test the algorithm on different computing platforms. Four different computing platforms and two different resolutions of images (640x480 and 1600x1200) were used in the experiments. Three of the computing platforms were desktop computers with different processor architectures running Windows 7 operating systems. The forth computing platform was the DM3730 processor based embedded (Beagleboard-XM) platform running Angstrom Linux. The embedded platform was chosen since the computation time and the number of calculations for the image processing is especially critical on the embedded platforms. The DM3730 on Beagleboard-XM contain 2 processors; ARM and DSP, but only the ARM side of the DM3730 processor was used in current experiments so that the results would be comparable with other platforms.

For every platform 100 laser line images, each containing 2 laser lines, per each resolution was used for laser line detection using adaptive undersampling method. Also the same amounts of images were used with the conventional method (not using undersampled images). For every image the image processing time was measured which was spent to detect the laser lines. Average processing time and thus frames processed per second (FPS) was calculated for each platform, for every image resolution and method. Table 2.1 shows the results of the laser line detection speeds.

It can be seen from the Table 2.1 that the increase of the laser line detection speed on the Beagleboard-XM was significant. The speed increase is close to 4 times on Beagleboard-XM platform. On other desktop platforms the speed increase is even higher, approaching close to 8.5 times. It can also be noted that, for every computing platform the speed increase was even higher with larger images (with more pixels), compared to smaller images. This is caused by the fact that the laser line on higher resolution images is proportionally smaller than

Table 2.1 Benchmarking of developed algorithm on different platforms [66 (III)].

Platform details	Benchmarking of algorithms with different resolutions			
	Conventional method 640x480 px. *Average fps.*	*Adaptively undersampled method 640x480 px.* *Average fps.*	*Conventional method 1600x1200 px.* *Aaverage fps.*	*Adaptively undersampled method 1600x1200 px.* *Average fps.*
Beagleboard-XM, DM3730 (ARM ® Cortex TM -A8 @1GHz + C64xx DSP @800MHz), 512MB of RAM	8 fps	27,68 fps	1,17 fps	4,64 fps
Intel(R) Core(TM)2 Duo CPU P7350 @2,00GHz, 4GB(2,73 GB usable) of RAM, 32 bit system	16,85 fps	114,00 fps	2,51 fps	21,16 fps
Intel(R) Core(TM) i5-3320M CPU @2,60GHz, 8GB(7,88 GB usable) of RAM, 64 bit system	44, 00 fps	286,38 fps	6,36 fps	52,35 fps
AMD Phenom(TM) II X3 B75 CPU @3,00GHz, 8GB(3,00 GB usable) of RAM, 32 bit system	23,03 fps	160,00 fps	2,66 fps	9,96 fps

the irrelevant parts of the image, which are not used by the adaptive undersampling method.

For Intel processors the speed increase was higher, probably resulted due to the fact that OpenCV has been developed by Intel's engineers and is probably so more optimized.

The average speed increase of the developed adaptive undersampling method, compared to conventional laser line detection method (non-under sampled images) is about 6 times. Considering the fact that 2 laser lines were detected instead of one the actual speed increase is 12 times compared to a single laser line scanner. This shows that the laser scanner speed can be increased significantly without increasing the laser scanner camera capturing frame rate.

The scanning speed increase can be further optimized by selecting more optimal under sampling level for the adaptive undersampling method and by utilizing all of the processor cores in the embedded multicore processors.

2.4 Conclusion of chapter 2

In this chapter, possible methods to speed up the road profile scanning were described. Various aspects of those methods led to a conclusion that in the case of road profile scanners an adaptive undersampling method combined with multiple lasers is the most suitable method to increase road profile scanning speed without increasing the camera frame rate or using custom, expensive hardware. Experiments were made on different image processing hardware platforms to assess the adaptive undersampling method and verify that the laser line detection speed is increased compared to the conventional method (not using undersampled images). The experiment showed that the speed increase with current setup was around 6 times with one laser line on the image and 12 times with two laser lines on one image. It was also noticed that the speed increase was even higher with larger images, compared to smaller images. The reason for this is that the laser line on higher resolution image is proportionally smaller than the other parts of the image which are not used by the adaptive undersampling method. The scanning speed can be further increased by finding the optimal level of undersampling in both horizontal and vertical directions, combining this method with ROI and/or using more lasers in parallel.

3 MODEL AND CALIBRATION OF THE ROAD PROFILE SCANNER

Calibration is an important step in obtaining an accurate measuring result with 3D structured light laser scanner. During the calibration a relation between the pixels on the 3D laser scanner camera image and the real world units is made. All distortions caused by camera and laser lenses and their positioning must be corrected.

In this chapter and in the paper [76 (V)] an overview of the relationships between the camera image, laser and real world units is given. Methods to correct the distortions and a proposed new method to find the laser line light plane parameters are described. Complete calibration procedure is given and experiments to assess the accuracy of the developed laser scanner and how much calibration is dependent on the laser line detection method is shown. Real comparative measurements were made also together with Estonian road maintenance authorities.

3.1 Pinhole camera model and laser light plane

The simplest approximation of a camera is the pinhole model, where the lens is substituted by an infinitely small hole located in the focal plane through which all the light passes and the image of the depicted object is projected onto the image sensor [77].

In order to convert the laser line in pixels captured by the camera sensor to the real world measurements in mm-s one must understand the relationship between the camera sensor and the laser light plane.

By knowing of the camera sensor width W and height H the full resolution image optical center in pixels can be calculated:

$$c_x = \frac{W}{2},\tag{3.1}$$

$$c_y = \frac{H}{2}.\tag{3.2}$$

Laser line coordinates on captured image in pixels are defined as u and v. Camera focal length f_x, f_y in pixels for a given focus depends on the lens, used by the camera, and can be estimated by using objects in front of the camera with known dimensions at different distances and poses.

Knowing that light emitted by the line laser forms a proper virtual laser light plane:

$$AX + BY + CZ + D = 0 \qquad (3.3)$$

and the laser line captured by the camera is located on this laser light plane we can calculate the laser line position in the camera coordinate system:

$$x' = \frac{u - c_x}{f_x}, \qquad (3.4)$$

$$y' = \frac{v - c_y}{f_y}. \qquad (3.5)$$

From this the real world coordinates of the laser line can be calculated:

$$Z = \frac{-D}{Ax' + By' + C}, \qquad (3.6)$$

$$X = x'Z, \qquad (3.7)$$

$$Y = y'Z. \qquad (3.8)$$

Pinhole camera, laser plane and its relationship is illustrated on Figure 3.1.

Image optical center in pixels cx, cy

Image point u, v

Camera sensor

Focal length fx, fy

Laser

Laser light plane:
AX+BY+CZ = -D

Camera field of view

Camera image

Laser line on image

Real world coordinates:
x' = (u-cx)/fx;
y' = (v-cy)/fy;
Z = -D/(Ax'+By'+C);
X = x'Z;
Y = y'Z;
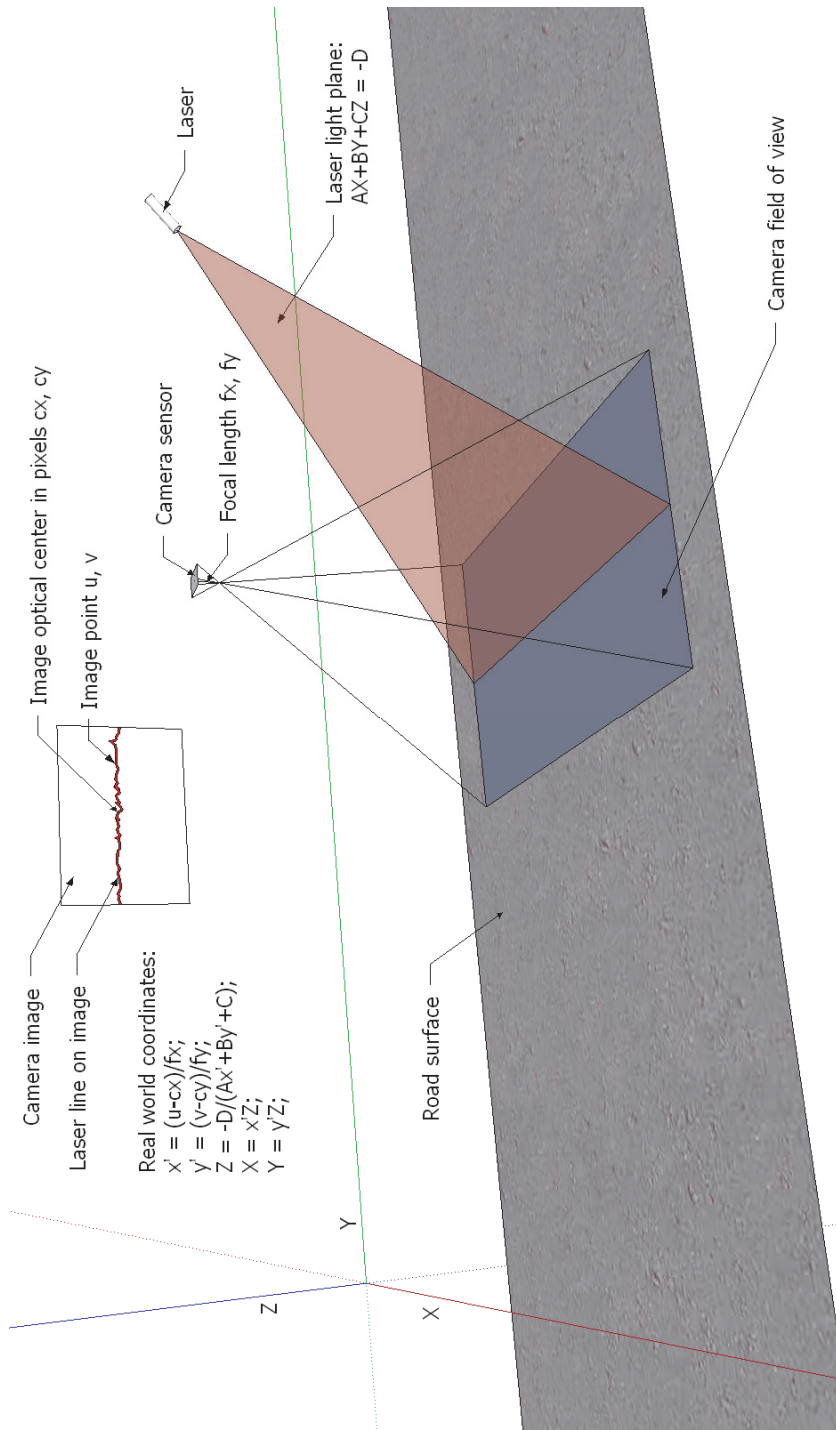
Road surface

Y

Z

X

Figure 3.1 Pinhole camera, laser plane and their relationship model.

3.2 Lens distortions

The ideal pinhole cameras do not have any image distortions, because the lens, being the main source of the distortions, is substituted with an infinitely small hole. Unfortunately this is not the case with real world cameras. Two main types of distortions exist: radial distortions and tangential distortions.

Radial distortions are caused by the lens symmetry. Radial distortions can usually be classified as either barrel distortions (image magnification decreases with distance from the optical axis), pincushion distortions (image magnification increases with distance from the optical axis) or the combination of those distortions called mustache distortions [77-78]. Different types of radial distortions are illustrated on Figure 3.2.
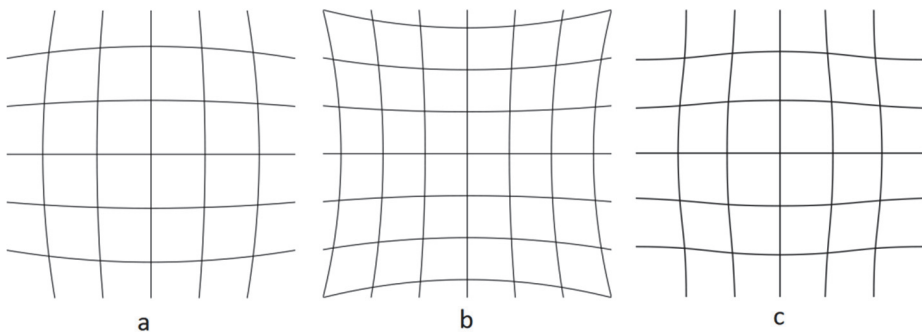
Figure 3.2 Barrel, (a), pincushion (b) and mustache distortions (c).

Tangential distortions occurs because the lens is not perfectly parallel to the camera sensor plane. Example of the tangential distortion is shown on Figure 3.3.
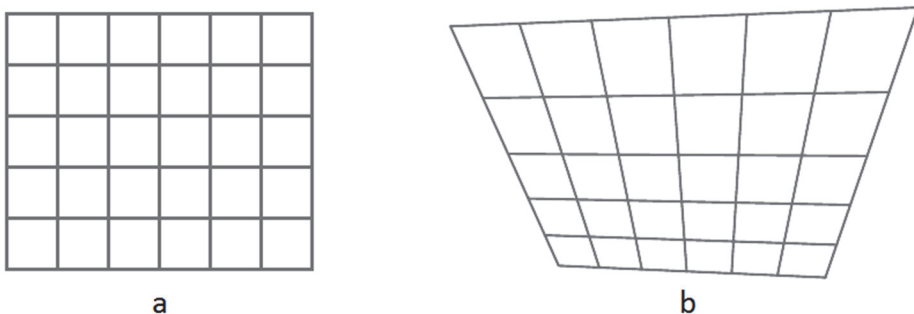

Figure 3.3 Real pattern (a), pattern observed by the camera (b).

Both of those distortions however can be taken into account and the camera image can be corrected. Radial distortions can be corrected with the following equations:

$$u_{corrected} = u(1 + k_1 r^2 + k_2 r^4 + k_3 r^6 + \ldots), \qquad (3.9)$$

$$v_{corrected} = v(1 + k_1 r^2 + k_2 r^4 + k_3 r^6 + \ldots), \qquad (3.10)$$

where $u_{corrected}$ and $v_{corrected}$ are image pixel coordinates (u, v) after corrections, k_n is n^{th} radial distortion coefficient and

$$r = \sqrt{u^2 + v^2}. \qquad (3.11)$$

Tangential distortions can be corrected with the equations:

$$u_{corrected} = u + [2p_1 uv + p_2(r^2 + 2u^2) + \cdots], \qquad (3.12)$$

$$v_{corrected} = v + [p_1(r^2 + 2v^2) + 2p_2 uv + \cdots], \qquad (3.13)$$

where p_n is n^{th} tangential distortion coefficient.

The same equations can be used also to correct only the laser line radial and tangential distortions.

3.3 Correcting the lens distortion

To calculate all those distortion coefficients Zhang [79] has proposed a method that requires only a two-dimensional pattern. This can be a printed chessboard pattern or a series of circles aligned as a grid with equal distances from each other on a sheet of paper or flat surface. Example of the pattern is illustrated on Figure 3.4.
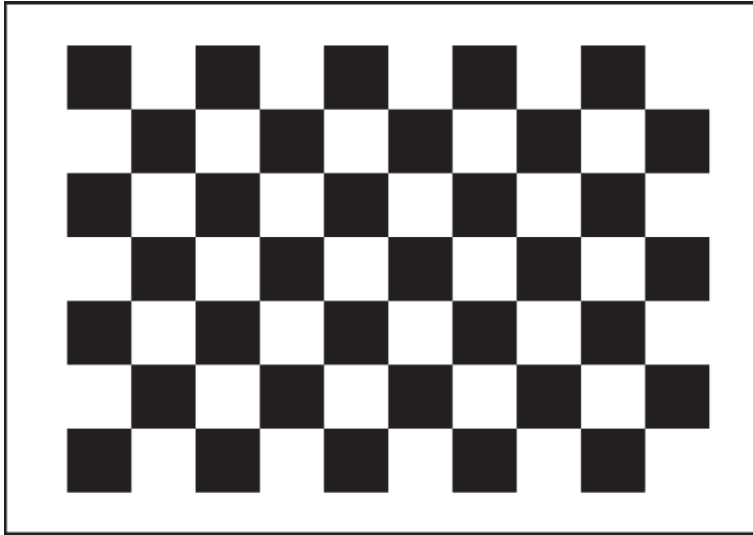
Figure 3.4 Example pattern used for lens distortion correction.

The corners of the pattern and the distance between those corners are used as reference points for the method. Several positions (angles) of the patterns must be presented to the camera with several distances from the camera. The more poses will result more data points for the algorithm to extract, which in turn yields a better optimization. The distribution of the pattern poses in front of the camera must be high to ensure that the obtained points are well distributed in 3D space. Using the known relative distance between those points the intrinsic parameters (focal length and the lens distortion) can be calculated and the lens distortion parameters are estimated using a linear least-squares approach. Next the extrinsic parameters (position and the orientation of the camera in 3D world) can be calculated for every pattern as the rotation R and translation T vectors. These rotation and translation vectors show how the pattern is positioned with respect to the camera or vice versa.

To correct the captured image the image pixels need to be remapped. For each pixel $(u,\ v)$ in the destination (corrected and rectified) image new coordinates ($u_{corrected}$, $v_{corrected}$) have to be calculated.

Example of an image before and after the lens distortion correction is presented on Figure 3.5.
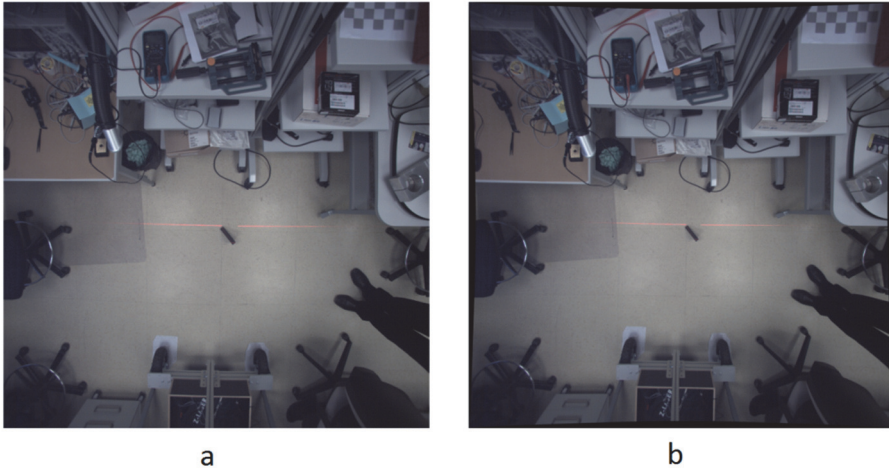
Figure 3.5 Example of an image before and after the correction.

3.4 Laser line straightness error

In addition to the distortions of the camera optics one must take into account the fact that projected laser lines are rarely straight. This is important when going into sub-pixel or sub-millimeter measurements. Mainly two types of straightness errors occur: curved profile and S-shaped profile [80]. Figure 3.6 illustrates those laser straightness errors.

Figure 3.6 Laser line straightness error, curved (a) and S-shaped (b) [80].

This means that the projected laser line deviates from the ideal line. The S-shaped error is caused by the imperfections of the lens (i.e. uneven lens surface). The curved profile is caused by the misalignment of the lens that is forming the laser line from the laser beam.

The error of the straightness can be calculated by determining the actual position of the laser line, the length of the line L, the best fit line and the maximum deviations Δ_1 and Δ_2 from the best fit line.
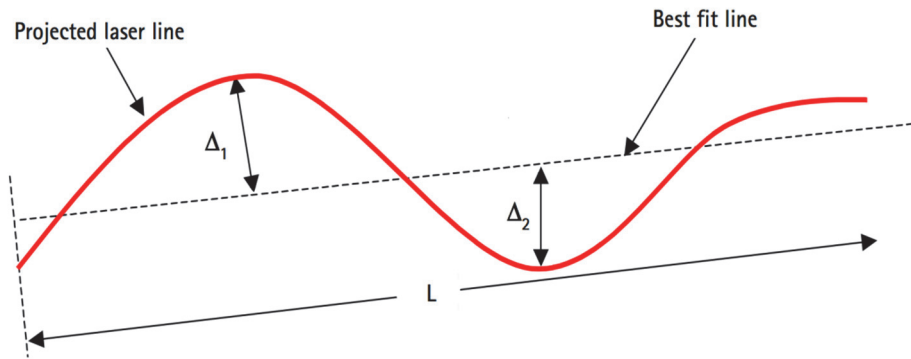
Figure 3.7 Parameters to determine the laser line straightness error [80].

The straightness error can then be calculated as:

$$\text{Straightness error } (\%) = \frac{\Delta_1 + \Delta_2}{L} * 100. \qquad (3.14)$$

Depending on the manufacturer the line straightness, line thickness and homogeneity distributions are already measured during the production process with high accuracy. The measurement results are stored in the database where the results can be easily obtained. Extract from the manufacturer report of the Z-Laser Z40M18S-F-660-lp90 (660 nm, 90° angle) laser straightness is depicted on Figure 3.8.
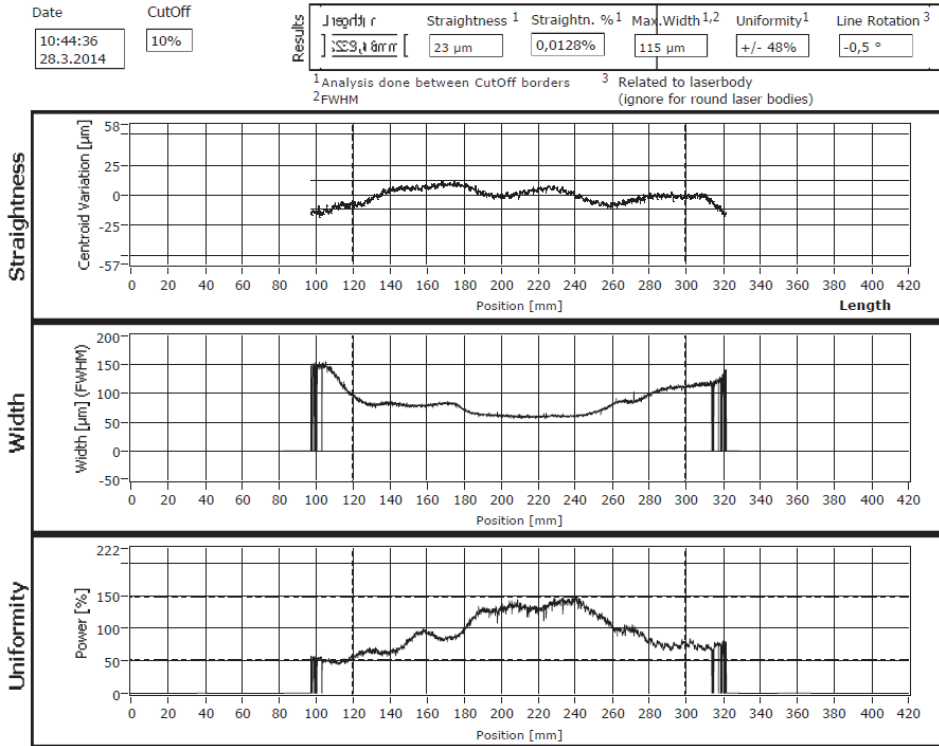
Figure 3.8 Extract from the Z-Laser Z40M18S-F-660-lp90 report.

As it can be seen from the report the measured straightness for this laser is ±23 μm. The measurements were made at the working distance of 200 mm. Increasing the working distance increases the measurement error linearly. At the working distance of 2000 mm the laser straightness deviates already ±0.23 mm. This is a quite considerable error while making sub-millimeter measurements from this distance and has to be taken into account.

3.5 Correction of the laser line straightness

As the straightness measurements are already made by the manufacturer, the measurement errors can be read from the file containing straightness error for every position of the line. Depending on the working distance the error must be corrected with the following equation:

$$\text{Corrected error} = \frac{\text{Straigtness error}}{\text{Working distance}} * Real\ working\ distance. \qquad (3.15)$$

3.6 Known method of finding the laser light plane parameters

As described earlier the laser line seen by the camera is located on the virtual laser light plane. In order to convert the laser line pixels on image to real world measurements this laser light plane parameters A, B, C and D must be found.

Some of the papers [71, 81] suggest finding of the laser line on known distances from the camera from which the mathematical laser light plane can be constructed.
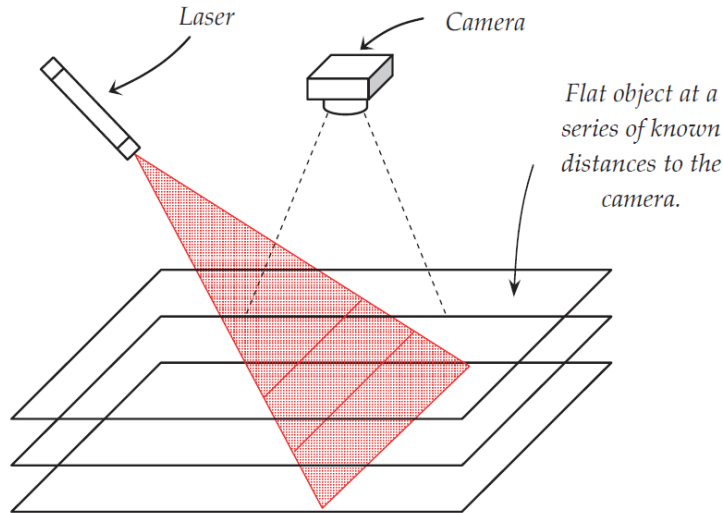
Figure 3.9 Obtaining laser lines at a known distances [71].

This method however may lead to inaccurate results due to the fact that the actual distance of the camera from the so called "know distance" is not accurate. Image sensors may not be parallel to the camera housing or the distance of the camera sensor from the housing is not usually specified by the camera producer thus needing the camera housing to be opened and the warranty broken. Thus the accuracy of the method depends greatly of the actual "known distance" determination accuracy.

3.7 Laser light plane linear interpolation method

To find the laser light plane parameters without knowing the laser and camera exact positions relative to each other and the distance from the ground a new method was developed. For this the laser line is projected on chessboard pattern with different poses of the chessboard pattern relative to the camera.

Figure 3.10 Laser line on chessboard patern with different poses [76 (V)].

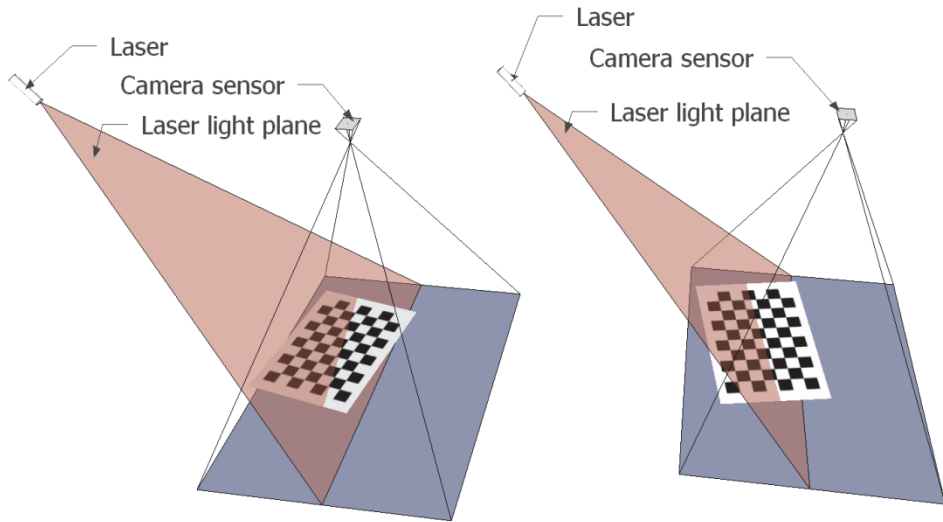Figure 3.10 illustrates the laser light plane and the laser intersection with the chessboard. While at least 2 poses of the chessboard are required to construct a laser plane mathematical description, actually the more poses are used the more accurate description of the laser light plane can be constructed. An important aspect of this method, when projecting the laser line on a flat chessboard pattern is that the laser should cross the chessboard pattern from one side of the chessboard to the opposite side of the chessboard pattern. In this case the laser lines lays on the chessboard pattern plane.

By knowing the camera intrinsic parameters (focal length, image optical center, distortion coefficients) and the chessboard size, the chessboard rotation and translation vectors (extrinsic parameters) can be calculated for every chessboard image by using the object pose estimation. Extrinsic parameters are translating coordinates of a point (X, Y, Z) to a coordinate system, fixed with respect to the camera. The rotation and translation transformation is the following (when $z' \neq 0$):

$$
\begin{bmatrix} x \\ y \\ z \end{bmatrix} = R \begin{bmatrix} X \\ Y \\ Z \end{bmatrix} + T. \tag{3.16}
$$

By this equation every point on the chessboard (and laser line, across the same chessboard) can be converted to the real world 3D points.

For this first the chessboard corners in pixels (C1(u,v) and C2(u,v)) are found. Then the laser line position is determined in pixels. By knowing the positions of the chessboard corners (*C1* and *C2*) and a laser line point between

those points (*L1(u,v)*) the ratio between chessboard corners and laser line point can be found in pixel units:

$$Ratio = \frac{C2(u,v) - C1(u,v)}{L1(u,v) - C1(u,v)}. \qquad (3.17)$$

Using this ratio the laser line point (*L1(X,Y,Z)*) in real world coordinates can be found:

$$L1(X,Y,Z) = C1(X,Y,Z) + Ratio\big(C2(X,Y,Z) - C1(X,Y,Z)\big). \qquad (3.18)$$

Following figure illustrates the chessboard pattern and the laser line on it for interpolating the laser line points from 2D coordinates to real world coordinate system.
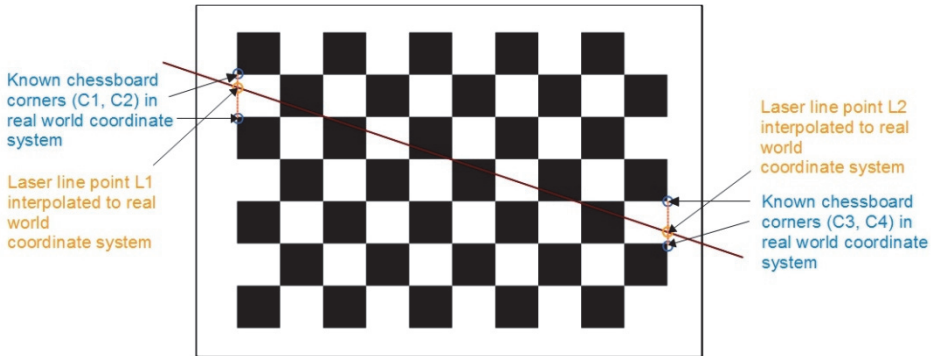
Figure 3.11 Interpolation of laser 2D points to real world coordinate system.

As it is known, there are at least three points needed to construct the mathematical plane equation. Thus at least 3 laser line points must be found in the real world coordinate system out of which at least one laser line point must lie on another chessboard. Therefore at least 2 poses of the chessboard is required to construct a laser plane mathematical description. The more poses are used the more accurate description of the laser light plane can be constructed.

To find the laser light plane parameters A, B, C and D the least square fitting (LSF) method is used. LSF uses the concept of minimizing the square sum of normal distances as (3.19) and (3.20) from all 3D points to the optimal plane to determine the parameters of best-fitted plane [82].

$$P_i = F_i(a, b, c, d) = \frac{|aX_i + bY_i + cZ_i + d|}{\sqrt{a^2 + b^2 + c^2}}, \qquad (3.19)$$

where the P_i denotes the normal distance from *i-th* point to the plane;

$$\sum_{i=1}^{m} P_i^2 => min, \qquad (3.20)$$

where *m* is the number of points.

3.8 Calibration process

The calibration process consists of three main steps: lens distortions calibration, laser line straightness calibration and finding of the laser light plane parameters.

The first step is the lens distortion correction step. This is needed as the very first step due to the fact that the image used as an input for other steps should be corrected image. Distorted image affects the results of other calibration steps and the final result would be incorrect. Several chessboard images are used to estimate the camera intrinsic parameters and extrinsic parameters for each of the chessboard pattern views. The estimation is based on the Zhang [79] method. The goodness of the estimation is assessed by the average re-projection error. This number gives a good estimation of precision of the found parameters. This should be as close to zero as possible. After successful intrinsic and extrinsic parameter detection the results are stored to a file. Intrinsic parameters are used later to create an undistortion map which is used to correct the image from the lens distortions (so-called additive correction).

After the lens distortion correction the laser line straightness calibration can be started. Parameters from the laser manufacturer report are read in from the file. Depending of the distance of the laser line from the camera the laser line distortion parameters are corrected. Then each laser line point is corrected by adding or subtracting the correction of the laser line distortion.

When laser line straightness parameters have been found the detection of the laser light plane constants can begin. For this several chessboard images, where laser line crosses the chessboard pattern, are used. All the images are undistorted from lens distortions with the parameters saved from the previous calibration steps. Laser line straightness on the image is then corrected. By finding the extrinsic parameters of every chessboard pattern and laser line points on the chessboard image in real world coordinates the laser light plane parameters can be found by using the least square fitting method to determine the parameters of best-fitted plane. When laser light plane parameters are found - the calibration process is finished.

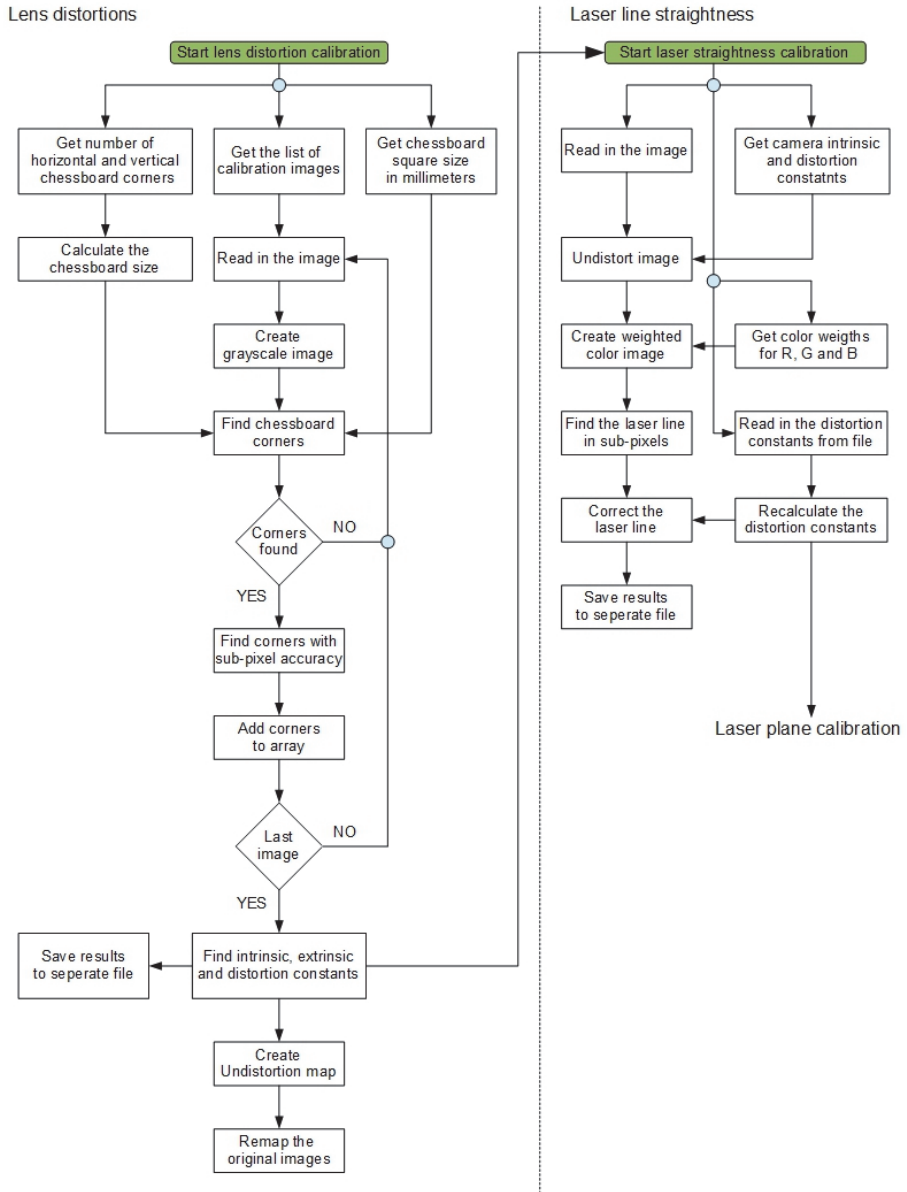The detailed calibration steps are described on the following flowchart.

Figure 3.12 Calibration process flowchart (part 1).

Laser plane parameters

Start laser plane calibration

Get laser line straightness constatnts

Get camera intrinsic and distortion constatnts

Get the list of images

Get number of horizontal and vertical chessboard corners

Get color weigths for R, G and B

Read in the image

Calculate the chessboard size

Undistort image

Create weighted color image

Create grayscale image

Find the laser line in sub-pixels

Find chessboard corners

Correct the laser line

NO

Corners found

YES

Determin laser points witch are on chessboard

Find corners with sub-pixel accuracy

Find the laser line points between the chessboard and calculate the ratio

Find the chessboard rotation and translation vectors

Interpolate laser line points to real world coordinate system

Convert chessboard corners to real world coordinate system

Save results to seperate file

Add laser line points to array

NO

Last image

YES

Least square fitting of laser line points to determin the parameters a, b, c, d of best-fitted plane
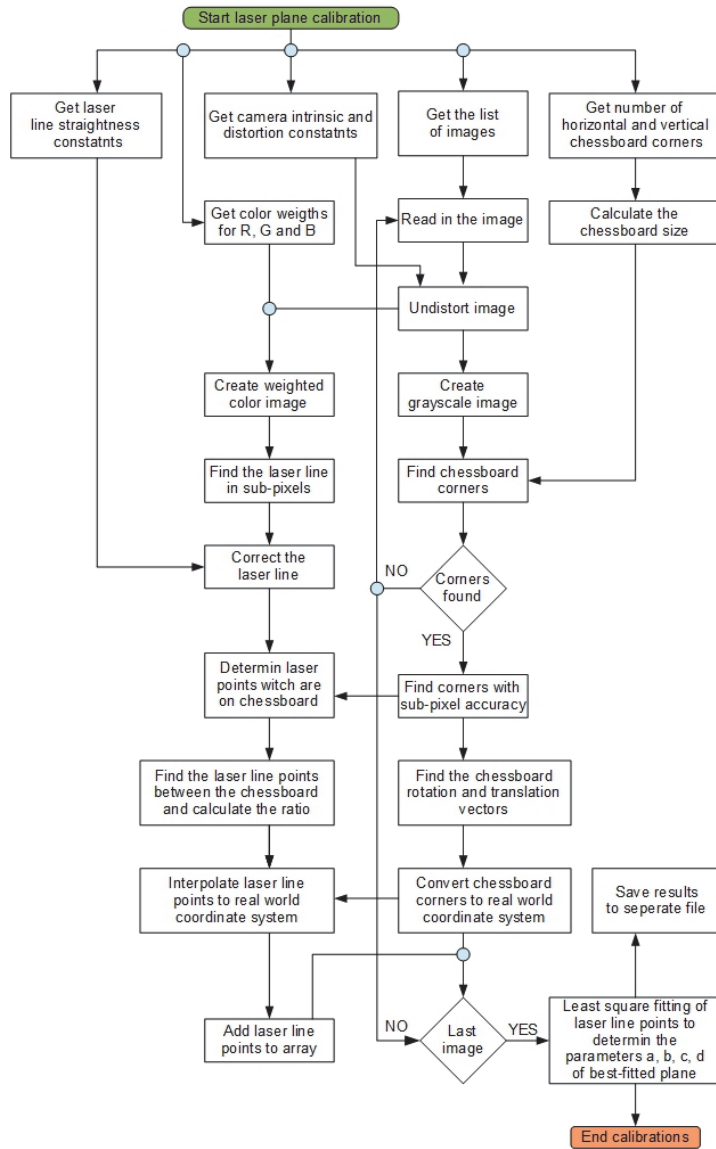
End calibrations

Figure 3.13 Calibration process flowchart (part 2).

3.9 Experiments – calibration dependency on line dectection method

As discussed before, calibration is an important step of laser scanners to be able to obtain an accurate measuring result. During the calibration process all distortions are corrected and a relation between the pixels in laser scanner camera image and the real world units is made.

Laser line detection method as part of the calibration process plays an important role in this calibration. The accuracy of the laser scanner is directly related to the precision of the laser line detection algorithm, used in the calibration process. Full - pixel resolution laser line detection algorithms are simpler and thus preferred in cases, where the accuracy of the laser scanner is not very important or where the processor resources are limited, like in the embedded real-time laser scanners. In other cases the one pixel resolution however is not sufficient, as the actual laser line center position can be located between two pixels. This is quite important if going into sub-millimeter measurements.

A series of experiments were made in order to asses how much the calibration and measurement results depend on the laser line detection with pixel or sub-pixel resolution in the calibration process and where is the trade-off between the complexity of the laser line detection algorithm and the laser scanner calibration and thus the measurement accuracy.

Two laser line detection methods were used in order to find the laser line from the chessboard images and calculate the laser light plane ABCD parameters. The first method with pixel resolution was using a second order Gaussian derivative [60]. The second method used to detect the laser line from the chessboard image was the laser line sub-pixel detection by convolution maximum correction with parabola, described previously. Figure 3.14 and Figure 3.15 show the differences of detected laser line from the same chessboard image with pixel and sub-pixel resolution methods. Several sets of chessboard images were chosen for laser light plane ABCD parameter detections with pixel and sub-pixel laser line methods.

Table 3.1 and Table 3.2 lists the ABCD parameters obtained with different image sets and laser line detection methods. It can be seen, that there are small differences between the A, B and C parameters obtained. The biggest variation is in the parameter A, which is related to the rotation of the laser light plane.
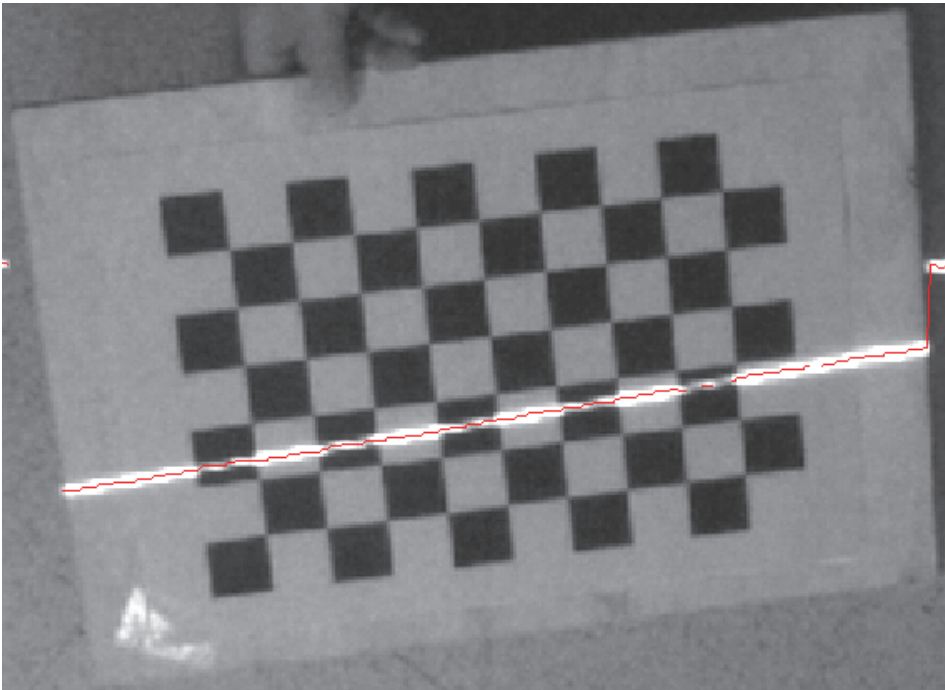
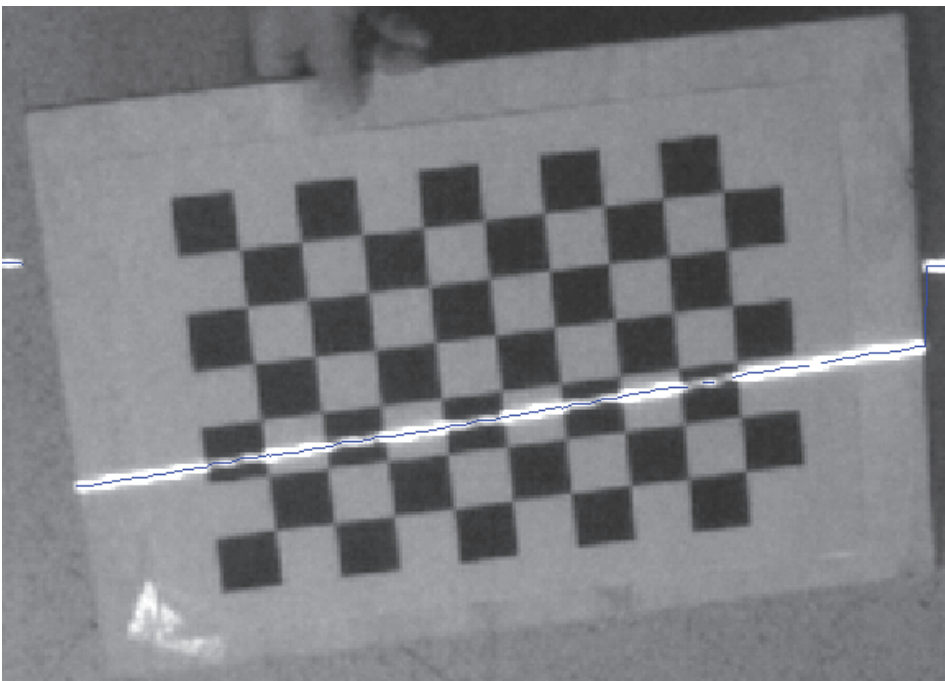*Figure 3.14 Laser line detection from the chessboard with pixel resolution [76 (V)].*

Figure 3.15 Laser line detection from the chessboard with sub-pixel [76 (V)].

Table 3.1 ABCD parameters with pixel resolution over different image sets [76 (V)].

	Image set 1	**Image set 2**	**Image set 3**	**StDev.**
A	1.066E-05	1.077E-05	1.069E-05	5.942E-08
B	6.863E-04	6.802E-04	6.799E-04	3.612E-06
C	4.789E-04	4.795E-04	4.795E-04	3.304E-07
D	-1.000E+00	-1.000E+00	-1.000E+00	0.000E+00

Table 3.2 ABCD parameters with sub-pixel resolution over different image sets[76 (V)].

	Image set 1	**Image set 2**	**Image set 3**	**StDev.**
A	1.114E-05	1.117E-05	1.104E-05	6.861E-08
B	6.862E-04	6.802E-04	6.798E-04	3.586E-06
C	4.789E-04	4.795E-04	4.795E-04	3.205E-07
D	-1.000E+00	-1.000E+00	-1.000E+00	0.000E+00

In order to see how the laser line detection with pixel or sub-pixel resolution in the calibration process influences the real measurement results, two objects with the heights of 6 mm and 25 mm were placed under the laser scanner and measured. Figure 3.16 shows the measured objects and the detected laser line.
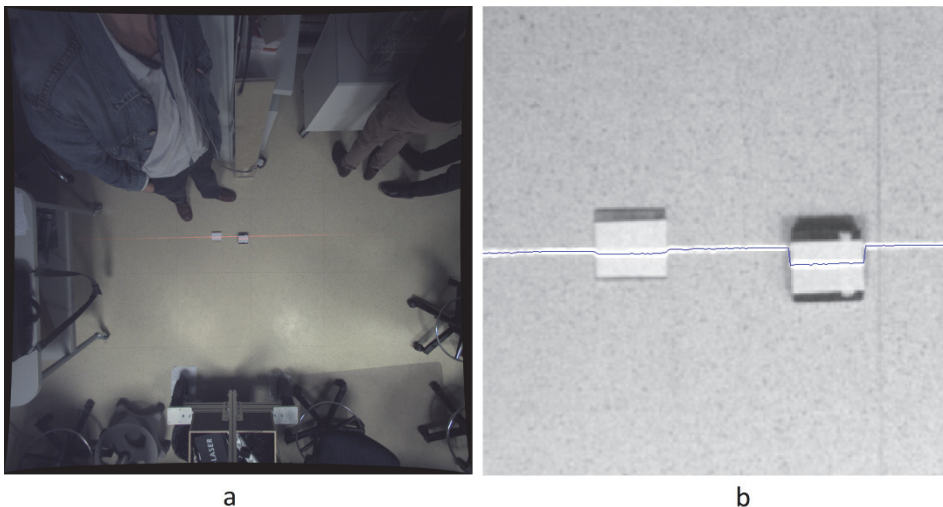

a   b

Figure 3.16 Measured objects and detected laser line on scanner image [76 (V)].

From the image the laser line was detected with sub-pixel resolution method. Pixel and sub-pixel ABCD parameters from the calibration process were used to convert the measurements to the real world millimeters. Figure 3.17 shows the detected laser line in real mm-s with pixel accuracy ABCD (a) and sub-pixel accuracy ABCD (b).
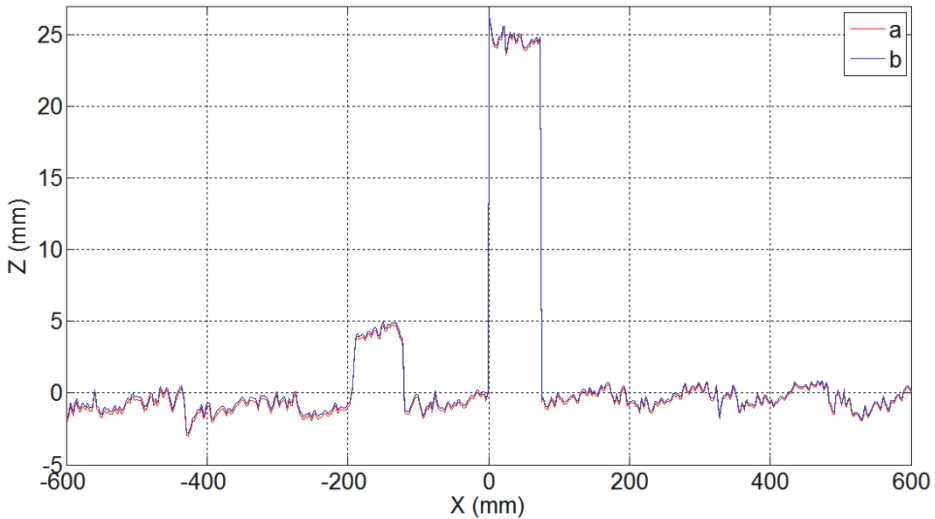

Figure 3.17 Measured objects in real mm-s with pixel and sub-pixel [76 (V)].

It can be seen that two objects are clearly distinguishable out of which one height is approximately 6 mm and the other is around 25 mm. The camera was in the height of ~1874 mm from the floor surface. The deviation between pixel accuracy ABCD (a) and sub-pixel accuracy ABCD (b) measurements can be seen more clearly from Figure 3.18 where smaller object can be seen more closely. It can be seen that there is actually rather noticeable difference between two measurements.

Figure 3.19 shows the deviation between two measurements Z1 (pixel accuracy ABCD) and Z2 (sub-pixel accuracy ABCD) across the whole laser line with different image sets (a, b, c, d). With current setup and image sets the deviation is between -1 and +1.2 mm, what is quite much for doing sub-millimeter measurements. It can be also seen that the deviation is rather systematic and linear from one side of the image to another. This comes mainly from the fact that the A parameter of the laser light plane was the one, which was the most influenced. As mentioned, A is the rotation parameter of the laser light plane.
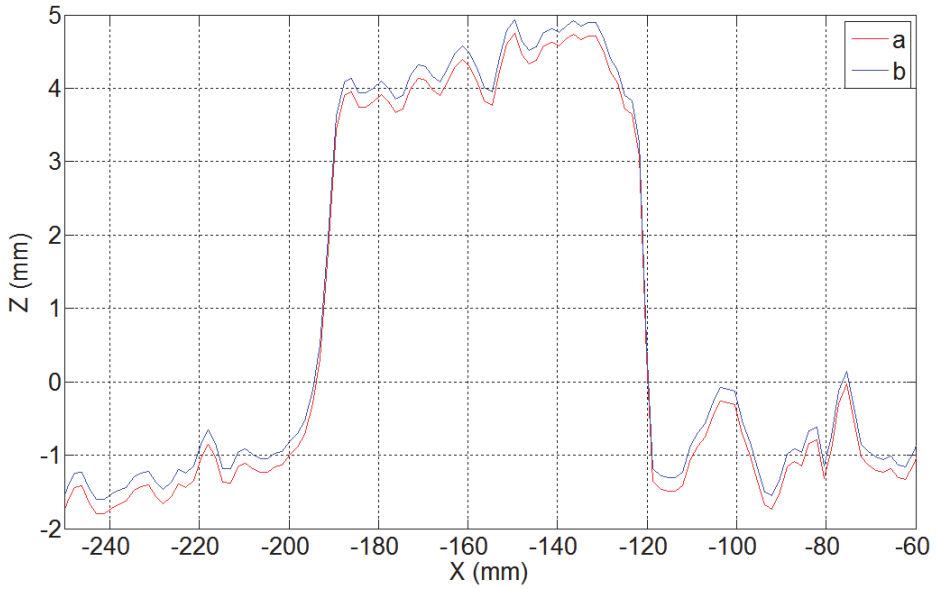
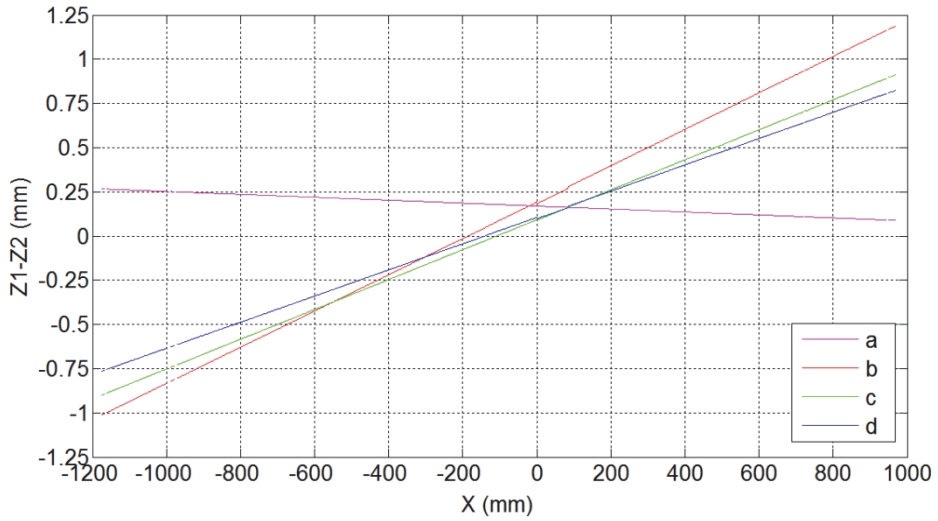*Figure 3.18 Smaller object in mm-s with pixel and sub-pixel accuracy [76 (V)].*

Figure 3.19 Deviation between measurements with various image sets [76 (V)].

Table 3.3 Measurements of objects with different ABCD parameters [76 (V)].

Measurement	Mean (mm)	StDev. (mm)	StDevE. (mm)	Diff. (%)
Real height	6.000	0	0	0
Height with pixel accuracy ABCD	5.369	0.241	0.024	10.520
Height with sub-pixel accuracy ABCD	5.554	0.241	0.024	7.430
Real height	25.000	0	0	0
Height with pixel accuracy ABCD	24.698	0.456	0.0450	1.210
Height with sub-pixel accuracy ABCD	24.864	0.455	0.0449	0.544

Deviation of the measurements of the reference objects, estimated with pixel and sub-pixel accuracy ABCD parameters are shown in Table 3.3. It can be seen that the sub-pixel laser line detection method in the calibration process has improved the measurement results and the measurement standard deviation has decreased. This comes from the fact that the found the ABCD parameters are more accurate. The experiments show that there is quite a noticeable dependency from the laser line detection method in the calibration process, which must be taken into account, when doing sub-millimeter accuracy measurements. However, if the measurement accuracy can be within few millimeters then pixel resolution laser line detection method in the calibration process is sufficient.

3.10   Experiments – transverse road profile measurement

In addition to the measurements of various reference objects in the laboratory, real profiles of a pavement surface were measured and compared with the standard straight edge rod and wedge measurement method, used by the road maintenance authorities in Estonia and in other countries. This enables to make measurements without expensive equipment while getting still good enough results. A road section with deep longitudinal crack was selected to evaluate the transverse profile measurement accuracy against traditional method. This allows to see better the horizontal and vertical resolution of the measurements. The measurement rod used was 4 meters long and measurement with the laser scanner were made from the 2 meter height. Common measurement width for both methods was around 1.5 meters in current setup. Figure 3.20 shows the measurement setup, measurement rod, the wedge on top of it and the developed laser scanner attached to mobile test rig.

Figure 3.20 Comparative measurements of real road transverse profile.

Figure 3.21 shows the measurement results with laser scanner (a) and with measurement rod (b). As can be seen from the figure, the laser measurement system has horizontal resolution about 1 mm, compared against 40 mm resolution with the measurement rod and wedge. This comes from the fact that the wedge is around 20 mm wide and typically the measurements are not taken after every millimeter, but less often. 26 measurements were taken with rod and wedge compared to 947 measurement points gained with laser scanner. It can be

seen that due to this rod and wedge measurement limited vertical resolution the crack in the pavement is missed. The wedge can not be placed in the bottom of the crack to be measured. Vertical resolution of the measurement rod method was around 1 mm which is also a bit bigger compared to the laser scanner measurement.

It can be said that the measurement results are generally very similar, but with the laser scanner the resolution is much better. Measurement with rod and wedge is more time consuming, but less expensive. If the measurements are made in large quantities, or on a long road section, then measurement with laser scanner has more benefits.
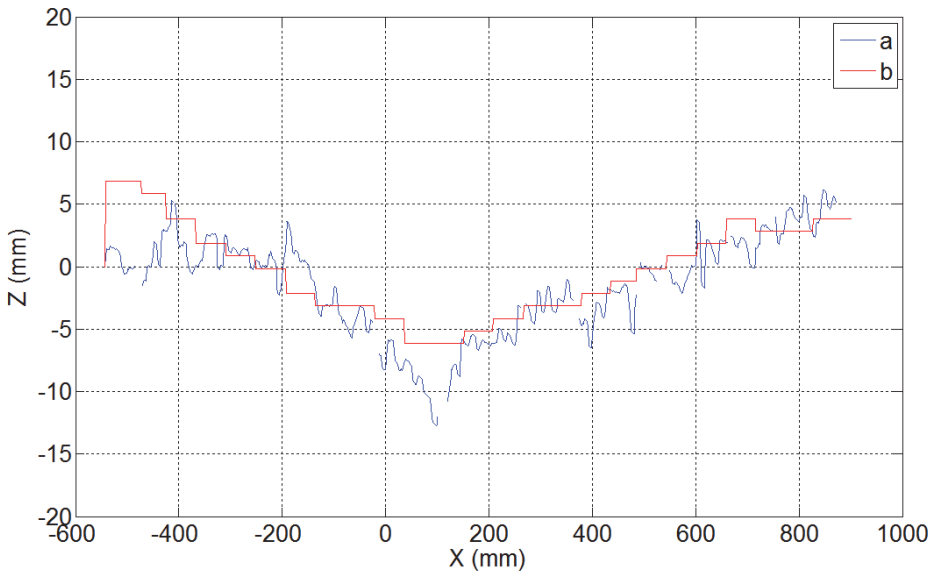

Figure 3.21 Measurement results with scanner (a) and measurement rod (b).

3.11   Conclusion of chapter 3

In the first part of this chapter an overview of the relationships between the camera image, laser and real world units is given. Methods to correct the distortions and a new method to find the laser line light plane parameters were described. Complete calibration procedure with flowchart was made and explained.

In the second part of this chapter a series of experiments were made. The main purpose of the experiments was to assess the accuracy of the developed laser scanner. Objects with known dimensions were measured and it was seen that the standard deviation of the measurements was less than 0.5 mm. Also experiments to see how much the laser line detection with pixel or sub-pixel resolution during the calibration process affects the measurement results were

performed. The measurement difference dependency from the laser line detection method was between -1 and +1.2 mm. This was the systematic error and it was caused by the fact that the A parameter, which was the most affected during the calibration process of the laser light plane, was not found so accurately in case of laser line detection with pixel resolution method. The A parameter is the rotation of the laser light plane.

In the final part of this chapter real-life profiles of a pavement surface were measured and compared with the standard rod and wedge measurement method, used by the road maintenance authorities in Estonia. It was seen that the measurement horizontal resolution with the developed scanner was about 1 mm, compared to 40 mm with the measurement rod and wedge method. Vertical resolution of the developed scanner was around 0.5 mm which is also less than the 1 mm of the rod and wedge method. Due to the better horizontal resolution the crack in the pavement was also detectable with the developed scanner, while it can not be detected with the rod and wedge method. Measurment with the developed scanner takes also significantly less time.

4 TIME AND LOCATION STAMPING OF THE PROFILES

One important aspect of the road profile scanners is how to associate captured images and road transverse profiles from them with absolute time and real world location. This is important to accurately determine the measurement location and time when the measurement platform speed is not constant or the camera is capturing the images asynchronously. Calculating IRI for example depends on the accuracy of the transverse profile locations.

There are plenty of known solutions [83-85] for synchronizing captured images in time with the special hardware. The problem with those solutions is that the hardware is complex; it needs real synchronization cables and special hardware, which makes the system clumsy and expensive. Also the typical lags in computer based networks are in tens of milliseconds.

There are also known solutions [86-87], where frames of the image acquisition streams are synchronized or related to each other by monitoring, and matching (in the algorithm), the moving objects (e.g. feature points) by various cameras, in parallel. The drawback of such solutions is that the frames are not still connected to the absolute time base, thus making it impossible to track the positions of the image frames. Also such algorithms are computationally sophisticated and time consuming, as the objects (feature points) are located at unknown co-ordinates and have unknown features. Such approach also depends much on the illumination conditions.

In order to precisely determine the laser line profile (road transverse profile), which is captured by the camera, absolute time and the position of it in real world a new solution has been proposed.

Patent application [88 (IV)] to Estonian patent office has been filled in for this solution in order to protect the intellectual property rights.

4.1 Time stamping solution with precisely modulated light in images

Figure 4.1 gives an overview of the proposed time stamping solution for the road profile measurement system. The solution consists of global navigation satellite system (GNSS) signal (1), GNSS receiver (2), light modulation controller (3) or a combination of those (4), light source; for example light emitting diode (LED) (5), laser line profile (6), road profile scanner camera (7), personal computer (PC) with image acquisition and processing software (8) and laser (9). The camera is running asynchronously at maximum speed. Camera is controlled by a computer.
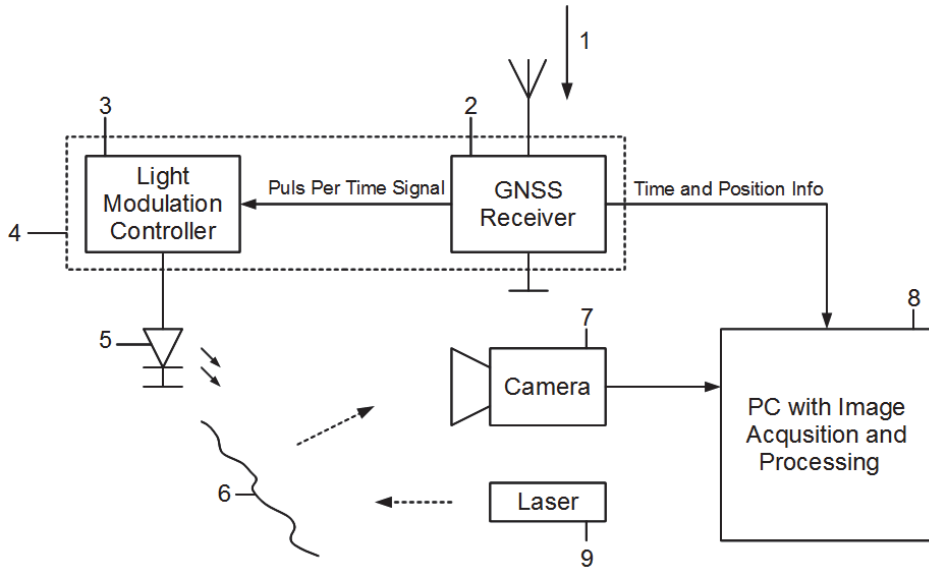
Figure 4.1Time stamping solution for road profile scanners.

The computer is also used to detect the laser line from images by using image processing algorithms. A time stamp is added to each camera image frame in the computer.

Accurate time stamp is obtained from the GNSS signal. GNSS signal contains the exact time and location information. GNSS signal is received with the GNSS receiver. The receiver sends the received time and location information to the computer. Pulse per second (PPS) signal from the GNSS receiver is driving the light modulating controller, which in turn regulates the light intensity of the light source.

One LED can be used as the light source. Also colored LED-s or a lot of single-color LED-scan be used as the light source. Seven segment indicator can also be used or any other suitable light source.

Different signals can be used to modulate the light source light intensity. The signal may be a pulse signal, a saw-tooth shaped signal, the pseudo-random pulse signal, or any other signal suitable for light source intensity controlling. Figure 4.2 shows some example signals (a1-a3) that can be used to modulate light source light intensity and camera image frames (b1-b3) taken asynchronously in parallel.

The modulated light intensity by source current signal Figure 4.2 (b1-b3). light intensity of the is captured by the camera (in asynchronous mode at maximum speed.
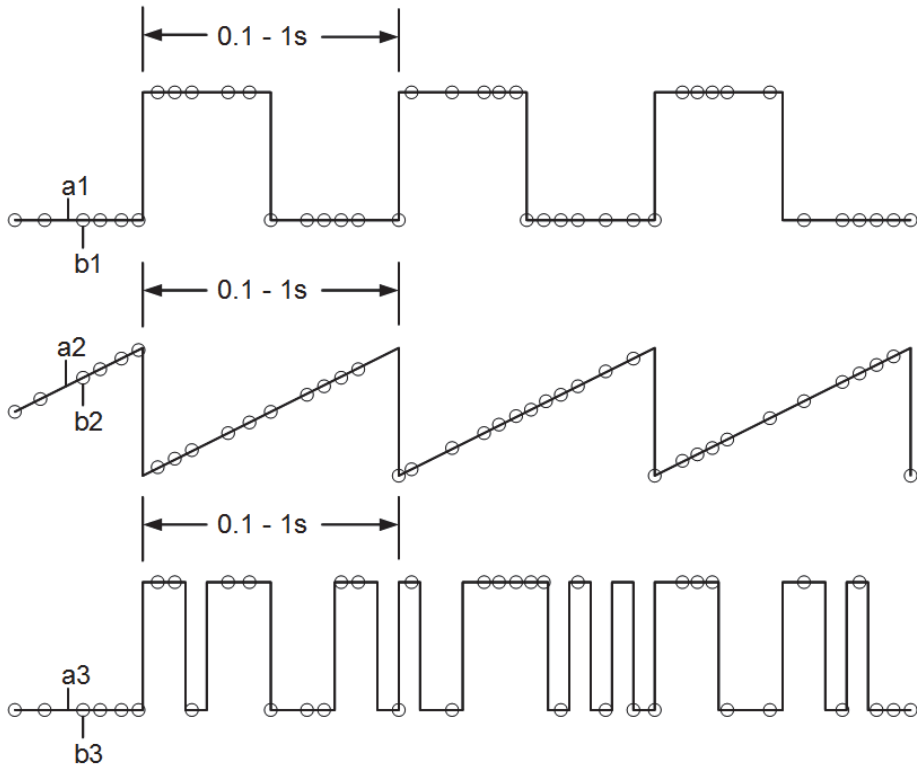
Figure 4.2 Various signals used to modulate light source light intensity [88 (IV)].

Knowing that the light intensity of the light source is changing synchronously and is driven by the GNSS signal, it is possible to calculate an exact time stamp for every frame captured by the camera. Thus every road profile will get an exact time stamp.

In addition to the time stamp an exact location information received from the GNSS signal is added to each frame captured by the camera. Thus every road profile will get an exact location information as well.

With this an absolute time and location of the digitized road section measured with the road profile measurement scanner is determined.

4.2 Experiments – modulated signal extraction from image

A set of experiments were made in the laboratory to extract the modulated light signal intensity from the camera image. LED was placed in the camera image corner. ROI was selected where the LED was placed. Figure 4.3 shows the camera image with LED pattern in the bottom left corner and with the selected ROI around it.
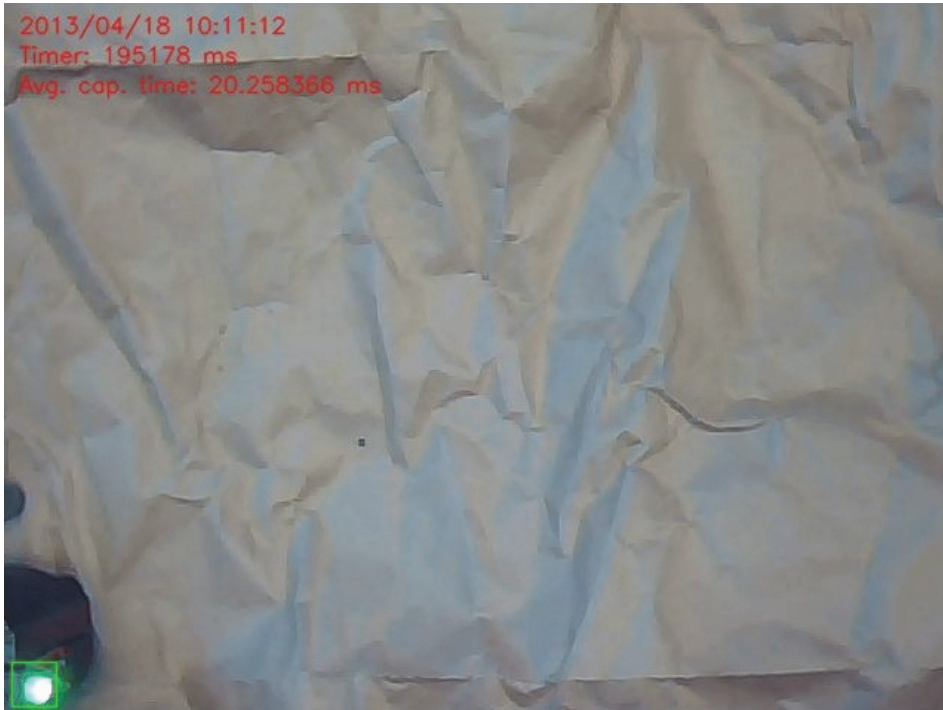
Figure 4.3 Modulated light extraction from camera image.

Signal generator was used to drive the LED. Several different waveforms (sawtooth, sinus and pulse signal) with the frequency of 1 Hz were used to drive the led and modulate the led light intensity. Camera was capturing asynchronously the image with ROI. The camera was capturing around 30 frames per second. Average intensity of the ROI was calculated from every camera image. Also time intervals between the consecutive image frames were measured as a reference in milliseconds.

Figure 4.4 and Figure 4.5 show the captured ROI average intensity (a) and the exitation signals (b) used to drive the light source. Circles in the acquired signal are the actual locations in time and the intensity of the signal at this time instants. It can be seen that the intensity and the time interval between the camera frames is not synchronous. This comes from the fact that the camera is typically capturing the images asynchronously. It can be also seen that the intensity of the signal is not exact sawtooth or sinus, like the driving signal, due to the LED voltage-current characteristics, nevertheless the periods and the frequency of the driving signal are clearly visible. It can be seen that the detected imagining signal in the ROI is close to 1 Hz like the driving signal.

Figure 4.6 shows the time deviation of the camera frame from the light source driving signal time. It can be seen that the deviation is between 7 to 40 ms. This is a lot considering that the camera was capturing around 30 frames per second, which means that the time between each frame is around 30 ms.
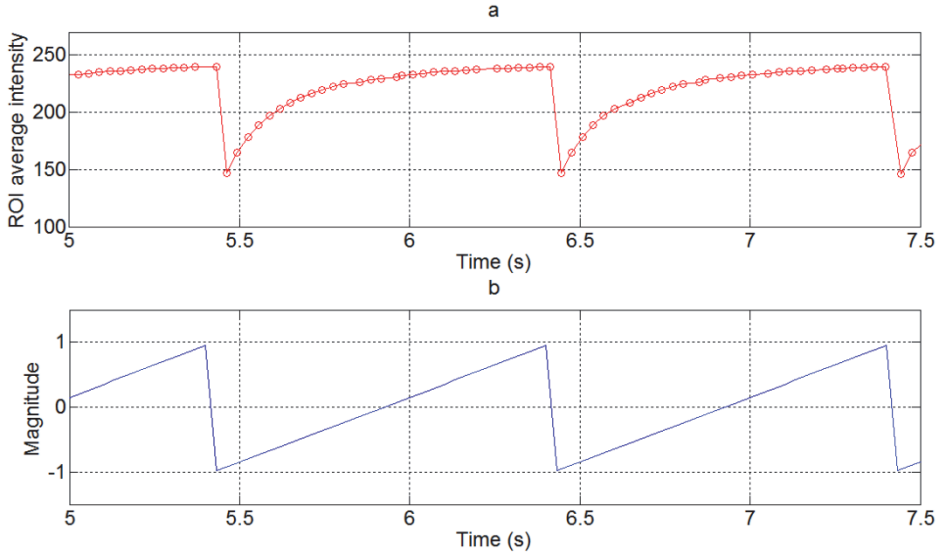
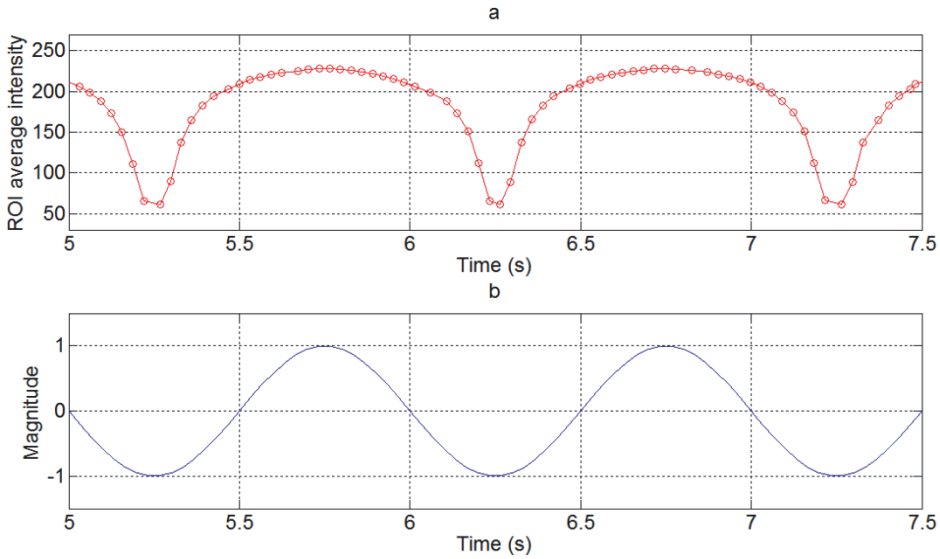*Figure 4.4 Captured light intensity from image and the real sawtooth signal.*

Figure 4.5 Captured light from image and the real sinusoidal signal.

Standard deviation of this deviation for the current setup was 8.4322 ms. It can be seen that in some cases the deviation is more than the one frame period time. Measurement location error of transverse profiles in the case of 100 km/h with this kind of time deviation can be up to 1.1 meters. The error is around 4% in the case of the camera frame rate of 30 frames per second and while getting a transverse profile after every 27.7 meters.
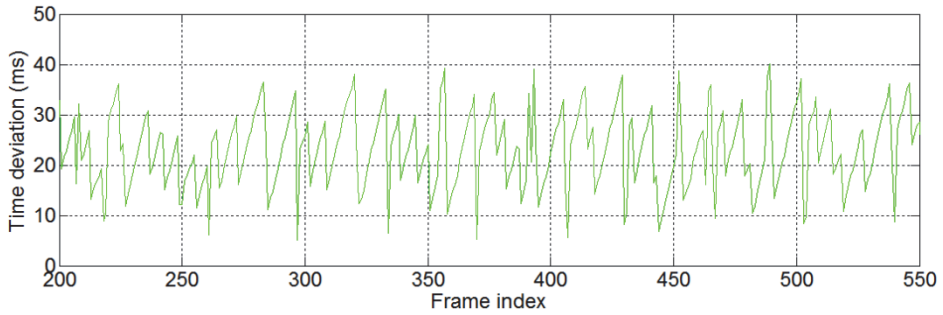
Figure 4.6 Time deviation of the frames from the actual signal of the light.

4.3 Conclusion of chapter 4

In this chapter a solution to precisely timestamp the laser line profile (road transverse profile) with absolute time and thus location of the road point was described. The solution by which a global navigation satellite system signal modulated light source is positioned in front of the laser scanner camera captures the modulated light intensity simultaneously with the laser line (road profile). Camera is capturing the images in the asynchronous mode with the maximum speed. By knowing that the light intensity of the light source is changing synchronously and is driven by the GNSS signal and the frequency of the signal is known, an exact time stamp for every frame captured by the camera can be calculated. Thus every road profile gets an exact time stamp.

Experiments were made in the laboratory to extract the modulated light signal intensity from the camera image and the camera frame time deviation from synchronous time was calculated. It was seen that the standard deviation for the current setup was 8.4322 ms. In such a case the correction of the transverse profile location is up to 4% for the measurement speed of 100 km/h. This corresponds to 1.1 meters for the camera frame rate of 30 FPS.

5 IMPLEMENTATION OF SYSTEM HARDWARE AND SOFTWARE

To evaluate and demonstrate the results, specific hardware and software was constructed. At first a smaller prototype of the final system was created called „mobile test rig". This allowed to make initial experiments and was used mostly during main software development period. Based on this „mobile test rig" the final system was constructed.

In this chapter an overview of the developed hardware and software is given.

5.1 Mobile test rig

In order to perform initial real life tests, a small mobile test platform was constructed. Draft drawing of mobile test rig with camera and laser mountings is illustrated on Figure 5.1.
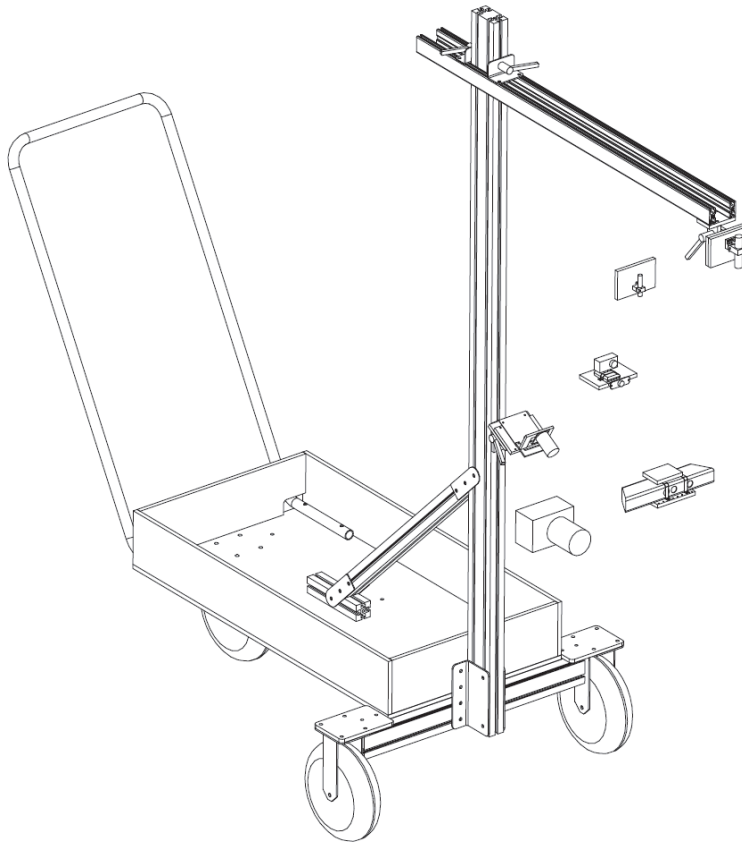

Figure 5.1 General overview of mobile test platform.

The mobile test platform has 3 inflatable wheels, so it can be moved around easily, what enables to test the laser line extraction and other image processing

algorithms on different surfaces. It is fully collapsible (yet rigid enough), for better transport purposes, measuring only 900 mm x 1225 mm x 2200 mm. The test platform can fit into car boot when packed together. It is small enough to be used also indoors, where it is more convenient to make initial tests and measurements before moving to outside. The test platform has been made from aluminum profiles with bolted fasteners. There is a set of fastenings for all basic systems components, which includes 3 different camera fastenings, 2 different laser fastenings, fastening for a data projector (in order to simulate different types of laser lines or multiple of lines), box where a laptop computer, batteries and other accessories like acceleration sensor and GPS receiver can be placed. All the laser and camera angles are adjustable. All laser and camera heights and distances can be changed. The camera and the laser can be raised up to 2 m in height giving almost 3 m of field of view depending of the lens used in front of the camera. The camera and laser locations are also interchangeable. Ximea MQ042CG-CM camera is used which has a resolution of 2048 x 2048 pixels and can capture full frame images up to 90 frames per second. The laser is Z-Laser's ZM18, which has many different line generation options for optics for experimenting purposes. Figure 5.2 shows the constructed mobile test platform.

Figure 5.2 Constructed mobile test platform on first outdoor experiments.

5.2 Measurement vehicle

After initial experiments with small mobile test rig a complete measurement system was constructed. The overall objective of the mechanical components was to facilitate the systems installation in a wide range of standard commercial

vehicles whilst minimizing the cost of adaptation of vehicles and installation of the system. Thus the same concept of using adjustable aluminum profiles was adopted. The vehicle could be a van, a passenger car, a special trailer or any other reasonable platform. The fixing and holding points of these rails are connected to the standard roof-rails and the tow-bar (or the rear-staircase of the van) of the vehicle. The tow-bar can optionally also give electrical power from the board of the vehicle to the electrical measurement subsystems. The adjustable metal rails give the flexibility in setting lasers, cameras, GPS systems and other electronic or mechanical solutions, to be mounted and enabling fast changes and adjustments in the configuration of the system. Also extended systems, e.g. with three lasers and three cameras can be easily assembled on the base of the same solution. Concept drawing of the developed mechanical system is depicted on Figure 5.3.
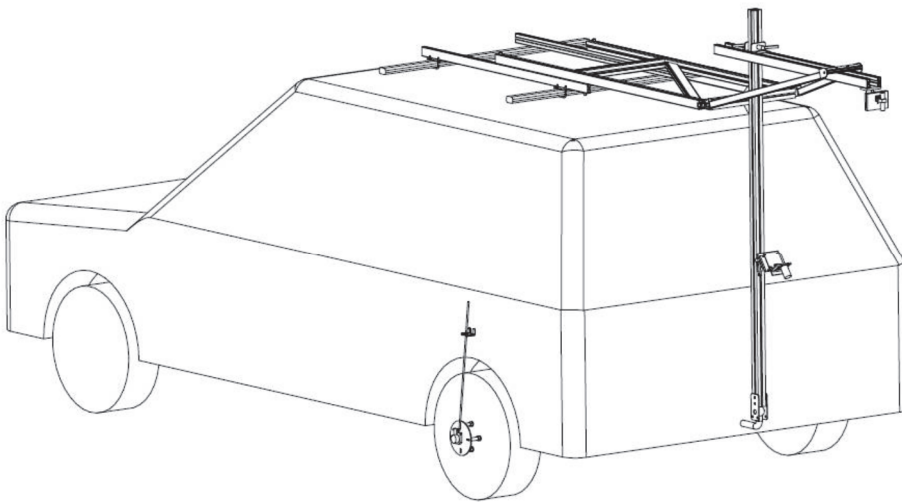

Figure 5.3 General overview of the measurement system installed on vehicle.

Van was chosen for the final system as it is higher than the standard vehicle, giving bigger field of view and thus larger measurement area. The van is also more stable giving more accurate results at the high speeds and on the rough surfaces. Figure 5.4 shows the constructed measurement system with the camera and the laser installed on van.

Figure 5.4 Measurement system with camera and laser installed on van.

5.3 Software

The software has been developed mostly as the C/C++ code and OpenCV libraries [78] have been used for some generic image processing tasks. Separate classes are made for laser line extraction, measurements, calibrations etc. This allows keeping the main data processing separate from Graphical User Interface [GUI], so it is easy to compile various end-user programs, by changing the GUI and combining the developed modules according to the specific needs, for Windows, Linux or Android. Current implementation of the software has been made in QT environment [89] for Windows. QT is multi platform open source GUI development environment allowing the same GUI to be also used in Linux Windows and Mac OSX.

The developed software currently supports Ximea MQ042CG-CM camera and standard USB web cameras. Software shows live display of acquired frames. Image files can be loaded as regular image format supported by OpenCV, but also from Raw16 format if the image depth is more than 8 bits per channel. Software also works with different video formats supported by OpenCV. From the "Capture Images" tab (Figure 5.5) camera lens undistortion can be applied and frames acquired from the camera can be saved either one-by-one at a time or all or as the whole sequence.
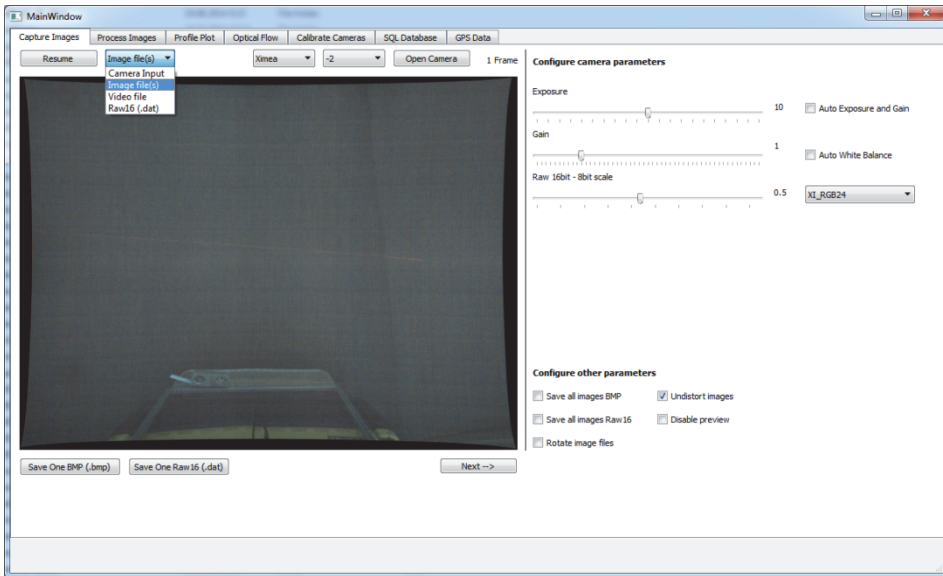
Figure 5.5 Camera configuration and image or video loading.

Laser line extraction parameters for developed method can be configured from the "Process Images" tab (Figure 5.6). Detected laser line(s) are plotted on greyscale image with red color. ROI can be applied which accelerates the laser line extraction process.

Figure 5.6 Laser line extraction configuration.
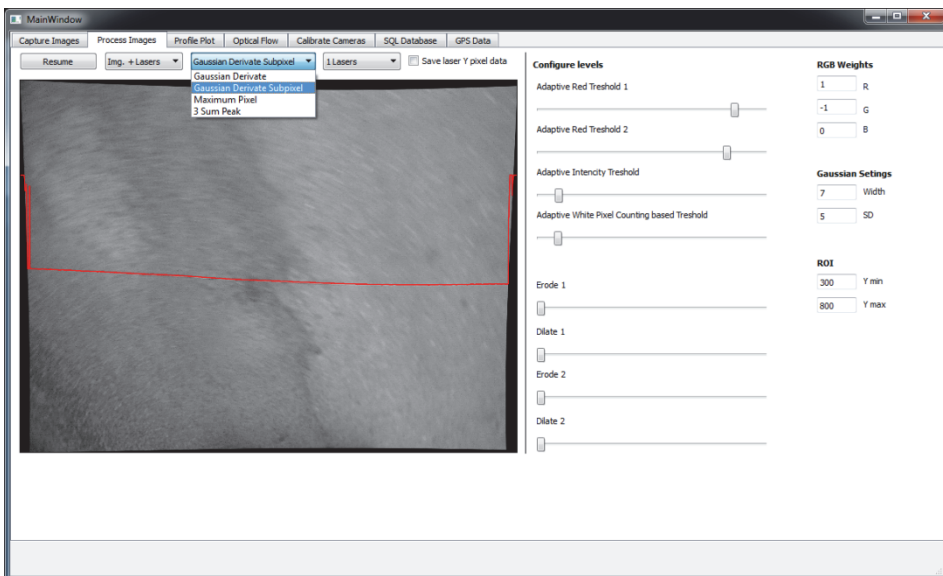
After laser line extraction and if the system calibration has been made the laser profile can be plotted in real world millimeters in "Profile Plot" tab (Figure 5.7). Profile can be zoomed in and investigated closely.
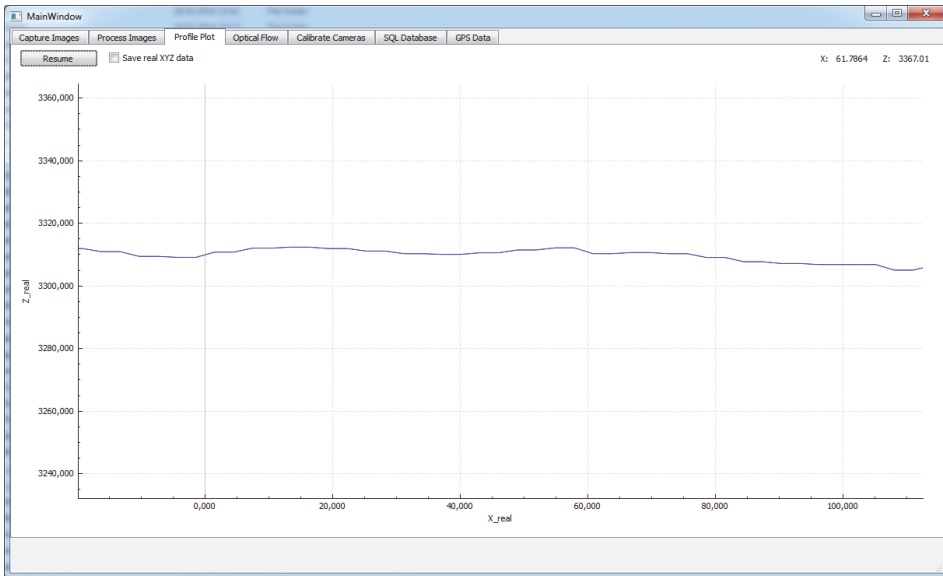
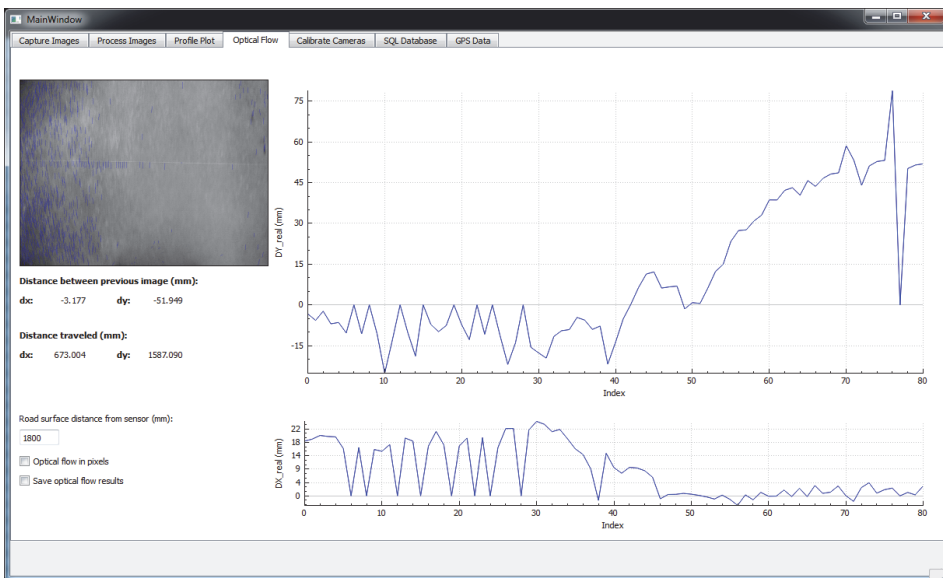*Figure 5.7 Road profile in real world mm-s from camera sensor perspective.*

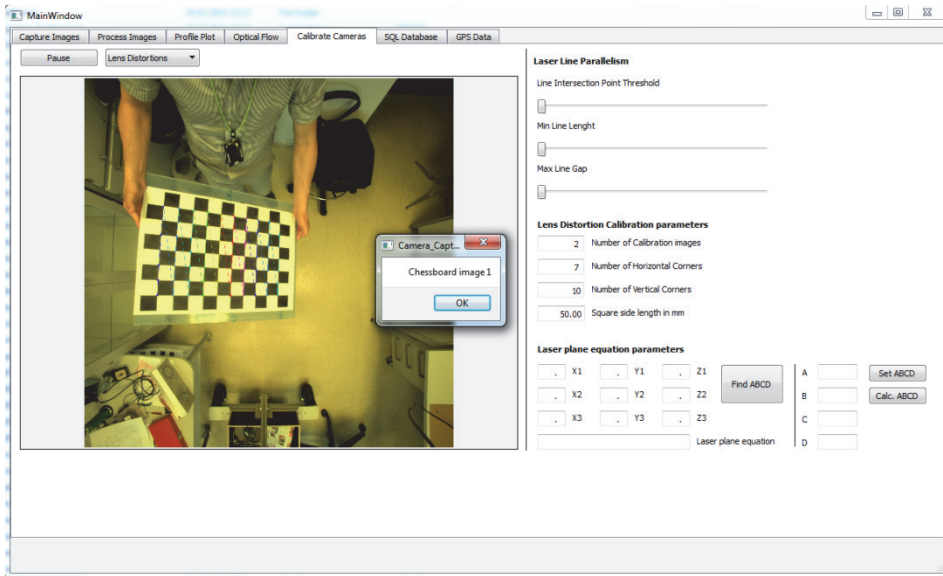*Figure 5.8 Optical flow between two captured frames in real world mm-s.*

Figure 5.9 Calibration of camera lens distortions and laser light plane.

Optical flow is calculated between two consecutive frames (laser line profiles) and cumulative plot of X and Y distances in either pixels or real world millimeters are plotted on "Optical Flow" tab (Figure 5.8). The distances between laser line profiles can be stored to file which is later used in 3D road profile reconstruction.

Lens distortions and laser light plane constant detection is made on "Calibrate Cameras" tab (Figure 5.9). For this chessboard parameters should be entered and images loaded for the calibration process. After successful calibration an XML file is stored containing all the necessary information. The calibration file is loaded automatically if available and the system calibration is not necessary to be made every time.

5.4 Conclusion of chapter 5

In this chapter, an overview of the developed hardware and software is given. At first a smaller prototype of the final system called „mobile test rig" was developed, which has a set of fastenings for all basic systems components. The "mobile test rig" was used during the main software development period, it is small and flexible solution for different indoor and outdoor experiments. Then a complete measurement system for vehicles was constructed. The objective of the mechanical components for measurement vehicle was to facilitate the systems installation in a wide range of standard commercial vehicles whilst minimizing the cost of adaptation and installation. The software has been developed mostly in C/C++ code using OpenCV libraries. Graphical user interface was developed in the QT environment.

6 CONCLUSION

6.1 Main results

The main objective formulated initially was to develop, optimize, implement and evaluate new improved 3D laser scanner and corresponding image processing algorithms for the road profile measurement system. As a result a 3D laser scanner system including all the mechanics and software was developed with completely new set of image processing algorithms and calibration processes. Four papers related to this thesis have been published and one patent application to the Estonian patent office (with further option to patent the invention in other countries) has been filled in for road profile time and location stamping solution in order to protect the intellectual property rights.

The main results of this thesis are listed below.

R1. In chapter 1 and paper [51 (II)] a new method based on second order Gaussian derivative convolution with different standard deviation convolution kernel parameters taking into account the variable laser line width was developed. The laser line detection dependencies, optimal standard deviations and the reduced uncertainties in the case of variable laser line width (caused by different material reflection coefficients) were shown with experiments.

R2. In chapter 1 and paper [52 (I)] two laser line detection methods "Parabola method" and "Upsampling method" and the combination of those were developed and tested to improve the laser line detection resolution from pixel to sub-pixel level. It was shown that both methods improved the laser line detection accuracy more than 20%. It was seen that the "Parabola method" is not as accurate as "Upsampling method", but is more computationally efficient and faster and is thus more preferable in the road profile measurement systems.

R3. The "Parabola Method" combined with "Variable Laser Line Detection Method" works well with noisy images, changing ambient light conditions, various road surfaces materials and low power lasers. This means that the developed road profile scanner is more safe to use and also less expensive than competitive solutions.

R4. In chapter 2 and paper [66 (III)] a new "Adaptive Undersampling Method" to increase the road profile scanning speed without increasing the camera frame rate or using custom, expensive hardware was developed. The main idea of this method is to process only the relevant parts of the images and skip the non-relevant parts that do not contain the laser line information. This was proven to be quite efficient method to increase the laser line detection speed. Experiments were made on different hardware platforms to assess the method and it was seen that the average speed increase with current setup was around 6 times with one laser line on image and 12 times with two laser lines on image. It

was also noticed that the speed increase was even higher with larger images, compared to smaller images. This is caused by the fact that the laser line on higher resolution images is proportionally smaller than the irrelevant parts of the image which are not used by the "Adaptive Undersampling Method".

R5. In chapter 3 a new *Laser Light Plane Linear Interpolation Method* for finding the laser light plane parameters together with the complete scanner calibration procedure and flowchart were developed and experimentally evaluated in the lab with objects of known dimensions as well as on real pavement (together with road maintenance authorities in Estonia). It was seen that the standard deviation of the measurements was less than 0.5 mm, which is a lot less than competitive solutions. In paper [76 (V)] the experiments to see how much the laser line detection with pixel or sub-pixel resolution during the calibration process affects the measurement results were made. The measurement difference dependency from the laser line detection method was between -1 and +1.2 mm which is a lot when doing sub-millimeter measurements, but can be corrected as it is the systematic error and was caused by inaccurate laser light plane detection with pixel accuracy laser line detection method. This also shows that the developed sub-pixel laser line detection *Parabola Method* plays an important role in getting the correct measurement results. With proper calibration procedure the developed scanner is easy to use and more accurate than most of the competitive solutions.

R6. In chapter 4 and in the patent application [88 (IV)] a novel solution to precisely time-stamp the laser line profile (road transverse profile) with absolute time and thus location on road was described. The solution by which a global navigation satellite system signal modulates a light source positioned in front of the laser scanner camera captures the modulated light intensity simultaneously with the laser line (road profile). Camera is capturing in the asynchronous mode with the maximum speed. By knowing that the light intensity of the light source is changing synchronously and is driven by the GNSS signal and the frequency of the signal is known, an exact time stamp for every frame captured by the camera can be calculated. Thus every road profile gets an exact time stamp. This is a novel solution and improves the transverse profile location up to 4% in case of measurement speed of 100 km/h. This is 1.1 meters in case of camera frame rate of 30 frames per second.

R7. In chapter 5 the developed hardware and software is described. At first a smaller prototype of the final system called „mobile test rig" was developed, which has a set of fastenings for all basic system components. The "mobile test rig" was used during the main software development period, it is small and flexible solution for different indoor and outdoor experiments. Then a complete measurement system for

vehicles was constructed. The objective of the mechanical components for measurement vehicle was to facilitate the systems installation in a wide range of standard commercial vehicles whilst minimizing the cost of adaptation and installation. The software has been developed mostly in C/C++ code using OpenCV libraries. Graphical user interface was developed in the QT environment.

The results of the thesis correspond to the research objectives, as defined in the introduction: R1 and R3 fulfill the objectives O4 and O6; R2 solves O2 ; R4 is the solution for O1 and O5; R5 solves O2 and O3; R6 fulfills the objectives O3, O7 and O8; R7 solves the objectives O7 and O8. So, all the objectives of the thesis have been achieved with new developed, investigated and tested solutions.

The work has also practical value listed below.

- Ready to be used C++ code with GUI for accurate laser scanner.
- Developed scanner can be reused also for other different purposes.
- Test and evaluation platforms and software source codes, full scale demonstrator of road profile scanner.
- Appropriate solutions for SME's providing smaller cost and reduced complexity of the road profile measurment system.

6.2 Future improvements

Future work could involve improving the calibration of the scanner, as it is the most critical part to have correct measurement results. Chessboard corner detection should be reviewed as in many cases the found chessboard corners were out of the grid. Predefined mask could be used to correct the chessboard corner locations. Also the camera sensor intensity and color distribution [90] has not been taken into account.

Experiments with using of optical flow [91-94] to calculate the scanner movement from camera image and pavement surface were made, but it needs further investigation, experiments and evaluation of the accuracy before it could be used in final solution.

The scanning speed can be further increased by find the optimal level of undersampling in both horizontal and vertical directions, combining this method with ROI and/or using more lasers in parallel.

There are several ways [95-97] to calculate camera tilt from the image. It is also possible to detect the tilt of the camera sensor by using multiline or multiple lasers on image and observing the distances between laser lines as it changes if the road surface is not parallel to laser light. Some experimental image sets were captured for future research.

Using of different laser line patterns like grid of lines or circles or dots was considered to get more information about the profile per camera image. Some experimental image sets were captured, but those were also left for future research.

7 REFERENCES

[1]   "Fugro Roadware," *http://www.roadware.com*, Visited: Jan. 29, 2015.

[2]   H. Wang, "Development of laser system to measure pavement rutting," University of South Florida, 2005.

[3]   D. Rose, "Surface-profiling system and method therefor," U.S. Patent 20020176608, Nov. 28, 2002.

[4]   D. Choi, M. D. Herbert, and V. Flores, "Road profile scanning method and vehicle using side facing sensors," U.S. Patent Application No. 20120203428, Aug. 09, 2012.

[5]   J. Laurent and M. Doucet, "Vision system and a method for scanning a traveling surface to detect surface defects thereof," U.S. Patent 7801333, Sep. 21, 2010.

[6]   J. L. Gardiner and I. C. Willis, "Apparatus for measuring carriageway surface properties," U.S. Patent 8159679, Apr. 17, 2012.

[7]   T. Fukuhara, "Apparatus mounted on vehicles for detecting road surface conditions," U.S. Patent 4653316, Mar. 31, 1987.

[8]   J. P. Powell, D. L. Bender, S. C. Saunders, L. W. Purnell, and A. S. Khattak, "Pavement inspection apparatus," U.S. Patent 4958306, Sep. 18, 1990.

[9]   K. Shoutaro, N. Tatsuhide, and O. Tetsuo, "Vehicle for evaluating properties of road surfaces," U.S. Patent 4700223, Oct. 13, 1987.

[10] D. Savastru, M. Sorin, R. M. Ion, "Scanning equipment for sampling road cross profiles," Ro. Patent 122110, Dec. 11, 2006.

[11] D. Savastru, M. Sorin, R. M. Ion, "Standard test method for measuring rut-depth of pavement surface," Ro. Patent 122929, Dec. 11, 2006.

[12] P. S. Huang and F.-P. Chiang, "Method and apparatus for three dimensional surface contouring using a digital video projection system," U.S. Patent 6438272, Aug. 20, 2002.

[13] H. Hans, "A device for measuring the profile of a roadway," WO. Patent Application No. 2003106924, Dec. 24, 2003.

[14] D. D. R. N. Zwingel, H. D. Steinbichler, and H. P. D. I. Misoph, "Contactless measurement of tunnel profile or road surface e.g. motorway," De. Patent 19513116, Oct. 11, 1996.

[15] R. D. Janke, M. Tasci, J. D. Davis, J. C. Tebbe, H. R. Butterfield, T. D. Roberts, D. A. Ruiz, K. M. Smith, and D. E. Martini, "Scanning device and method for analyzing a road surface," U.S Patent 7546765, Jun. 16, 2009.

[16] D. J. Elton and M. E. Harr, "Non-contact road profilometer and deflection meter," U.S. Patent 4571695, Feb. 18, 1986.

[17] L. E. Kuntz, "Profile indicating system for roadways," U.S. Patent 4135304, Jan. 23, 1979.

[18] "Automatic measuring system for longitudinal and traverse unevenness of road," Kr. Patent Application No. 20010068235, Jul. 23, 2001.

[19] T. Fukuhara, H. Sato, and A. Yoneya, "Method for measuring road surface longitudinal profile," U.S. Patent 6647636, Nov. 18, 2003.

[20] K. Homma, H. Nogi, K. Yamada, M. Kitazume, M. Uzawa, and M. Aoki, "Method of and apparatus for measuring irregularities of road surface," U.S. Patent 4878754, Nov. 07, 1989.

[21] W. J. Herr, "Highway profile measuring system," U.S. Patent 5510889, Apr. 23, 1996.

[22] D.-M. Docros, "Method for measuring the profile of a road," U.S. Patent Application No. 20030000097, Jan. 02, 2003.

[23] S.-D. WEE, "Apparatus for automatically inspecting road surface pavement condition," U.S. Patent 7562563, Jul. 21, 2009.

[24] R. A. Ferguson, D. N. Pratt, P. R. Turtle, I. B. MacIntyre, D. P. Moore, P. D. Kearney, M. J. Best, J. L. Gardner, M. Berman, M. J. Buckley, J. E. Breen, and R. Jones, "Road pavement deterioration inspection system," U.S. Patent 6615648, Sep. 09, 2003.

[25] Y. Masuyama, J. Katayama, and N. Kusakari, "Road surface state estimating system and road surface state measuring apparatus," U.S. Patent 7197425, Mar. 27, 2007.

[26] D. R. Fohey, "Non-contact sensor, system and method with particular utility for measurement of road profile," U.S. Patent 4456829, Jun. 26, 1984.

[27] H. Watanabe, N. Takeuchi, and T. Arimoto, "Apparatus for measuring a shape of road surface," U. S. Patent 5745225, Apr. 28, 1998.

[28] I. Shingo, "Correction data synchronizing device for road surface condition measuring device," Jp. Patent 09-189536, Jan. 11, 1996.

[29] E. B. Spangler, "Method and system for measurement of road profile," U.S. Patent 4422322, Dec. 27, 1983.

[30] M. Per, "Road surface and tyre condition monitoring apparatus," Gb. Patent 2486930, Jul. 04, 2012.

[31] L. M. Mara, "Rapid road repair vehicle," U.S. Patent 5947636, Sep. 07, 1999.

[32] E. Mueller, S. Otterbein, D. Kunz, R. Kallenbach, E. Mueller, S. Otterbein, D. Kunz, and R. Kallenbach, "Signal derivation system for real=time evaluation of road surface profile under motor vehicle - has monitors for vertical deflections of wheels and with data reduction signal processing to classify profiles," De. Patent 4133238, Apr. 08, 1993.

[33] J. Takiguchi, N. Kajiwara, Y. Shima, R. Kurosaki, and T. Hashizume, "Measurement apparatus, measurement method, and feature identification apparatus," U.S. Patent Application No. 20100034426, Feb. 11, 2010.

[34] D. Savastru, M. Sorin, R. M. Ion, "Method and equipment for testing road longitudinal profiles in dynamic regim," Ro. Patent 122109, Dec. 11, 2006.

[35] T. Keiji, F. Toshihiko, "Detector for road surface crack," Jp. Patent 60-122306, Dec. 05, 1983.

[36] U. J. Yong, "System for measuring and analyzing pavement crack," Kr. Patent Application No. 20000056726, Sep. 15, 2000.

[37] I. Haruo, S. Nobuyosh , "Measuring method for state of road surface," Jp. Patent 09-166435, Dec. 18, 1995.

[38] D. Michihisa, M. Shigemi, H. Shinichi , "Apparatus for measuring crack of road surface," Jp. Patent 04-240556, Jan. 23, 1991.

[39] S. Koji, F. Toshihiko T. Mitsuo, "Automatic analyzing device for road surface state," Jp. Patent 64-049909, Aug. 20, 1987.

[40] A. Hideaki, "Measuring instrument for road surface property," Jp. Patent 63-284409 , May 15, 1987.

[41] "ViaTech AS," *http://www.viatech.no/*, Visited: Jan. 29, 2015.

[42] "Pathway Services Inc.," *http://www.pathwayservices.com*, Visited: Jan. 29, 2015.

[43] "Pavemetrics Systems inc.," *http://www.pavemetrics.com*, Visited: Jan. 29, 2015.

[44] "Pavement Management Services," *http://pavement.com.au/*, Visited: Jan. 29, 2015.

[45] "International Cybernetics," *http://www.intlcybernetics.com*, Visited: Jan. 29, 2015.

[46] "Roadscanners Oy," *http://www.roadscanners.com*, Visited: Jan. 29, 2015.

[47] "SITECO Informatica," *http://www.sitecoinf.it/*, Visited: Jan. 29, 2015.

[48] L. Amoureus, M. P. Bomers, R. Fuser, and M. Tosatto, "Integration of Lidar and Terrestrial Mobile Mapping Technology for the Creation of a

Comprehensive Road Cadastre," presented at the The 5th International Symposium on Mobile Mapping Technology, Padua, Italy, 2007.

[49]   J. Laurent, J. F. Hébert, D. Lefebvre, and Y. Savard, "Using 3D Laser Profiling Sensors for the Automated Measurement of Road Surface Conditions," in *7th RILEM International Conference on Cracking in Pavements*, A. Scarpas, N. Kringos, I. Al-Qadi, and L. A, Eds. Springer Netherlands, 2012, pp. 157–167.

[50]   "Maintenance Planning Systems for road, rail and airport authorities," *http://www.viatech.no/download/Jorn/ViaTech.pdf*, Jan. 29, 2015.

[51]   A. Mõlder, O. Märtens, T. Saar, and R. Land, "Extraction of the Variable Width Laser Line," in *Proceedings of the 14th Biennial Baltic Electronics Conference*, Tallinn, Estonia, 2014, pp. 157-160.

[52]   A. Molder, O. Martens, T. Saar, and R. Land, "Laser Line Detection with Sub-Pixel Accuracy," *Elektron. Ir Elektrotechnika*, vol. 20, no. 5, pp. 132–135, May 2014.

[53]   J. Wu, J. S. Smith, and J. Lucas, "Weld bead placement system for multipass welding [using transputer-based laser triangulation vision system]," *Sci. Meas. Technol. IEE Proc.*, vol. 143, no. 2, pp. 85–90, Mar. 1996.

[54]   K. Sung, H. Lee, S. Choi, and S. Rhee, "Development of a multiline laser vision sensor for joint tracking in welding," *Weld. J.*, pp. 79–85, Apr. 2009.

[55]   J. Canny, "A Computational Approach to Edge Detection," *IEEE Trans. Pattern Anal. Mach. Intell.*, vol. PAMI-8, no. 6, pp. 679–698, Nov. 1986.

[56]   J. M. S. Prewitt, "Object enhancement and extraction," *Pict. Process. Psychopictorics*, pp. 75–149, 1970.

[57]   R. Lienhart and J. Maydt, "An extended set of Haar-like features for rapid object detection," in *2002 International Conference on Image Processing. 2002. Proceedings*, 2002, vol. 1, pp. I–900–I–903.

[58]   J. Forest, J. . Teixidor, J. Salvi, and E. Cabruja, "A Proposal for Laser Scanners Sub-Pixel Accuracy Peak Detector," 2003.

[59]   V. Matiukas and D. Miniotas, "Detection of Laser Beam's Center-line in 2D Images," *Electron. Electr. Eng.*, no. 7, pp. 67–70, 2009.

[60]   L. Qi, Y. Zhang, X. Zhang, S. Wang, and F. Xie, "Statistical behavior analysis and precision optimization for the laser stripe center detector based on Steger's algorithm," *Opt. Express*, vol. 21, no. 11, pp. 13442–13449, Jun. 2013.

[61] C. Steger, "Unbiased extraction of lines with parabolic and Gaussian profiles," *Comput. Vis. Image Underst.*, vol. 117, no. 2, pp. 97–112, Feb. 2013.

[62] M. Lopez, J. A. Vilan, J. M. Matias, and J. Taboada, "Quality Control of Wood-Pulp Chips Using A 3D Laser Scanner and Functional Pattern Recognition," in *IEEE International Symposium on Industrial Electronics, 2007. ISIE 2007*, 2007, pp. 1773–1778.

[63] P. Pelgrims, G. V. de Velde, and B. V. de Vondel, "Sub-pixel edge detection," DE NAYER Instituut, Oct. 2004.

[64] S. Winkelbach, S. Molkenstruck, and F. M. Wahl, "Low-Cost Laser Range Scanner and Fast Surface Registration Approach," in *Pattern Recognition*, K. Franke, K.-R. Müller, B. Nickolay, and R. Schäfer, Eds. Springer Berlin Heidelberg, 2006, pp. 718–728.

[65] T. Acharya and P.-S. Tsai, "Computational Foundations of Image Interpolation Algorithms," *Ubiquity*, vol. 2007, no. October, pp. 4:1–4:17, Oct. 2007.

[66] A. Molder, O. Martens, T. Saar, and R. Land, "Adaptively undersampled image processing for fast multiline laser detection," in *2013 IEEE 8th International Symposium on Intelligent Signal Processing (WISP)*, 2013, pp. 60–64.

[67] S. Yamazaki, A. Nukada, and M. Mochimaru, "Hamming Color Code for Dense and Robust One-shot 3D Scanning," in *British Machine Vision Conference*, 2011, pp. 96.1–96.9.

[68] K. T. Chanin Sinlapeecheewa, "3D profile measurement using color multi-line stripe pattern with one shot scanning," *Integr. Comput.-Aided Eng.*, vol. 12, pp. 333–341, 2005.

[69] "High Speed Camera, sensitive global shutter CMOS sensor, Camera Link," *http://www.alliedvisiontec.com/emea/products/cameras/camera-link/bonito.html*, Mar 24, 2014.

[70] X. Sun, J. Huang, and W. Liu, "Decision model in the laser scanning system for pavement crack detection," *Opt. Eng.*, vol. 50, no. 12, pp. 127207–127207–10, 2011.

[71] K. Tornslev, "3D scanning using multibeam laser," Technical University of Denmark, Lyngby, 2005.

[72] A. Majumder and S. Irani, "Contrast Enhancement of Images Using Human Contrast Sensitivity," in *Proceedings of the 3rd Symposium on Applied Perception in Graphics and Visualization*, New York, NY, USA, 2006, pp. 69–76.

[73] K. Jack, "Chapter 3: Color Spaces," in *Video Demystified: A Handbook for the Digital Engineer, 4th Edition*, 2005, pp. 15–34.

[74] P. J. S. G. Ferreira, "Iterative and Noniterative Recovery of Missing Samples for 1-D Band-Limited Signals," in *Nonuniform Sampling*, F. Marvasti, Ed. Springer US, 2001, pp. 235–281.

[75] "The Kaleida Graph Guide to Curve Fitting," *http://www.synergy.com/Tools/curvefitting.pdf*, Visited: Feb. 01, 2015.

[76] A. Mõlder, O. Märtens, T. Saar, and R. Land, "Laser Scanner Calibration Dependency on the Line Detection Method," *Elektron. Ir Elektrotechnika*, accepted Feb. 18, 2015, in print.

[77] R. Andersson, "A calibration method for laser-triangulating 3D cameras," Linköpings university, Linköping, Sweden, 2008.

[78] "OpenCV Documentation," *http://docs.opencv.org*, 28-Jan-2015.

[79] Z. Zhang, "A flexible new technique for camera calibration," *IEEE Trans. Pattern Anal. Mach. Intell.*, vol. 22, no. 11, pp. 1330–1334, Nov. 2000.

[80] "Properties of Structured Light - Application Note," Coherent, Jan. 29, 2015.

[81] I. Frosio, N. Alberto Borghese, P. Tirelli, G. Venturino, and G. Rotondo, "Flexible and low cost laser scanner for automatic tyre inspection," in *2011 IEEE Instrumentation and Measurement Technology Conference (I2MTC)*, 2011, pp. 1–5.

[82] C. M. Huang and Y. H. Tseng, "Plane Fitting Methods of LIDAR Point Cloud."

[83] M. A. Azzopardi, "Method and apparatus for generating and transmitting synchronized video data," U.S. Patent 8654251, Feb. 18, 2014.

[84] G. R. Hewes and F. W. W. JR, "Multi-sensor video frame synchronization apparatus and methods," U.S. Patent 8717422, May 06, 2014.

[85] G. Litos, X. Zabulis, and G. Triantafyllidis, "Synchronous Image Acquisition based on Network Synchronization," in *Conference on Computer Vision and Pattern Recognition Workshop, 2006. CVPRW '06*, 2006, pp. 167–167.

[86] T. Chen, S.-Y. Kung, and Y.-T. Lin, "Frame synchronization in a multi-camera system," U.S. Patent 6340991, Jan. 22, 2002.

[87] J. Hoerentrup and M. Schlosser, "Video processing apparatus and method for detecting a temporal synchronization mismatch," WO. Patent Application No. 2013092248 A1, Jun. 27, 2013.

[88] O. Märtens, A. Mõlder, R. Land, T. Saar, M. Reidla, D. Reid, and A. Girfanov, "Meetod ja seade täpsete ajatemplitega pideva pildivoo hõivamiseks," Estonian patent application No. P201400044, Dec. 18, 2014.

[89] "Qt Project," *http://qt-project.org/*, Visited: Feb. 01, 2015.

[90] Micron Technology, "MT9D131 Developer Guide." 2007.

[91] B. K. P. Horn and B. G. Schunck, "Determining Optical Flow," Apr. 1980.

[92] H. Frenz and M. Lappe, "Absolute travel distance from optic flow," *Vision Res.*, vol. 45, no. 13, pp. 1679–1692, Jun. 2005.

[93] T. Brox and J. Malik, "Large Displacement Optical Flow: Descriptor Matching in Variational Motion Estimation," *IEEE Trans. Pattern Anal. Mach. Intell.*, vol. 33, no. 3, pp. 500–513, Mar. 2011.

[94] H. Liu, R. Chellappa, and A. Rosenfeld, "Fast two-frame multiscale dense optical flow estimation using discrete wavelet filters," *J. Opt. Soc. Am. A Opt. Image Sci. Vis.*, vol. 20, no. 8, pp. 1505–1515, Aug. 2003.

[95] J. Hjelmström and A. Johannesson, "Method for determining the tilt of an image sensor," EU Patent 2549227, Sep. 11, 2013.

[96] Y. Tamura, "Projector with tilt angle measuring device," EU Patent 1517550 B1, Okt. 19, 2011.

[97] M. Kimura, "Image processing device, image processing method, image processing program, recording medium with image processing program recorded therein, and image processing processor," U.S. Patent 8180176, May 15, 2012.

ACKNOWLEDGMENTS

ABSTRACT

This thesis describes image processing solutions for precise road profile measurement systems.

Existing road profile measurement systems are fairly complex, consisting of several instruments which are necessary to collect the data required by the users (road maintainers, road constructors, national technical control centers, airfields, etc) of it. Calibration, installation of the system and usage of existing solutions is rather sophisticated. This has made the road profile measurement systems quite expensive and thus not affordable for smaller companies, who would benefit of owning such a system.

In this thesis several image processing aspects of the road profile scanners were improved while reducing the calibration complexity and facilitating the systems installation in a wide range of standard commercial vehicles, whilst minimizing the cost of adaptation and installation.

In the introduction part of this thesis an overview of road profile measurement systems and the state of art has been given. The motivation and goals of this thesis are described.

In the first chapter an overview of existing laser line detection methods has been given, several new methods are developed and tested to improve the laser line detection resolution, compared to existing solutions to sub-pixel level and reduce the dependency of the laser line detection algorithms from the noise and the variation of the laser line width.

In the second chapter the road profile measurement system speed aspects have been investigated and a new adaptive undersampling method to increase road profile scanning speed without increasing the camera frame rate or using custom hardware has been described.

In the third chapter an overview of the relationships between the camera image, laser and real world units is given. Methods to correct the distortions and a new method to find the laser line light plane parameters are described. Complete calibration procedure is given and experiments to assess the accuracy of the developed laser scanner are described.

In the fourth chapter a new solution to precisely time-stamp the laser line profile (road transverse profile) with absolute time and thus location on road has been described. Experiments were made to extract the exact time from image with modulated light on it.

In the fifth chapter an overview of the developed mobile test rig hardware, software and the final complete system has been described.

In the final chapter, the main results of this thesis are described. The proposed methods and solutions are summarized. In addition to this, a potential list of future research activities are described.

KOKKUVÕTE

Käesolev väitekiri kirjeldab pilditöötluse lahendusi täpsetele tee profiili mõõtesüsteemidele.

Olemasolevad tee profiili mõõtesüsteemid on üsna keerulised, koosnedes paljudest instrumentidest, mis on vajalikud, et koguda erinevaid tee andmeid, mida kasutavad mitmed organisatsioonid (teehooldajad, tee-ehitajad, riiklikud teede tehnokontrolli keskused, lennuväljad jne) erinevatel eesmärkidel. Olemasolevate süsteemide kalibreerimine, paigaldamine ja kasutamine on võrdlemisi keeruline, mis on muutnud tee profiili mõõtesüsteemi üsna kalliks ja seega ei ole see taskukohane väiksematele ettevõtetele, kellel oleks sellisest süsteemist samuti kasu.

Antud töös on parendatud tee profiili mõõtmise süsteemi mitmeid olulisi pilditöötluse aspekte, vähendades samal ajal kalibreerimise keerukust ja lihtsustades süsteemi paigaldmist, mis võimaldab selle kasutamist väga laial valikul tarbesõidukitel, vähendades oluliselt ka antud süsteemi kohandamis- ja paigaldamiskulusid.

Sissejuhatavas peatükis antakse ülevaade tee profiili mõõtmise süsteemist ja teadaolevatest tipplahendustest. Kirjeldatud on käesoleva väitekirja motivatsioon ja eesmärgid.

Esimeses peatükis tehakse ülevaade olemasolevatest laserjoone leidmise meetoditest. Mitu uut meetodit on välja töötatud, uuritud ja testitud, parandades laserjoone leidmise eraldusvõimet sub-piksli täpsuseni võrreldes teadaolevate lahendustega, vähendadades sealjuures sõltuvust mürast ja laserjoone laiuse variatsioonist.

Teises peatükis uuritakse tee profiili mõõtmise süsteemi toime kiiruse aspekte ja kirjeldatakse uut adaptiivset alavõendamise pilditöötluse meetodit, et tõsta tee profiili skaneerimise kiirust ilma kaamera kaadrisageduse tõstmise või keerulise eririistvara kasutamiseta.

Kolmandas peatükis antakse ülevaade kaamerapildi, laseri ja reaalse maailma mõõtmete vahelistest seostest. Kirjeldatud on uus meetod laseri valguse tasapinna parameetrite leidmiseks. Toodud on täielik kalibreerimisprotsessi kirjeldus. Ekperimentaalses osas on uuritud arendatud skanneri täpsust ja seda mõjutavaid tegureid.

Neljandas peatükis on toodud uudne lahendus laserjoone profiilide (tee põikiprofiil) märgistamiseks täpsete ajatemplitega. Kirjeldatud on katsetulemused täpse ajatempli tuvastamiseks moduleeritud valgusallikaga pildilt.

Viiendas peatükis kirjeldatakse loodud mobiilset testkäru, tarkvara ja lõpliku tee profiili mõõtmissüsteemi lahendust.

Viimases peatükis on toodud töö peamised põhitulemused ja kokkuvõtted. Lisaks on välja pakutud potentsiaalsed uurimisvaldkonnad tulevikus.

APPENDICES

Paper I

A. Molder, O. Martens, T. Saar, and R. Land, "Laser Line Detection with Sub-Pixel Accuracy," *Elektron. Ir Elektrotechnika*, vol. 20, no. 5, May 2014, pp. 132-135.

Laser Line Detection with Sub-Pixel Accuracy

A. Molder[1], O. Martens[1, 2], T. Saar, R. Land[1]

[1]*Thomas Johann Seebeck Department of Electronics, Tallinn University of Technology,*
Ehitajate St. 5, 19086, Tallinn, Estonia
[2]*ELIKO Competence Centre,*
Maealuse 2/1, Tallinn 12618, Estonia
ago@kodutalu.ee

Abstract—Due to the fact that the image sensors have a fixed resolution and pixel size – a lot of image processing algorithms are limited with pixel resolution. One of those image processing algorithms is related to 3D laser scanners and in particularly to the laser line detection from images. This pixel quantization resolution, however, in many cases is not sufficient and greatly limits the laser scanner precision. In particularly the problem is highlighted in the linearly growing or declining surfaces, but also in strait lines where the actual laser line centre position is between two pixels. In this paper two laser line centre position detection methods with sub-pixel accuracy have been proposed and investigated. The methods have been tested on real images and as seen from the results at the end of the paper, the methods greatly improve the laser line detection accuracy and resolution.

Index Terms—Sub-pixel, laser line, 3D laser scanner, parabola.

I. INTRODUCTION

Many laser line detection algorithms [1], [2] for 3D laser line scanners detect the laser line with pixel resolution. This is mainly related to the fact that the camera sensor, capturing the laser line image, has a fixed resolution and pixel size. In one aspect-the theoretical limit for the spatial resolution is determined by the Nyquist-Shannon sampling theorem. Changes at higher frequencies, than the half of the sample rate cannot be accurately detected. The laser line is typically 1 to 10 pixels wide, in real images of interest. This one pixel accuracy however is not sufficient in many cases, if going into sub-millimetre measurements with line laser scanners. The accuracy of the laser scanner is directly related to the precision of the laser line detection algorithm and in many cases the actual laser line centre position is located between two pixels. This is highlighted particularly in a linearly growing or declining surfaces, but also on very rough surfaces as for example the pavement surface with small rocks.

Several laser line sub-pixel detection methods exist. Some of them are proposing to first detect the laser line edges [3] and then to estimate the real laser line centre position with

interpolation. Furthermore, sub-pixel edge detection [4] by cubic interpolation has been also proposed to enhance this method. Unfortunately this method can produce inaccurate results, when laser scattering can cause asymmetric laser line profile with non-precise edge positions. This can cause the mathematical mean point of the laser line to deviate from the actual laser line centre. The proposed methods take into account also the intensity profile and thus are less dependent of the laser line edge positions.

Other methods [5] propose to detect the laser line centre position with sub-pixel accuracy by calculating the weighted average of the "brightest" pixel coordinates in each column. This method can still cause inaccurate results, if the laser line peak has a flat top and uneven number of brightest pixels. The result in this case is also affected by the fact, how many pixels are chosen as "brightest" pixels and where the threshold level has been set.

As known, cross-section of the laser line is similar to the Gaussian distribution from the image pixel intensity perspective. Thus Gaussian profile fitting is also a popular method [6] to detect laser line centre position with sub-pixel resolution and accuracy. With this method, however, a maximum position of the fitted Gaussian profile is detected instead of the actual laser profile peak position. This can lead to inaccurate results when the laser line width is changing. In case, if the laser line has multiple peaks a specially modified Gaussian function has to be used.

To detect real centre position of the laser line with sub-pixel accuracy we have proposed two new methods to find the best method for accurate laser line centre position detection with sub-pixel accuracy. Firstly a method is proposed, where laser line detection method (inverted second order Gaussian derivate kernel convolution to the laser line brightness profile) is combined with the sub-pixel correction estimation of the convolution maximum by parabola. Secondly a robust method to upsample the image before laser line detection has been proposed, improving also the laser line detection results to sub-pixel accuracy, compared with the original image.

The proposed methods have been tested on real life images and the results show, that these methods improve the laser line detection accuracy, to the sub-pixel level.

II. LASER LINE SUB-PIXEL DETECTION BY CONVOLUTION MAXIMUM CORRECTION WITH PARABOLA

The inverted second order Gaussian derivate is used for the

laser line extraction as a kernel for convolution to the brightness (e.g. grey value) profile. The convolution is calculated for every image column to detect the position of the laser line with pixel accuracy. Figure 1 shows the laser line grey value profile and its convolution results with optimal inversed Gaussian second order derivate kernel.
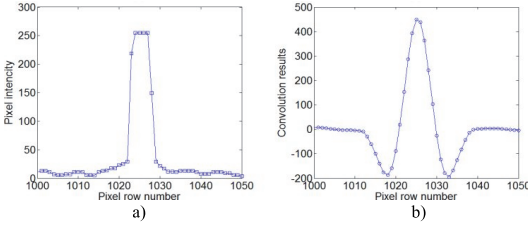

Fig. 1. Laser line cross section grey value profile (a) and convolution curve with inversed Gaussian second order derivate kernel (b).

As seen from Fig. 1(a) the actual grey value profile is rather flat in the laser line centre position. The convolution maximum was found on the 1025 of pixel row. By looking the convolution curve Fig. 1(b) around the maximum area more closely, it can be seen, that the top of the curve is not symmetrical.

To estimate the real centre position of the laser line a point before the maximum (x1, y1), the maximum point (x2, y2) and one point after the maximum (x3, y3) can be taken. With those points it is possible to find a parabola equation

$$y = ax^2 + bx + c, \qquad (1)$$

that passes through all these points. By solving the equation system:

$$y = ax^2 + bx + c, \qquad (2)$$

$$y2 = a(x2)^2 + b(x2) + c, \qquad (3)$$

$$y3 = a(x3)^2 + b(x3) + c, \qquad (4)$$

the constants a, b and c can be easily found:

$$a = \frac{((y2 - y1)(x1 - x3) + (y3 - y1)(x2 - x1))}{((x1 - x3)((x2)^2 - (x1)^2) + (x2 - x1)((x3)^2 - x1^2))}, \quad (5)$$

$$b = \frac{((y2 - y1) - a((x2)^2 - x1^2))}{(x2 - x1)}, \qquad (6)$$

$$c = y1 - a(x1)^2 - b(x1). \qquad (7)$$

With those constants the parabola vertex x_{max} and y_{max} coordinates can be expressed with the following equations:

$$x_{max} = -\frac{b}{2a}, \qquad (8)$$

$$y_{max} = a(x_{max})^2 + b(x_{max}) + c. \qquad (9)$$

Figure 2 shows a parabola constructed with points x1, y1 = (1024, 394); x2, y2 = (1025, 448.6); x3, y3 = (1026, 363.1) and the real maximum of the constructed parabola is located at x_{max}, y_{max} = (1024.89, 449.45). This parabola

vertex is found for every convolution maximum of every pixel column and by this the laser line has been found by sub-pixel accuracy.
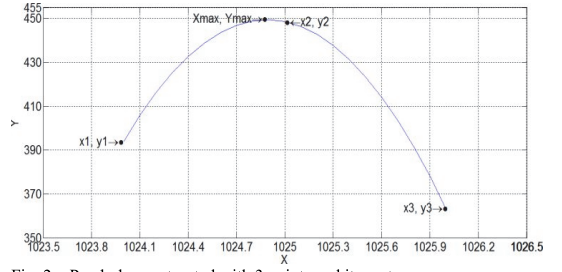

Fig. 2. Parabola constructed with 3 points and its vertex.

III. IMAGE UPSAMPLING METHOD

One efficient approach to increase the laser line resolution and thereby the accuracy is to upsample the images. After upsampling the image, the laser line can be found in sub-pixel accuracy compared with the original image. Many algorithms exists [7] to upsample the image, using different methods. Many image editing software like Irfanview and image processing libraries like OpenCV already include those different upsampling methods, making this quite robust and easy method to implement. Figure 3 shows a laser line image before upsampling and Fig. 4 after the upsampling. After upsampling the image, the laser line is detected with the proposed variable width laser line detection method.
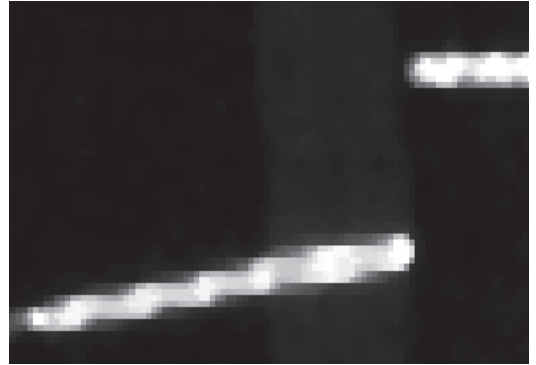

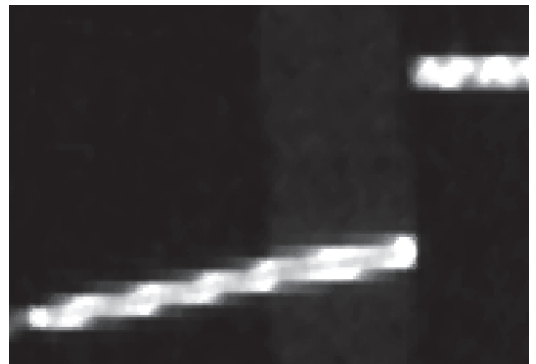Fig. 3. Laser line image before upsampling.

Fig. 4. Laser line image after upsampling 2 times.

IV. RESULTS

To verify the proposed methods they were tested on several real life images. Laser lines were extracted with pixel and then with sub-pixel resolution (and accuracy). In particularly, as the problem is especially highlighted in the
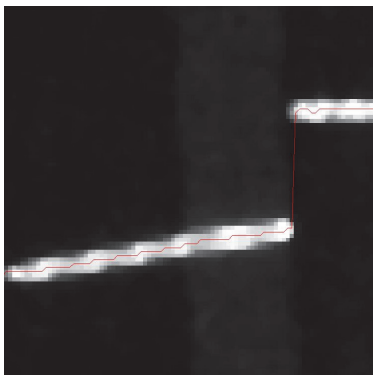

Fig. 5. Detected laser line with 1 pixel accuracy from original image.
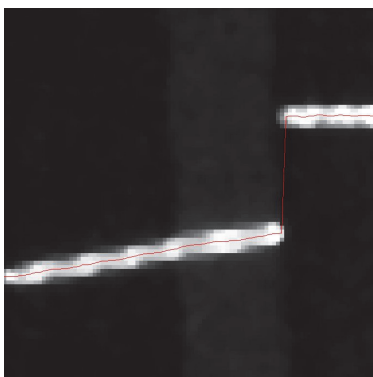

Fig. 6. Detected laser line with sub-pixel accuracy (convolution maximum correction with parabola method).

First the convolution maximum correction with parabola method was tested. Figure 5 shows a linearly growing laser line and a detected laser line with pixel accuracy and Fig. 6 with sub-pixel accuracy. It can be visually seen that our method has improved the laser line detection accuracy.

Secondly the upsampling method with the same image was tested. For comparison purpose the same image region of interest was selected to verify the method. Figure 7 shows for demonstration the detected laser line with upsampled image. It is clearly visible, that the upsampling method also improves the laser line detection accuracy. Furthermore the results seem similar or even better to the first proposed method.

For experimental purposes the convolution maximum correction with parabola method was also tested on upsampled image. Figure 8 shows the result of this combined method. It can be seen, that the accuracy has been improved, compared with the upsampled pixel accuracy image. The disadvantage of these upsampling methods is that the upsampling increases the number of pixels with the power of the upsampling level selected. This in turn decreases the laser line detection speed and increases the required processing power, which is often critical in real

linearly growing or declining surfaces, but also in strait lines where the actual laser line centre position is between two pixels, those part of our test images were selected to verify the proposed methods.
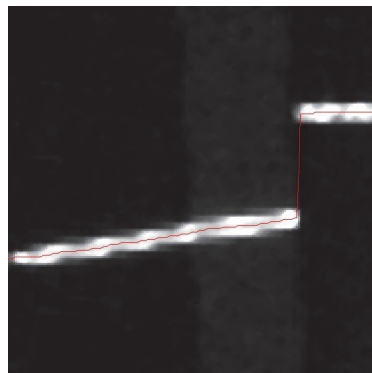

Fig. 7. Detected laser line from upsampled image with its pixel accuracy.
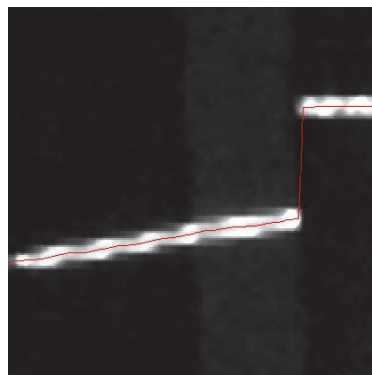

Fig. 8. Detected laser line from upsampled image with sub-pixel accuracy (convolution maximum correction with parabola method).

time systems. The speed decrease can be compensated with adaptively undersampling the image, as proposed by our previous works. Finding the optimal up and down sampling level is probably the key element of this method.

Figure 9 and Fig. 10 presents 2 laser line sections (laser line on fairly straight (few pixel fluctuations over 2 meters) floor surface and on linearly declining surface) detected by pixel and sub-pixel accuracies from original and upsampled image. It can be seen from Fig. 9 and Fig. 10, that all of the proposed methods improve the laser line detection accuracy.

In order to assess the real improvement the methods are compared to reference. It is known that in the real world both those laser line sections (linearly declining surface and strait floor surface) are straight (ideal) lines. By fitting the ideal line through the detected laser line points for every method the deviation from the ideal line can be found. This indicates how good the method is compared to the originally pixel accuracy method from original image. The less deviation from the ideal line the better the method. Figure 11 shows the deviation in pixels from the reference (ideal) line at position 0 on linearly declining surface. It can be seen that in case of pixel accuracy method from the original image Fig. 11(a) the deviation varies from 1 to -1,

while all the proposed methods Fig. 11(b)–Fig. 11(d) deviate much less in between 0.6 to -0.6.
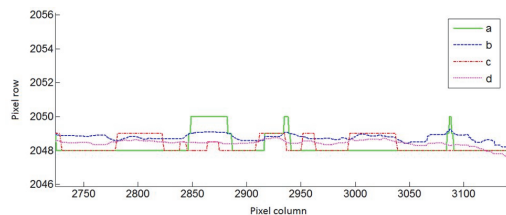

Fig. 9. Detected laser line on fairly strait floor surface with pixel accuracy form original image (a), sub-pixel accuracy with convolution maximum correction method from original image (b), pixel accuracy from upsampled image (c) and sub-pixel accuracy with convolution maximum correction and upsampling method combination (d).
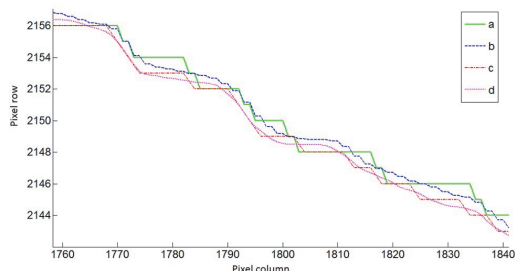

Fig. 10. Detected laser line on linearly declining surface with pixel accuracy form original image (a), sub-pixel accuracy with convolution maximum correction method from original image (b), pixel accuracy from upsampled image (c) and sub-pixel accuracy with convolution maximum correction and upsampling method combination (d).
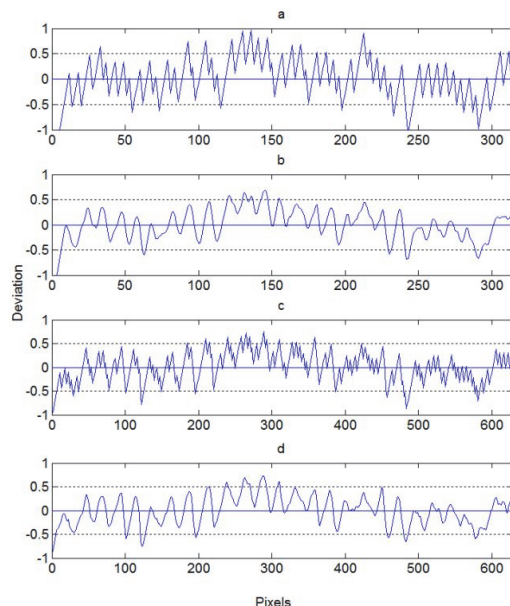

Fig. 11. Deviation from the ideal line at position 0. Pixel accuracy form original image (a), sub-pixel accuracy with convolution maximum correction method from original image (b), pixel accuracy (sub-pixel accuracy compared to original image) from upsampled image (c) and sub-pixel accuracy (sub-sub-pixel compared to original image) with convolution maximum correction and upsampling method combination (d).

Root Mean Square Error (RMSE) was calculated for all the methods which were fitted with ideal lines for both line

sections (declining surface and straight floor surface). Average RMSE for the both line section was calculated. It can be seen from the Table I that all the methods have improved the laser line detection. The RMSE has decreased more than 20 % for all the proposed methods. The most accurate method is the pixel accuracy method from the upsampled image. The RMSE has decreased more than 25 % compared to original image for this method.

Taking into account, that if using the upsampling method the pixel count is increased by the power of the upsampling level selected and thus the needed processing power increases also, the first proposed convolution maximum correction with parabola method seems to be more reasonable for fast and precise imaging systems.

TABLE I. RMSE OF METHODS BY IDEAL LINE FITTING.

Method name	RMSE (declining surface)	RMSE (straight floor surface)	RMSE (Average)	%
Pixel accuracy upsampled image	0,30448	0,36489	0,33469	25.294
Sub -pixel with convo-lution maximum correction original image	0,31929	0,37900	0,34915	22.019
Sub -pixel with convolution maximum correction upsampled image	0,30476	0,40238	0,35357	21.032
Pixel accuracy original image	0,41422	0,48125	0,44773	0

V. CONCLUSIONS

This paper presents two laser line detection algorithms with sub-pixel resolution and accuracy. The methods have been described and the Matlab model has been created. The methods were tested with real life images. The detected laser lines were compared with reference (ideal) line for every method and the RMSE was calculated. The results show visually and by RMSE that all the proposed methods have improved the laser line detection accuracy to subpixel level.

REFERENCES

[1] K. Sung, H. Lee, Y. S. Choi, S. Rhee, "Development of a multiline laser vision sensor for joint tracking in welding", *The Welding Journal,* pp. 79-s, 2009. [Online]. Available: http://www.aws.org/wj/supplement/wj0409-79.pdf
[2] M. Lopez, J. A. Vilan, J. M. Matias, J.Taboada, "Quality control of wood-pulp chips using a 3D laser scanner and functional pattern recognition", *Industrial Electronics,* pp. 1773–1778, 2007.
[3] V. Matiukas, D. Miniotas, "Detection of laser beam's center-line in 2D images", *Elektronika ir Elektrotechnika*, no. 7, pp. 67–70, 2009.
[4] P. Pelgrims, G. V. D. Velde, B. V. D Vondel, "Sub-pixel edge detection", *De Nayer Instituut Onderzoeksgroep Digitale Technieken*, 2004.
[5] S. Winkelbach, S. Molkenstruck, F. M. Wahl, "Low-cost laser range scanner and fast surface registration approach", *LNCS 4174*, 2006, pp. 718–728.
[6] Li Qi, Y. Zhang, X. Zhang, S. Wang, F. Xie, "Statistical behavior analysis and precision optimization for the laser stripe center detector based on Steger's algorithm", *Optics express,* vol. 21, no. 11, pp. 13442–134493, 2013. [Online]. Available: http://dx.doi.org/ 10.1364/OE.21.013442
[7] T. Acharya, P. S. Tsai, "Computational foundations of image interpolation algorithms", *ACM Ubiquity*, vol. 8, 2007 [Online]. Available: http://citeseerx.ist.psu.edu/viewdoc/download?doi=10.1.1. 122.2248&rep=rep1&type=pdf

Paper II

A. Mõlder, O. Märtens, T. Saar, and R. Land, "Extraction of the Variable Width Laser Line," in *Proceedings of the 14th Biennial Baltic Electronics Conference (BEC)*, Tallinn, Estonia, 6-Oct-2014, pp. 157-160.

Extraction of the Variable Width Laser Line

Ago Mõlder, Olev Märtens, Tõnis Saar and Raul Land

Thomas Johann Seebeck Department of Electronics

Tallinn University of Technology

Tallinn, Estonia

ago@kodutalu.ee

Abstract— **the aim of this paper is to develop a laser line detection algorithm which reduces the uncertainties what are caused by the unknown laser line width on the laser scanner images. Due to the fact that different surfaces reflect light in different ways the laser line on captured images is not always with constant width. The line width is also depending of the laser optics used. In 3D laser line scanners a correct detection of laser line is essential, because the laser line extraction accuracy affects greatly the precision of the developed 3D laser scanner. In this paper a method to use different standard deviations for inverted second order Gaussian derivative convolution mask to find the optimal standard deviation for every line section has been proposed. The results show a great dependency between standard deviation of the convolution kernel and laser line width. The experiments show that the optimal standard deviation of the convolution kernel is not constant over the whole laser line. Furthermore the optimal standard deviation for every line section reduces the uncertainties that were caused by the unknown laser line width.**

Keywords—image processing; 3D laser line scanner; laser line calibration; Gaussian kernel, second order derivative

I. INTRODUCTION

Several laser line detection methods are used to extract laser line(s) from 3D laser scanner images. Some of the methods [1, 2] use the most intensive pixel or so called peak detection methods. Unfortunately this method can produce inaccurate results while processing oversaturated, noisy or wider than 1 pixel wide laser line peaks (example: Fig. 1 (b)). Often different edge detection methods [3, 4] are used to find the laser line edges. Based on the edge co-ordinates a laser line centre can be calculated, but laser scattering can result in asymmetric laser line profile which can cause the mathematical mean point to deviate from the actual laser line centre. First order Gaussian derivative zero crossings have also been used [5] to extract laser line centre positions. With this method the laser line width is not taken into the consideration and random noise peaks influence the end result quite a lot. Some methods [6] even use multiple first order Gaussian derivatives to extract laser line edges instead of usual edge detection operators, but these methods use fixed distance of those found first order derivatives to find the laser line and is not thus optimal method in case of variable laser width.

As known, the laser line cross-section is similar to the Gaussian distribution from the image pixel intensity perspective. Thus some of the laser line extraction methods [7,

8] use the Gaussian second order derivative kernel to find the laser lines from images, and as this seems to be a reasonable approach then the variable width laser line extraction method is also based on this assumption.

Most of the above mentioned methods assume that the laser line is of constant width over the whole image, but in reality this is not always the case. Due to the fact that various surfaces reflect light in different ways the laser line width changes. Some materials reflect more energy back to the camera sensors than others. As a consequence, some areas of the laser line appear wider and some laser line areas narrower. In addition, the laser line width varies at different distances from the camera. The closer to the camera the wider the laser line appears. Laser line width on the image also depends of the laser optics used. For example some line lasers are produced with Gaussian distribution optics, where in the middle of the line the line is wider and in the line ends the line, is narrower.

The assumption that the line width is constant affects the laser line extraction accuracy and thus also the 3D laser scanner precision. In sub-millimeter level this is a critical factor.

To achieve a greater autonomy of the laser line extraction algorithm from the line width perspective and reduce the uncertainty what is caused by the unknown laser line width a laser line extraction method that calculates optimal line width parameters for every laser line section during the laser line extraction process has been proposed. The calculated parameters can be used for one time system calibration or for real time system optimization. The method has been tested on real images and the results are presented at the end of the paper. The method has been tested on several real life images.

II. THE BASES OF THIS LASER LINE EXTRACTION METHOD

As mentioned before laser line cross-section is similar to the Gaussian distribution

$$g(n, \sigma) = \frac{1}{\sqrt{2\pi}\sigma} e^{-\frac{n^2}{2\sigma^2}} \qquad (1)$$

with a width of N where $-\left(\frac{N-1}{2}\right) \leq n \leq \left(\frac{N-1}{2}\right)$ and σ is the standard deviation of a Gaussian random variable. Fig. 1 presents a Gaussian distribution and a similar laser profile cross-section.

14th Biennial Baltic Electronics Conference (BEC2014)
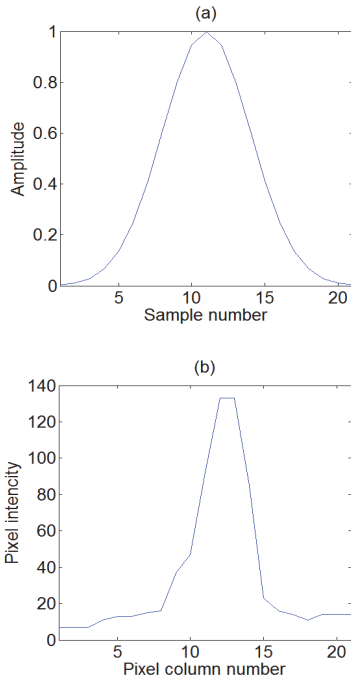Tallinn, Estonia, October 6-8, 2014

Fig. 1. (a) Gaussian distribution, (b) real laser cross-section profile.

To find a laser line, an inverted second order derivative of the Gaussian distribution is taken

$$g''(n, \sigma) = -\frac{n^2 - \sigma^2}{\sqrt{2\pi}\sigma^5} e^{-\frac{n^2}{2\sigma^2}} \qquad (2)$$

which is convolved to the gray value profile f(n) of every image column

$$s''(n, \sigma) = g''(n, \sigma) * f(n) \qquad (3)$$

In the laser line centre position the convolution has a local maximum.

III.   VARIABLE WIDTH LASER LINE EXTRACTION

In order to take into account the change in the line width over the entire image inverted second order derivations of the Gaussian distribution with several different standard deviations in the range of $1 \leq \sigma \leq 4$ are taken with an increment of 0.5 steps. Too big standard deviation range and small step size make the method slow and calculation intensive. Optimal step size and range will be investigated in subsequent studies. With this several convolution kernels are formed. Fig. 2 presents inverted second order Gaussian derivatives with different standard deviations. By changing the standard deviation of the convolution kernel several convolution maximums in laser line centre positions are
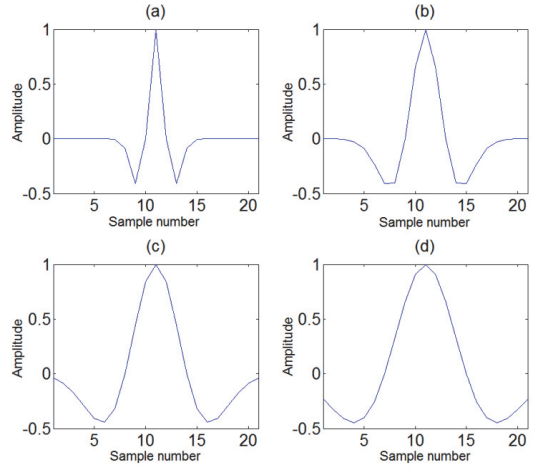
Fig. 1 Inverted second order Gaussian derivatives with standard deviations (a) 1, (b) 2, (c) 3 and (d) 4.

found. Out of those maximums a maximum of maximums for the final laser line is selected. For every image column or a section of the laser line the optimal standard deviation value out of witch the convolution was the maximum is stored. This standard deviation vector can then be used for one time system calibration. The optimal standard deviation can also be found during the laser line extraction process for every image. Fig. 3 presents a block diagram of the proposed method.

Fig. 3 Block diagram of the proposed method.

158

IV. SYSTEM SETUP

In order to perform real life tests, a small mobile test platform was constructed. The test platform has 3 inflatable wheels, so it can be moved around which enables to test the laser line extraction method on different surfaces. It is fully collapsible (yet rigid enough), for better transport purposes, measuring only 900 mm 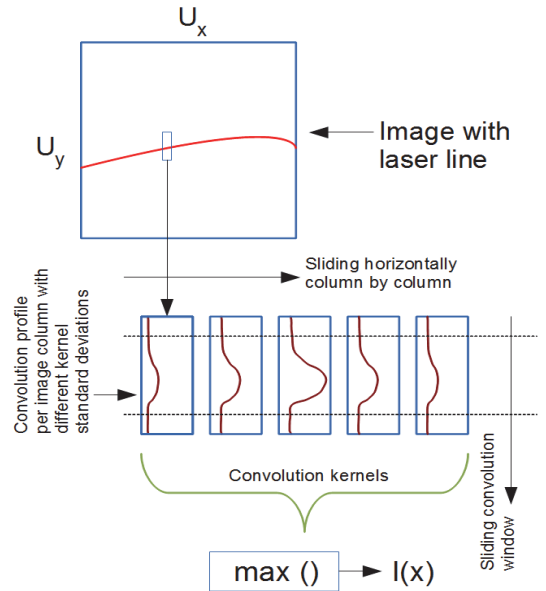x 1225 mm x 2200 mm. The test platform has been made from aluminium profiles with bolted fasteners. There is a set of fastenings for all basic systems components, which includes 3 different camera fastenings, 2 different laser fastenings, fastening for a data projector (in order to simulate different types of laser lines), box where a laptop computer, batteries and other accessories can be placed. All the laser and camera angles are adjustable. All laser and camera heights and distances can be changed. The camera and the laser can be raised up to 2 m in height. The camera and laser locations are also interchangeable. Ximea MQ042CG-CM camera is used which has a resolution of 2048 x 2048 pixels and can capture full frame images up to 90 frames per second. The main laser is Z-Laser's ZM18, which has many different line generation optics for experimenting purposes. Fig. 4 shows the mobile test platform. Matlab model was developed in order to test the method.

Fig. 4 Mobile test platform with adjustable camera and laser.

V. RESULTS

In order to assess and verify the method, several real life images where used to find the optimal standard deviation for every image column for better laser line extraction. Fig. 5 shows the correlation between the standard deviation of the convolution kernel and the maximum of the convolution results with different standard deviation convolution kernels. Three different laser line widths where used, marked as line a = 3 px, line b = 5 px and line c = 7 px marked on Fig. 5. It can be seen from the Fig. 5 that with different laser line widths the maximum convolution is different as expected. The optimal or the maximum of the maximum convolutions is clearly visible and depends on the standard deviation.

It was also noticed that with different convolution kernel sample count (the convolution kernel width) the optimal
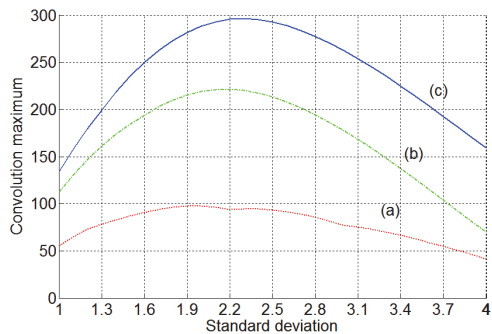

Fig. 5 Maximum convolution compared to standard deviation with 3 different line widths. Line a = 3 pixels wide, line b = 5 pixels wide and line c = 7 pixels wide. Correlation kernel sample count is 13 pixels.
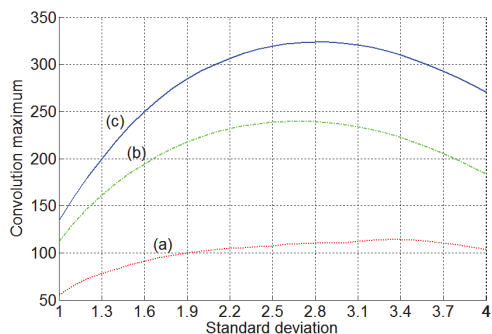
Fig. 6 Maximum convolution compared to standard deviation with 3 different line widths. Line a = 3 pixels wide, line b = 5 pixels wide and line c = 7 pixels wide. Correlation kernel sample count is 19 pixels.

standard deviation of the convolution kernel was changing. Fig. 6 shows a shifted optimal convolution kernel standard deviations compared to Fig. 5. The relationship between the convolution kernel sample count and its standard deviation will be investigated in subsequent studies.

Fig. 7 shows an example of the image used to test the proposed method. It can be seen that the laser that is used is with Gaussian distribution optics, meaning that in the middle of the laser line the laser line is wider and it is narrower in the ends of the laser line. Also on top of the checkerboard black squares it can be seen that there is much less energy and thus the laser line is also narrower.

Fig. 7 Example test image with Gaussian distribution optics where line is wider in the middle of the line and narrower in the ends.

159

Fig. 8 Extracted laser line with fixed and optimal standard deviation

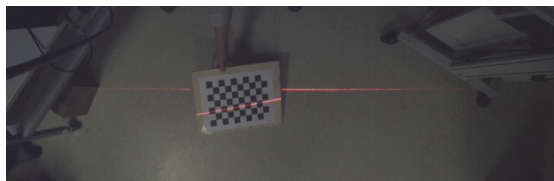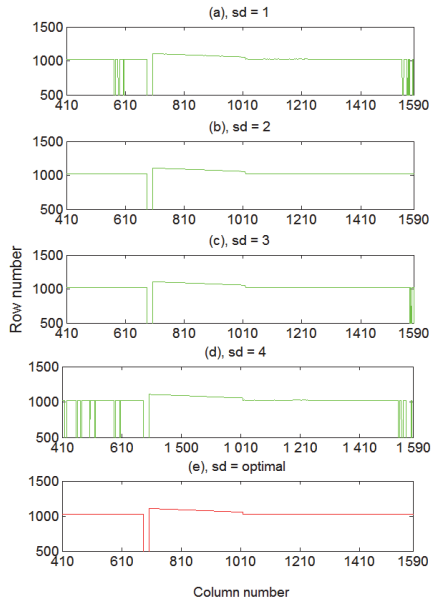Fig. 8 (a-d) represents an extracted laser line with different fixed standard deviation convolution kernels. Fig. 8 (e) shows an extracted laser line with optimal standard deviation convolution kernels for every pixel column. It can be seen that the laser line (Fig. 8 (e)) has been detected with less missing samples than with the fixed standard deviation convolution kernels. Although some fixed standard deviation convolution kernels (Fig. 8 (b)) can give quite good results it is not an optimal standard deviation for every pixel column. Closer inspection shows that the laser line deviates from the laser line detected with optimal standard deviation convolution kernel. Fig. 9 shows a laser line section deviation from the optimal laser line. This deviation becomes critical when it is necessary to detect the laser line with sub-pixel accuracy.

Fig. 10 shows the distribution of standard deviations of the optimal convolution kernels over the whole laser line image. As seen from the figure the optimal standard deviation is not
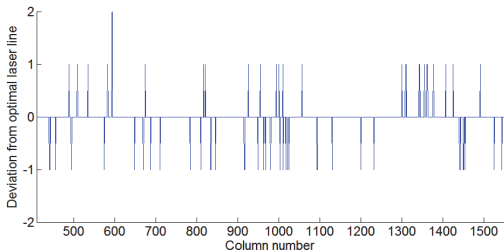

Fig. 9 Laser line (fixed standard deviation convolution kernel) deviation from optimal laser line (optimal standard deviation convolution kernel).
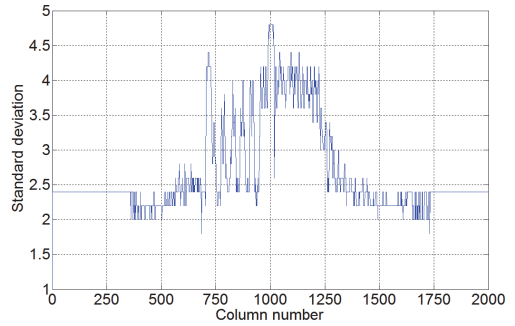

Fig. 10 Standard deviation distribution over the whole laser line.

a constant over the laser line, furthermore, the standard deviation is higher in the middle part of the image and lower in both ends of the laser line. This is within correlation with the Fig. 7 laser line width due to the laser Gaussian distribution optics. It can be also seen from Fig. 10 (Pixel column 740 - 900) that in places where the laser line was on dark squares and is thus narrower due to less energy the optimal standard deviation is smaller than in white squares.

CONCLUSIONS

This paper presents a variable width laser line extraction method. Experimental results show a great dependence between Gaussian second order derivate convolution kernel standard deviation and laser line width. The experiments show that the optimal standard deviation of the convolution kernel is not constant over the whole laser line. The proposed standard deviation vector can be used as a look up table for one time system calibration or as for real time system optimization. The results show that the proposed method decreased the uncertainty what is caused by the unknown laser line width and thus improves the laser line extraction accuracy.

REFERENCES

[1] J.Wu, J.S. Smith, and J. Lucas, "Weld bead placement system for multipass welding", Science, Measurement and Technology, Vol. 143, March 1996, pp. 85-90.
[2] K. Sung, H. Lee, Y.S. Choi, and S. Rhee, "Development of a multiline laser vision sensor for joint tracking in welding", The Welding Journal, April 2009, pp. 79-s.
[3] J. Canny, "A computation approach to edge detection", Pattern Analysis and Machine Intelligence, IEEE Transactions, Vol. 8, No. 6, November 1986, pp.679-698.
[4] J. M. S. Prewitt, "Object enhancement and extraction", Picture Processing and Psychopictorics, 1970, pp. 75-149.
[5] J. Forest, J.M. Teixidor, J. Salvi, and E. Cabruja, "A proposal for laser scanners sub-pixel accuracy peak detector".
[6] V. Matiukas and D. Miniotas, "Detection of laser beam's center-line in 2D images", Electronics and electrical engineering, 2009. pp. 67-70.
[7] Li Qi, Y. Zhang, X. Zhang, S. Wang, and F. Xie, "Statistical behavior analysis and precision optimization for the laser stripe center detector based on Steger's algorithm", Optics express, June 2013, Vol. 21, No. 11, pp. 13442-13449.
[8] C. Steger, "Unbiased extraction of lines with parabolic and Gaussian profiles", Computer Vision and Image Understanding, Vol. 117, No. 2, February 2013, pp 97–112.

Paper III

A. Molder, O. Martens, T. Saar, and R. Land, "Adaptively undersampled image processing for fast multiline laser detection," in *2013 IEEE 8th International Symposium on Intelligent Signal Processing (WISP)*, 2013, pp. 60–64.

Adaptively Undersampled Image Processing for Fast Multiline Laser Detection

Ago Molder, *IEEE member*, Olev Martens, *IEEE member*, Tonis Saar, Raul Land, *IEEE member*

Thomas Johann Seebeck Department of Electronics
Tallinn University of Technology, Ehitajate tee 5, 19086 Tallinn, Estonia
ago@kodutalu.ee

Abstract— In many image processing applications one of the main problem is how to create algorithms, which are fast enough to be implemented on embedded (with limited resources) computing platforms, like DM3730 processor based development boards (Beagleboard-XM). One such image processing area is related to laser scanners, which are usually implemented on multi-core high performance personal computers. In this paper an adaptively undersampled image processing method for fast multiline laser detection has been proposed. The combination of adaptive undersampling and multiline laser detection significantly reduces the calculation operations, needed for laser line detections, thus making this method highly suitable for limited embedded platforms. This method has been tested with real multiline laser images on pavement surface, on 4 different computing platforms and the results are presented at the end of the paper.

Keywords— *Multiline laser, laser scanning, adaptive undersampling, image processing, embedded platform, computationally efficient*

I. INTRODUCTION

Laser scanners are widely used for quality control in woodworking industries [1], automatic tire inspection [2], road profile measurements and crack detection for road maintaining [3] and elsewhere [4].

An alternative of using laser scanning system is to use structured light based scanning solutions. Several so called "one shot" scanning methods have been developed [5, 6]. They have the advantage of a high scan rate compared to the laser line scanners, but they are significantly more sensitive to illumination changes and are more sophisticated to implement. Also using a special projector to generate structured light images makes the cost of scanning system much higher compared to laser scanners. Due to these limitations laser scanning systems are more widely used in various applications.

Traditional laser scanners [7] use one camera and one laser in the combination to get one section profile of object under investigation. To get more section profiles the object under investigation has to be moved in respect to the laser scanner. In this case the number of laser profiles of the objects gained per second depends greatly on camera capturing speed. If the camera is capturing, for example, 30 frames per second then - 30 object section profiles will be gathered every second. In order to increase the scanning rate the camera capturing rate must be increased. For this high speed cameras can be used [8]. However higher frame rate cameras are significantly more expensive and with the increasing of frame rate the data transfer rates and thus image processing performance must be significantly increased. In embedded real-time image processing systems, processor resources are very limited. The computation time for laser line detection and the number of operations required for that is very critical. Therefore the image acquisition and processing should be robust, fast and smart.

One efficient approach to increase laser scanner speed is to use multiline lasers to gain more profiles per image captures and thus increasing the profile scanning rate without increasing the camera capturing rates. This method has been successfully used in welding industries [9] to check the quality of welding joints and on road profile systems for crack detection [10]. Unfortunately using of solely multiline lasers for increasing profile scanning speed is mostly not sufficient on embedded real-time image processing platforms with limited processing power.

As known - large part of the image processing algorithms handles the images independent of the content of the images. In order to save the processor time and resources only the high-interest areas of images should be processed by image processing algorithms. Resulted from the fact that the laser line(s) to be detected on an image, captured by the camera, is marginal - in sense of the line width (typically some pixels), compared, with the camera image height (480 pixels, for example) - a lot of processor resources will be wasted for processing of the non-relevant parts of an image.

In order to speed up laser profile scanning an adaptively undersampled image processing method has been proposed in this paper, for fast multiline laser detection. In our previous works adaptive undersampling methods has been used for other applications [11, 12], giving hope that adaptive undersampling method could be a reasonable approach also for multiline laser detection. Our method is not fixed with limited number of laser lines and is thus also adaptive in this sense.

The method has been tested and benchmarked on several computing platforms; including 3 desktop computers and one DM3730 processor based Beagleboard-XM embedded computing platform.

II. METHOD

A. Preprocessing

In order to get a good result, laser line must be distinguishable from the background. For testing purposes the laser lines were projected on a pavement background, as the pavement has a lot of different colors, making the laser line detection particularly difficult. As seen from the Fig. 1 - two laser lines are visible on the original laser scanner image. The image shows, that one of the laser line most characterizing indicators is color of it. Lasers are manufactured for several colors, but red color lasers are more widely used due to its price, compared with other color versions of lasers.

In order to find the red colored laser line - the red channel image is extracted from the original image. As seen from the Fig. 2 - not only red parts of an image are bright in the red channel, as white regions are also bright in the red channel image, since white color is combined of maximum intensities of every color channel (red, green, blue).

Since by our proposed method we first detect initial laser line positions and then, based on this initial laser line positions we adaptively undersample the original image, then it is not necessary to implement image preprocessing for all image regions. Thus we undersample the images horizontally, which will be used for image preprocessing and the initial laser line detection. Fig. 3 represents a horizontally undersampled image. The image was horizontally undersampled by 15 times.

To extract only the red color information, the areas, which are common with the green and blue channels has to be removed. This can be done by subtracting the sum of green and blue channel intensities from the red channel image [13]. Fig. 4 shows the result of only red color detection to extract laser lines. In this case only parts of the laser line which, are red colored, are detected.

Since the laser light and its color are usually quite intense, compared to the background and if the camera settings are not been adapted continuously, some parts of the laser line image tend to saturate and the laser line becomes white. This saturation is utilized by some laser line detection methods [14],
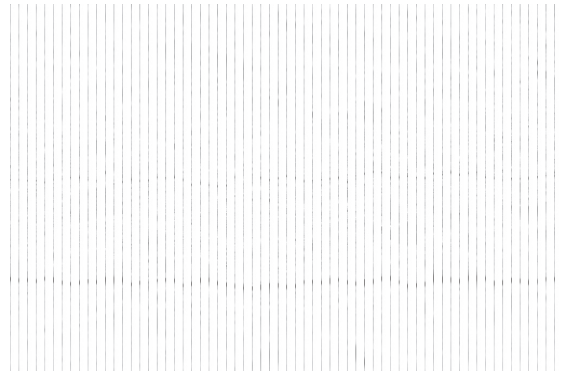

Fig. 2 *Red channel image.*

Fig. 3 Horizontally undersampled red channel image

Fig. 1 *Original multiline laser image.*

Fig. 4 *Red color detection on horizontally undersampled image*

where the laser line is detected from the red channel image by finding the highest average intensity level position in a column and using that position as the laser line for that column. Resulted from the fact, that various materials have very different reflective properties, this method is not always very good, as some parts of the laser line may be just under the threshold level and thus this information will be lost. Fig. 5 represents and intensity based threshold image, where some parts of laser lines remained under the threshold level.

In order to get a good result with various materials and various backgrounds - a combination of maximum intensity method and the red color detection method has been used. Two images are combined by using logical OR operation. Every relevant pixel of both undersampled images is compared to each other and the highest value of both pixels is always used for the combined image. Fig. 6 represents the combined horizontally undersampled image, where black regions of the image are presumed to be a part of the initial laser lines.

Also other methods [15] may be considered for initial image preprocessing instead of the red color detection and intensity based threshold methods, as image preprocessing depends greatly on the image background. In our case the selected method was sufficient and the main emphases of the method relies on adaptively undersampling the image.

B. Initial laser line detection

After preprocessing the horizontally undersampled image has been obtained, where black regions of the image are presumed to be a part of the initial laser lines. Since the image contains multiple laser lines, a peak detection method has been used on the image, obtained from the preprocessing. For every relevant column a sum of 3 predefined pixel arrays has been calculated. In the case, if second sum is greater than the first and third sum – a peak has been detected and a position of laser line, corresponding to the peak count is written to a separate initial laser line array. At the same time the peak count is stored as separate value as laser line count for every relevant column.
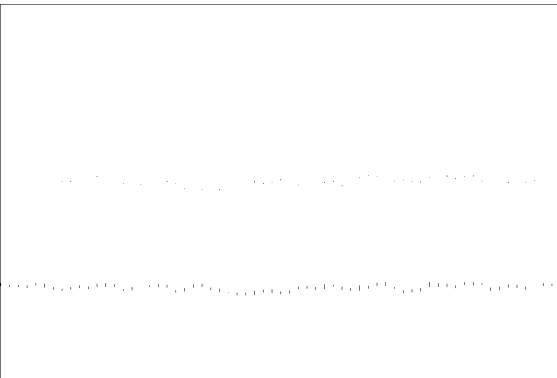

Fig. 6 *Combined red color and intensity based threshold images.*

Fig. 7 shows one column of horizontally undersampled image, where 2 clear peaks are visible. After the peaks are detected - an initial laser line image can be constructed. For every detected laser line one dot per row is used. Fig. 8 represents an initial laser line image.

C. Adaptively undersampling the image

In order to find the laser line more precisely - an adaptively undersampled image is created from the red channel image by using the points of the initial laser line as references. A predefined number of pixels are taken from the red channel image, around the initial laser line position for every column. Until the initial laser line position does not change, for rows, that do not have initial laser line position – the last known initial laser line position is used. On the constructed image only all relevant regions of the image would be highlighted and all the unnecessary and non-relevant parts of an image are excluded. Adaptively undersampled image, in such way, is shown in Fig. 9

Fig. 5 *Intensity based tresholding of red color channel on horizontally undersampled image.*

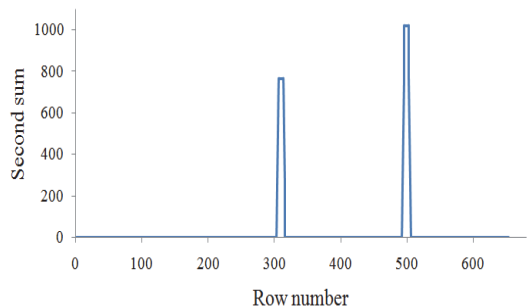Fig. 7 *Peaks in one column of preprocessed binary image.*

Fig. 8 *Initial laser lines.*

Fig. 10 *Final laser lines detected from undersampled image.*
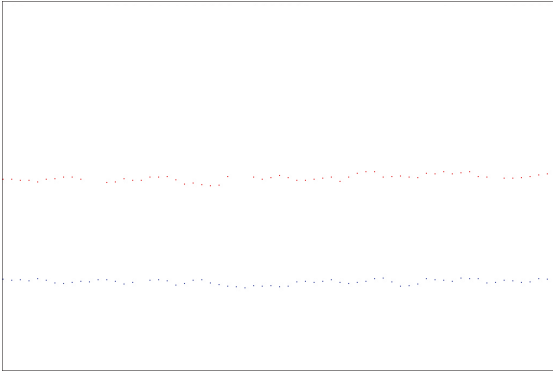
D. Final laser line detection

From the adaptively undersampled image final laser line can be extracted. For this a peak detection method is used for the second time for every detected initial laser line. Only the regions that are not white and are so part of the undersampled image, are used. It can be seen from the Fig. 10, that some of the line parts have not been fully detected, but missing sample recovery methods [16] can be used further for this purpose.

III. RESULTS

In this paper adaptive and computationally efficient undersampled image processing method for multiline laser detection was presented.

In order to assess and verify the laser line detection speed and the increase of it, compared to the conventional method (not using undersampled images) - a C++ code was developed with using of the OpenCV libraries. The proposed method was tested with two different resolutions of images (640x480 and 1600x1200) and four different computing platforms were used.
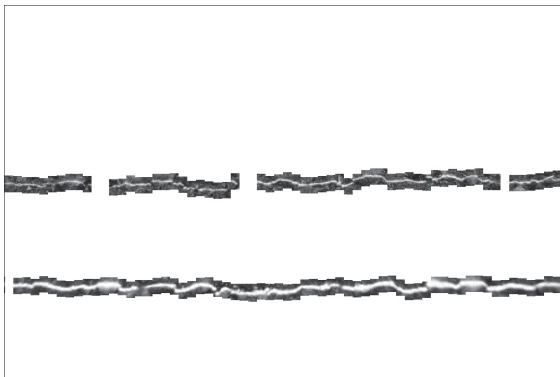

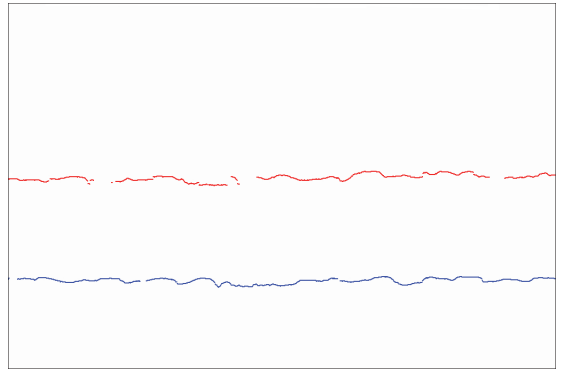Fig. 9 *Adaptively undersampled image based on initial laser line detection.*

Since computation time and the number of calculations for the image processing are very critical on the embedded platforms - the method was tested on the DM3730 processor based embedded (Beagleboard-XM) platform. The Beagleboard-XM was using Angstrom Linux and the method was tested on the ARM side of the DM3730 processor. For comparison purposes the method was also tested on 3 desktop computing platforms, running under Windows 7 operating systems. For every platform 100 images were tested and the average processing time and thus frames processed per second (fps) was calculated.

It can be seen from the Table 1, that the increase of the speed on the Beagleboard-XM was significant. The processing speed has been increased 3.46 to 8.43 times, depending on the resolution of images. It can also be noted that, for every computing platform the speed increase was even higher with larger images, compared to smaller images. On Intel processors the speed increase was higher, probably resulted from the fact that OpenCV was developed by Intel's engineers. The average speed increase of our method, compared to conventional laser line detection method (non-undersampled images) is about 6 times. Considering the fact that 2 laser lines were detected instead of one the actual speed increase is 12 times compared to a single laser line scanner.

IV. FUTURE WORK

Future work includes better preprocessing method development for detecting laser lines with low intensity in highly noisy conditions. Further benchmarking and optimizations will be done on handling more laser lines and utilizing DSP side of DM3730 processor.

Camera calibration and the evaluation of measurement errors will be performed in order to develop an accurate profile measuring instrument. Various sample reconstruction and prediction methods will be used in order to improve the accuracy of detected laser lines.

TABLE I.   BENCHMARKING OF DEVELOPED ALGORITHM ON DIFFERENT COMPUTING PLATFORMS

NR	Platform details	Algorithm benchmarking on different platforms			
		Conventional method 640x480 image average processing frame rate	*Our adaptively undersampled method 640x480 image average processing frame rate*	*Conventional method 1600x1200 image average processing frame rate*	*Our adaptively undersampled method 1600x1200 image average processing frame rate*
1	Beagleboard-XM, DM3730 (ARM ® Cortex TM -A8 @1GHz + C64xx DSP @800MHz), 512MB of RAM	8 fps	27,68 fps	1,17 fps	4,64 fps
2	Intel(R) Core(TM)2 Duo CPU P7350 @2,00GHz, 4GB(2,73 GB usable) of RAM, 32 bit system	16,85 fps	114,00 fps	2,51 fps	21,16 fps
3	Intel(R) Core(TM) i5-3320M CPU @2,60GHz, 8GB(7,88 GB usable) of RAM, 64 bit system	44, 00 fps	286,38 fps	6,36 fps	52,35 fps
4	AMD Phenom(TM) II X3 B75 CPU @3,00GHz, 8GB(3,00 GB usable) of RAM, 32 bit system	23,03 fps	160,00 fps	2,66 fps	9,96 fps

V.   CONCLUSIONS

This paper presents efficient, accurate and adaptively undersampled image processing method for fast multiline laser detection. C++ model of our method has been developed, described and tested with real images of multiline lasers on pavement surface. Four different computing platforms have been used for testing, including one embedded limited recourses Beagleboard-XM platform.

The results show that our method significantly increased the frame rate per second to detect multiple laser lines without increasing the camera capturing frame rate. Our approach is accurate and is suitable for fast multiline laser scanner systems.

REFERENCES

[1] M. Lopez, J.A. Vilan, J.M. Matias, J.Taboada, "Quality Control of Wood-Pulp Chips Using A 3D Laser Scanner and Functional Pattern Recognition", Industrial Electronics, 2007

[2] I. Frosio, N.A. Borghese, P. Tirelli, G. Venturino, G. Rotondo, "Flexible and Low Cost Laser Scanner for Automatic Tire Inspection", Instrumentation and Measurement Technology Conference (I2MTC), 2011

[3] J. Laurent, D. Lefebvre, E. Samson, "Development of a New 3D Transverse Laser Profiling System for the Automatic Measurement of Road Cracks", 6th Symposium on Pavement Surface Characteristics: SURF 2008

[4] Y. Jin, L. Zhang, C. Wu, Z. Zhu, "Detection of 3D Curve for Shoe Sole Spraying Based on Laser Triangulation Measurement", IEEE International Conference on Automation and Logistics Shenyang, China, 2009

[5] S. Yamazaki, A. Nukada, M. Mochimaru, "Hamming Color Code for Dense and Robust One-shot 3D Scanning", The British Machine Vision Conference (BMVC), 2011

[6] C. Sinlapeecheewa, K. Takamasu, "3D Profile Measurement Using Color Multi-Line Stripe Pattern With One Shot Scanning", Integrated Computer-Aided Engineering 12, 333–341, 2005

[7] "Principle of the laser scanning technique", Http://blog.computedvision.com/technology-in-machine-vision/3d-laser-scanners/, Retrieved March 24, 2013

[8] "High Speed Camera, sensitive global shutter CMOS sensor, Camera Link", Http://www.alliedvisiontec.com/emea/products/cameras/camera-link/bonito.html, Retrieved March 24, 2013

[9] K. Sung, H. Lee, Y.S. Choi, S. Rhee, "Development of a Multiline Laser Vision Sensor for Joint Tracking in Welding", The Welding Journal, 2009

[10] X.M. Sun, J.P Huang, W.Y. Liu, "Decision Model in the Laser Scanning System for Pavement Crack Detection", Optical Engineering 50(12), 2011

[11] O. Martens, T. Saar, A. Gavrijaseva, A. Molder, "Variable-Resolution Image Processing for Validation of Coins", In: Proceedings: IEEE International Symposium on Intelligent Signal Processing: WISP2011, 176 – 179, 2011

[12] A. Molder, O. Martens, T. Saar, "Adaptively Undersampled, Circular Histogram Based Image Processing for Rotation Invariant Coin Detection", 13th biennial Baltic Electronics Conference: BEC2012, 2012

[13] L. Lepisto, A. Launiainen, I. Kunttu, "Red Eye Detection Using Color and Shape", Local and Non-Local Approximation in Image Processing, 2009

[14] J.Wu, J.S. Smith, J. Lucas, "Weld bead placement system for multipass welding", Science, Measurement and Technology, 1996

[15] H.N. Ta, D. Kim, S. Lee, "A Novel Laser Line Detection Algorithm for Robot Application", 11th International Conference on Control, Automation and Systems 2011 in KINTEX, 2011

[16] P. J. S. G. Ferreira. Iterative and Noniterative Recovery of Missing Samples for 1-D Band-Limited Signals, Sampling Theory and Practice, 235-282, 2001

CURRICULUM VITAE

1. Personal data

   Name: Ago Mõlder
   Date and place of birth: 08.05.1984, Pärnu, Estonia
   E-mail address: ago@kodutalu.ee

2. Education

Educational institution	Graduation year	Education (field of study/degree)
Tallinn Polytechnic School	2003	Telecommunication
Tallinn University of Technology	2007	Electronics and biomedical engineering/B.Sc.
Tallinn University of Technology	2009	Electronics engineering/M.Sc

3. Language competence/skills (fluent, average, basic skills)

Language	Level
Estonian	Fluent
English	Fluent
Russian	Basic skills

4. Professional employment

Period	Organisation	Position
2002 – 2002	EMTS Ltd.	Electronics engineer
2003 – 2004	Kodutalu Ltd.	Log Marker
2005 – 2005	Starman Inc.	Technician
2005 – 2013	Starman Inc.	Network designer
2012 – present	ELIKO Competence Center	Research Engineer
2013 – present	Ericsson Estonia Inc.	Software developer

5. Research activity, including honours and thesis supervised

Research topics:
Signal processing, image processing

Research projects:
- Energy efficient electronic systems (SF0140061s12 SF, 01.01.12 - 31.12.13).
- Innovative, Highly Efficient Road Surface Measurement and Control System (VFP567 FP7-SME, 01.08.12 - 31.07.14).
- Research of the adaptively oversampled and modulated conversion and processing algorithms of signals(ETF8905, 01.01.11 - 31.12.13).
- Smart composites: design and manufacturing (AR12139, 01.07.12 - 30.06.15).

ELULOOKIRJELDUS

1. Isikuandmed

   Nimi   Ago Mõlder
   Sünni aeg ja -koht: 08.05.1984, Pärnu, Eesti
   E-maili aadress: ago@kodutalu.ee

2. Hariduskäik

Õppeasutus	Lõpetamise aeg	Haridus (eriala/kraad)
Tallinna Polütehnikum	2003	Telekommunikatsioon
Tallinna Tehnikaülikool	2007	Elektroonika ja biomeditsiinitehnika/ bakalaureus
Tallinna Tehnikaülikool	2009	Elektroonika/magister

3. Keelteoskus (alg-, kesk- või kõrgtase)

Keel	Tase
Eesti	Kõrgtase
Inglise	Kõrgtase
Vene	Algtase

4. Teenistuskäik

Periood	Asutus	Amet
2002 – 2002	EMTS Ltd.	Elektr. insener
2003 – 2004	Kodutalu OÜ	Palkide märkija
2005 – 2005	Starman AS	Tehnik
2005 – 2013	Starman AS	Projekteerija
2012 – tänaseni	ELIKO TAK	Teadur
2013 – tänaseni	Ericsson Eesti AS	Tarkvara arendaja

5. Teadustegevus, sh tunnustused ja juhendatud lõputööd

Uurimisvaldkonnad:
Signaalitöötlus, pilditöötlus

Teadus- arendusprojektid:
- Energiasäästlikud elektroonikasüsteemid (SF0140061s12 SF, 01.01.12 - 31.12.13).
- Innovative, Highly Efficient Road Surface Measurement and Control System (VFP567 FP7-SME, 01.08.12 -31.07.14).
- Adaptiivselt ülevõendatud ja moduleeritud signaalide muundamise ja töötlemise algoritmide uurimine (ETF8905, 01.01.11 - 31.12.13).
- Smart composites: design and manufacturing (AR12139, 01.07.12 - 30.06.15).

DISSERTATIONS DEFENDED AT
TALLINN UNIVERSITY OF TECHNOLOGY ON
INFORMATICS AND SYSTEM ENGINEERING

1. **Lea Elmik**. Informational Modelling of a Communication Office. 1992.

2. **Kalle Tammemäe**. Control Intensive Digital System Synthesis. 1997.

3. **Eerik Lossmann**. Complex Signal Classification Algorithms, Based on the Third-Order Statistical Models. 1999.

4. **Kaido Kikkas**. Using the Internet in Rehabilitation of People with Mobility Impairments – Case Studies and Views from Estonia. 1999.

5. **Nazmun Nahar**. Global Electronic Commerce Process: Business-to-Business. 1999.

6. **Jevgeni Riipulk**. Microwave Radiometry for Medical Applications. 2000.

7. **Alar Kuusik**. Compact Smart Home Systems: Design and Verification of Cost Effective Hardware Solutions. 2001.

8. **Jaan Raik**. Hierarchical Test Generation for Digital Circuits Represented by Decision Diagrams. 2001.

9. **Andri Riid**. Transparent Fuzzy Systems: Model and Control. 2002.

10. **Marina Brik**. Investigation and Development of Test Generation Methods for Control Part of Digital Systems. 2002.

11. **Raul Land**. Synchronous Approximation and Processing of Sampled Data Signals. 2002.

12. **Ants Ronk**. An Extended Block-Adaptive Fourier Analyser for Analysis and Reproduction of Periodic Components of Band-Limited Discrete-Time Signals. 2002.

13. **Toivo Paavle**. System Level Modeling of the Phase Locked Loops: Behavioral Analysis and Parameterization. 2003.

14. **Irina Astrova**. On Integration of Object-Oriented Applications with Relational Databases. 2003.

15. **Kuldar Taveter**. A Multi-Perspective Methodology for Agent-Oriented Business Modelling and Simulation. 2004.

16. **Taivo Kangilaski**. Eesti Energia käiduhaldussüsteem. 2004.

17. **Artur Jutman**. Selected Issues of Modeling, Verification and Testing of Digital Systems. 2004.

18. **Ander Tenno**. Simulation and Estimation of Electro-Chemical Processes in Maintenance-Free Batteries with Fixed Electrolyte. 2004.

19. **Oleg Korolkov**. Formation of Diffusion Welded Al Contacts to Semiconductor Silicon. 2004.

20. **Risto Vaarandi**. Tools and Techniques for Event Log Analysis. 2005.

21. **Marko Koort**. Transmitter Power Control in Wireless Communication Systems. 2005.

22. **Raul Savimaa**. Modelling Emergent Behaviour of Organizations. Time-Aware, UML and Agent Based Approach. 2005.

23. **Raido Kurel**. Investigation of Electrical Characteristics of SiC Based Complementary JBS Structures. 2005.

24. **Rainer Taniloo**. Ökonoomsete negatiivse diferentsiaaltakistusega astmete ja elementide disainimine ja optimeerimine. 2005.

25. **Pauli Lallo**. Adaptive Secure Data Transmission Method for OSI Level I. 2005.

26. **Deniss Kumlander**. Some Practical Algorithms to Solve the Maximum Clique Problem. 2005.

27. **Tarmo Veskioja**. Stable Marriage Problem and College Admission. 2005.

28. **Elena Fomina**. Low Power Finite State Machine Synthesis. 2005.

29. **Eero Ivask**. Digital Test in WEB-Based Environment 2006.

30. **Виктор Войтович**. Разработка технологий выращивания из жидкой фазы эпитаксиальных структур арсенида галлия с высоковольтным p-n переходом и изготовления диодов на их основе. 2006.

31. **Tanel Alumäe**. Methods for Estonian Large Vocabulary Speech Recognition. 2006.

32. **Erki Eessaar**. Relational and Object-Relational Database Management Systems as Platforms for Managing Softwareengineering Artefacts. 2006.

33. **Rauno Gordon**. Modelling of Cardiac Dynamics and Intracardiac Bio-impedance. 2007.

34. **Madis Listak**. A Task-Oriented Design of a Biologically Inspired Underwater Robot. 2007.

35. **Elmet Orasson**. Hybrid Built-in Self-Test. Methods and Tools for Analysis and Optimization of BIST. 2007.

36. **Eduard Petlenkov**. Neural Networks Based Identification and Control of Nonlinear Systems: ANARX Model Based Approach. 2007.

37. **Toomas Kirt**. Concept Formation in Exploratory Data Analysis: Case Studies of Linguistic and Banking Data. 2007.

38. **Juhan-Peep Ernits**. Two State Space Reduction Techniques for Explicit State Model Checking. 2007.

39. **Innar Liiv**. Pattern Discovery Using Seriation and Matrix Reordering: A Unified View, Extensions and an Application to Inventory Management. 2008.

40. **Andrei Pokatilov**. Development of National Standard for Voltage Unit Based on Solid-State References. 2008.

41. **Karin Lindroos**. Mapping Social Structures by Formal Non-Linear Information Processing Methods: Case Studies of Estonian Islands Environments. 2008.

42. **Maksim Jenihhin**. Simulation-Based Hardware Verification with High-Level Decision Diagrams. 2008.

43. **Ando Saabas**. Logics for Low-Level Code and Proof-Preserving Program Transformations. 2008.

44. **Ilja Tšahhirov**. Security Protocols Analysis in the Computational Model – Dependency Flow Graphs-Based Approach. 2008.

45. **Toomas Ruuben**. Wideband Digital Beamforming in Sonar Systems. 2009.

46. **Sergei Devadze**. Fault Simulation of Digital Systems. 2009.

47. **Andrei Krivošei**. Model Based Method for Adaptive Decomposition of the Thoracic Bio-Impedance Variations into Cardiac and Respiratory Components. 2009.

48. **Vineeth Govind**. DfT-Based External Test and Diagnosis of Mesh-like Networks on Chips. 2009.

49. **Andres Kull**. Model-Based Testing of Reactive Systems. 2009.

50. **Ants Torim**. Formal Concepts in the Theory of Monotone Systems. 2009.

51. **Erika Matsak**. Discovering Logical Constructs from Estonian Children Language. 2009.

52. **Paul Annus**. Multichannel Bioimpedance Spectroscopy: Instrumentation Methods and Design Principles. 2009.

53. **Maris Tõnso**. Computer Algebra Tools for Modelling, Analysis and Synthesis for Nonlinear Control Systems. 2010.

54. **Aivo Jürgenson**. Efficient Semantics of Parallel and Serial Models of Attack Trees. 2010.

55. **Erkki Joasoon**. The Tactile Feedback Device for Multi-Touch User Interfaces. 2010.

56. **Jürgo-Sören Preden**. Enhancing Situation – Awareness Cognition and Reasoning of Ad-Hoc Network Agents. 2010.

57. **Pavel Grigorenko**. Higher-Order Attribute Semantics of Flat Languages. 2010.

58. **Anna Rannaste**. Hierarcical Test Pattern Generation and Untestability Identification Techniques for Synchronous Sequential Circuits. 2010.

59. **Sergei Strik**. Battery Charging and Full-Featured Battery Charger Integrated Circuit for Portable Applications. 2011.

60. **Rain Ottis**. A Systematic Approach to Offensive Volunteer Cyber Militia. 2011.

61. **Natalja Sleptšuk**. Investigation of the Intermediate Layer in the Metal-Silicon Carbide Contact Obtained by Diffusion Welding. 2011.

62. **Martin Jaanus**. The Interactive Learning Environment for Mobile Laboratories. 2011.

63. **Argo Kasemaa**. Analog Front End Components for Bio-Impedance Measurement: Current Source Design and Implementation. 2011.

64. **Kenneth Geers**. Strategic Cyber Security: Evaluating Nation-State Cyber Attack Mitigation Strategies. 2011.

65. **Riina Maigre**. Composition of Web Services on Large Service Models. 2011.

66. **Helena Kruus**. Optimization of Built-in Self-Test in Digital Systems. 2011.

67. **Gunnar Piho**. Archetypes Based Techniques for Development of Domains, Requirements and Sofware. 2011.

68. **Juri Gavšin**. Intrinsic Robot Safety Through Reversibility of Actions. 2011.

69. **Dmitri Mihhailov**. Hardware Implementation of Recursive Sorting Algorithms Using Tree-like Structures and HFSM Models. 2012.

70. **Anton Tšertov**. System Modeling for Processor-Centric Test Automation. 2012.

71. **Sergei Kostin**. Self-Diagnosis in Digital Systems. 2012.

72. **Mihkel Tagel**. System-Level Design of Timing-Sensitive Network-on-Chip Based Dependable Systems. 2012.

73. **Juri Belikov**. Polynomial Methods for Nonlinear Control Systems. 2012.

74. **Kristina Vassiljeva**. Restricted Connectivity Neural Networks based Identification for Control. 2012.

75. **Tarmo Robal**. Towards Adaptive Web – Analysing and Recommending Web Users` Behaviour. 2012.

76. **Anton Karputkin**. Formal Verification and Error Correction on High-Level Decision Diagrams. 2012.

77. **Vadim Kimlaychuk**. Simulations in Multi-Agent Communication System. 2012.

78. **Taavi Viilukas**. Constraints Solving Based Hierarchical Test Generation for Synchronous Sequential Circuits. 2012.

79. **Marko Kääramees**. A Symbolic Approach to Model-based Online Testing. 2012.

80. **Enar Reilent**. Whiteboard Architecture for the Multi-agent Sensor Systems. 2012.

81. **Jaan Ojarand**. Wideband Excitation Signals for Fast Impedance Spectroscopy of Biological Objects. 2012.

82. **Igor Aleksejev**. FPGA-based Embedded Virtual Instrumentation. 2013.

83. **Juri Mihhailov**. Accurate Flexible Current Measurement Method and its Realization in Power and Battery Management Integrated Circuits for Portable Applications. 2013.

84. **Tõnis Saar**. The Piezo-Electric Impedance Spectroscopy: Solutions and Applications. 2013.

85. **Ermo Täks**. An Automated Legal Content Capture and Visualisation Method. 2013.

86. **Uljana Reinsalu**. Fault Simulation and Code Coverage Analysis of RTL Designs Using High-Level Decision Diagrams. 2013.

87. **Anton Tšepurov**. Hardware Modeling for Design Verification and Debug. 2013.

88. **Ivo Müürsepp**. Robust Detectors for Cognitive Radio. 2013.

89. **Jaas Ježov**. Pressure sensitive lateral line for underwater robot. 2013.

90. **Vadim Kaparin**. Transformation of Nonlinear State Equations into Observer Form. 2013.

92. **Reeno Reeder**. Development and Optimisation of Modelling Methods and Algorithms for Terahertz Range Radiation Sources Based on Quantum Well Heterostructures. 2014.

93. **Ants Koel**. GaAs and SiC Semiconductor Materials Based Power Structures: Static and Dynamic Behavior Analysis. 2014.

94. **Jaan Übi**. Methods for Coopetition and Retention Analysis: An Application to University Management. 2014.

95. **Innokenti Sobolev**. Hyperspectral Data Processing and Interpretation in Remote Sensing Based on Laser-Induced Fluorescence Method. 2014.

96. **Jana Toompuu**. Investigation of the Specific Deep Levels in p-, i- and n-Regions of GaAs p^+-pin-n^+ Structures. 2014.

97. **Taavi Salumäe**. Flow-Sensitive Robotic Fish: From Concept to Experiments. 2015.